Natural Resources Canada | Ressources naturelles Canada

GEOLOGICAL SURVEY OF CANADA
OPEN FILE 7632

2012 Haida Gwaii Mw 7.7 Earthquake Response -

Ocean Bottom Seismometer Relocation and Geophone Orientation Analysis and Quality Control of Wide-Angle P-wave Refraction Data

M. Riedel, M.M. Côté, P.J. Neelands, G. Middleton, G. Standen, R. Iuliucci, M. Ulmi, C.D. Stacey, R. Murphy, D. Manning, C. Brillon, G.D. Spence

2014

Canada

GEOLOGICAL SURVEY OF CANADA
OPEN FILE 7632

2012 Haida Gwaii Mw 7.7 Earthquake Response - Ocean Bottom Seismometer Relocation and Geophone Orientation Analysis and Quality Control of Wide-Angle P-wave Refraction Data

M. Riedel[1], M.M. Côté[1], P.J. Neelands[1], G. Middleton[1], G. Standen[2], R. Iuliucci[3], M. Ulmi[1], C.D. Stacey[1], R. Murphy[4], D. Manning[4], C. Brillon[1], G.D. Spence[5]

[1] Natural Resources Canada, Geological Survey of Canada - Pacific, 9860 West Saanich Road, Sidney, British Columbia, Canada
[2] Geoforce Consultants Ltd., 1 Endeavour Drive, Dartmouth, Nova Scotia, Canada
[3] Dalhousie University, Department of Oceanography, Halifax, Nova Scotia, Canada
[4] Natural Resources Canada, Geological Survey of Canada – Atlantic, 1 Challenger Drive, Dartmouth, Nova Scotia, Canada
[5] University of Victoria, School of Earth and Ocean Sciences, Victoria, British Columbia, Canada

2014

doi:10.4095/295551

This publication is available for free download through GEOSCAN (http://geoscan.nrcan.gc.ca/).

Recommended citation
Riedel, M., Côté, M.M., Neelands, P.J., Middleton, G., Standen, G., Iuliucci, R., Ulmi, M., Stacey, C.D., Murphy, R., Manning, D., Brillon, C., and Spence, G.D., 2014. 2012 Haida Gwaii Mw 7.7 Earthquake Response - Ocean Bottom Seismometer Relocation and Geophone Orientation Analysis and Quality Control of Wide-Angle P-wave Refraction Data; Geological Survey of Canada, Open File 7632, 79 p. doi:10.4095/295551

Publications in this series have not been edited; they are released as submitted by the author.

Abstract

Canada's second largest instrumentally recorded earthquake occurred on October 27th, 2012, off the west coast of Moresby Island, Haida Gwaii. Analysis of seismic waveforms and the pattern of aftershocks indicate that it was a thrust earthquake with a magnitude of Mw = 7.7. To accurately locate earthquakes, recording stations need to be positioned such that they surround the epicenter and the sound speed at which seismic waves travel through the earth's crust must be known. The land stations on Haida Gwaii are all to the east of the aftershock sequence, thus making these offshore earthquake locations uncertain and making depths for those events almost impossible to calculate accurately. Only sparse information from seismic refraction work conducted in the early 1980ies on the offshore velocity structure around the epicenter is known. Therefore, a series of 14 ocean bottom seismometers (OBS) were deployed for the duration of 1 month between December 6, 2012 and January 5, 2013 to record a portion of the aftershock sequence. An active source seismic program was conducted in January 2013 prior to the OBS recovery to acquire information on the sediment- and crustal structures to aid in the earthquake location analyses. However, the initial refraction data were not recorded on any of the 14 OBS as the batteries on all of the OBS stations had drained by the time of the survey. An extra set of six OBS was re-deployed and a total of four single-channel seismic profiles were acquired across these six OBS stations for a smaller-scale detailed refraction velocity experiment. Using the active source seismic data, each of the six OBS of the second deployment were re-located on the ocean floor, which is a critical pre-requisite for any velocity analysis. The OBS instruments drifted on average by 200m to the NW of the deployment drop-position. New offset information for the relocated OBS stations were calculated, and used for an initial exemplary but non-ray-tracing based 1D refraction velocity analysis on selected OBS stations to demonstrate the general utility of the OBS refraction data. Additional particle motion analyses were conducted for five of the six OBS stations of the second refraction survey to define the geophone orientation. One of these six stations (OBS-5) appeared to have identical horizontal components and therefore could not be used for a geophone-orientation determination. Long-range refraction seismic arrivals from the active-source experiment with a single 520 cubic inch G-gun were identified on some of the Haida Gwaii land-stations with offset ranges of up to 58 km. This information can potentially be used for a deep-crustal refraction velocity analysis. At this stage, only basic information on these land-station data is documented for potential future analyses.

1 Introduction

Canada's second largest instrumentally recorded earthquake occurred at 8:05 p.m. on October 27th, 2012, off the west coast of Moresby Island, Haida Gwaii (Figure 1). Analysis of seismic waveforms and the pattern of aftershocks indicate that it was a "thrust" earthquake. Thrust earthquakes have the potential to generate large tsunamis, and post-seismic field surveys for this event predict wave heights in some bays and inlets along the coast of Moresby Island as large as 8 m (Leonard and Bednarski, 2014). In the first month after the earthquake more than 20,000 aftershocks were recorded. The majority of these are less than magnitude 2. The initial locations of aftershocks from this earthquake (Figure 1) cover an area of 150 km in length and 50 km in width. They extend seaward from beneath the west coast of Moresby Island to more than 50 km offshore. The central zone of the aftershock sequence is the target of the seismic experiment described in this report. The distribution of the OBS stations was chosen to cover a reasonable area of the aftershock sequence centered on the epicenter, covering mostly the Queen Charlotte terrace (Figure 2). The deployment occurred in December with a recovery mission in January (for additional details, see cruise reports by Riedel et al., 2014a, b), which restricted the operations due to heavy seas and high winds. The study area was therefore limited in extent to avoid large distances between individual OBS stations. A total of nine instruments were available as part of the Natural Resources Canada (NRCan) instrument pool at the Bedford Institute of Oceanography in Dartmouth, NS. An additional five instruments from Dalhousie University were used through collaboration with Dr. Keith Louden.

The active source seismic experiment consisted of two surveys, both conducted with a single 520 cubic inch G-gun and a single-channel streamer. The first survey was not recorded on the regional grid of 14 OBS stations deployed to acquire the aftershock earthquake sequence, as batteries had run out to supply the OBS with sufficient energy to record waveforms. Therefore, a second survey was completed where six OBS were refurbished onboard and re-deployed (Figure 3). A total of four crossing lines were acquired across the six OBS stations with the same seismic source and streamer as used for the first survey.

In this report we summarize the necessary OBS pre-processing steps required prior to any detailed ray-tracing based velocity analysis. These pre-processing steps include the shot-time and location definition, digital data conversion to SEGY standard, OBS relocation analysis, and instrument depth estimation. The OBS relocation analysis was difficult due to a malfunctioning

of the time-server during data acquisition at sea, and we propose one possible solution for correcting the uncertain time-drift of the shot-times. Due to this additional uncertainty, we utilized a more complex OBS relocation analysis (Zykov, 2006) as the one used in the OBS experiment conducted in the Canadian Arctic in 2013, described by Riedel et al., (2014) for which the same NRCan-owned OBS instruments were used as the ones utilized in the Haida Gwaii earthquake experiment.

2 Seismic acquisition equipment and constraints

The seismic airgun and single-channel streamer used in this experiment were provided through the GSC-Atlantic division. A single G-gun with a volume of 520 cubic inch was used. The Sulzer compressor from the GSC-Pacific division was used and the capacity of this compressor allowed firing the airgun every 30 seconds at the fastest rate. The airgun was fired with a pressure of 1800 psi. The single-channel streamer was a unit consisting of 48 individual Teledyne B-1 acceleration canceling hydrophones, bundled to six channels each with 8 hydrophones. These six channels are then combined at the amplifier to one single channel. In order to maintain a uniform tow-depth beneath the sea surface, three passive birds were attached to the streamer and the tow-depth was between one to three meters. A layback of ~70 m (200 feet) was used. The streamer consists of a ~9 m (27 feet) long dead section, followed by the ~45m (150 feet) long oil-filled active section, and a second ~9m (27 feet) long dead section.

3 Shot-time definition and non-linear drift correction

The OBS experiment was conducted without a special time server that auto-corrects the times of the shot-logging computer and trigger. Instead, a manual fix of the shot-time logger was applied during the Haida Gwaii experiment, where the watch-keepers had to manually synchronize the shot-time logger every 10 minutes (600 seconds). The hope was that this manual synchronising would suffice to achieve the micro-second shot-time accuracy required for the OBS relocation and subsequent velocity analyses. The OBS themselves do suffer from a clock-drift, which can be corrected as the clock of each OBS instrument was synchronized to a

reference before deployment and after recovery. The time-drift corrections for the OBS clocks are listed in Table 1.

After an initial shot time definition and conversion of the seismic data so that arrival times could be picked from the traces, two rather unusual time-drifts were identified in the seismic data (Figure 4). The first instant occurred at the beginning of the survey, only after 11 shots were fired, i.e. about 5 minutes into the survey (Figure 5a). As seen in the seismic data of OBS-6 the direct arrivals from the airgun appear to reverse, although the ship continued to approach the OBS station along the main E-W transect. A second "reversal" of the direct arrivals occurred in the middle of the survey at shot #1029 (Figure 5b). Again, the ship is approaching the OBS along a straight line (parallel to the main transect) and the direct arrival times should progressively become smaller. Yet, a similar "reversal" occurs as seen at the beginning of the survey. The arrivals for both these instances are too late for what is expected given the straight-line geometry of the survey. The individual OBS clocks were all synchronized before and after retrieval and are all different from each other and not linked to the ship's clock. The two "reversals" of arrivals occur on all OBS stations at the same time, which rules out an OBS-clock error (which would be rather random). We concluded that no other explanation than a shot-time drift can account for this behaviour. As the arrival times were defined based on no changes to the shot times (other than the clock-time drift occurring on the OBS itself) we analysed the shot time data for unusual jumps or delays. We calculated the time difference between individual shots, which should have been in the order of ~ 30 seconds (Figure 6). The time of the first shot is used as the "absolute" reference of the survey. As can be seen on Figure 6, the shot time interval is on the order of 29.92 seconds, close to the expected value. However, two very large deviations occur at the two times noted previously, where the trigger time interval is by ~ 100 ms shorter. A closer look into the trigger-time interval data (Figure 7) shows that after the shot-logger was apparently synchronized the times are adjusted back to the regular trigger interval in an exponential fashion over a time of 10 minutes (or 20 shots) at these two incidents. As the trigger intervals are apparently shorter than expected (and initially defined), this explains why the seismic data on the OBS are apparently delayed. However, the trigger-intervals are not corrected back in an instant, but creep back to normal times over the period of 10 minutes. Therefore, the shots are delayed in a cumulative fashion and a cumulative adjustment needs to be applied (Figure 8). This can also be noticed, when comparing the direct arrival times when the vessel

was exactly on top of the OBS instruments. In case of OBS-6, there is a 580 ms time difference (Figure 4) between both crossings (shot No. 232 and shot No. 1828).

While observing the large deviations of the trigger-time interval, it is also evident, that over all other 10 minute intervals, the trigger times are not constant and drift, often with an opposite sense than the two large incidences (Figure 8). The cumulative delay therefore is slowly getting smaller (Figure 8) after each of the two large “reversal” incidences.

After applying the cumulative delay to the shot time tables and adding a bulk shift of 930 ms to adjust the direct arrival time when on top of each OBS to match (on average) the expected travel time from the known water depth and the single channel data, a new conversion to SEGY data format was performed. As seen in Figure 9, this cumulative time-correction successfully adjusted the reversal of arrival times in a broad sense. However, some inaccuracies remain in the data. Especially for the second reversal instance, the data appear overcorrected by up to a maximum of 70 ms at the first trace after the jump occurred (Figure 9d). The overcorrection is only seen for 8 traces, after which all arrivals appear to be along the expected arrival times. As there is no measurable or otherwise objective (and thus defendable) reason to manually adjust these differences and introduce further bias, we decided not to apply any additional corrections to these 8 traces. Accordingly, these traces are omitted from later analysis, such as the OBS relocation analysis. In the case of the first incidence, the time-corrected data appear to be properly corrected as the direct arrival times slowly get smaller as the ship approaches the OBS station. At the beginning of the survey, the vessel was not in full survey speed but gradually adjusted to stable conditions, thus the arrival times do not fully align linearly. Any potential over- (or under-) correction cannot be easily identified. However, the OBS relocation code allows correcting for any additional delays or biases (as described in section 4.2) and therefore no additional manual time-adjustments were made to the data.

4 Relocation analysis

4.1 SEGY-data generation

Based on the initial corrections to the shot times recorded by the time server, the data tables for seismic data conversions are generated using the Shottab.exe software developed by Dalhousie University (Dave LeBlanc and Prof. Dr. Keith Louden, 2002). The initial shot-time tables as well the corrected versions completed after OBS relocation are provided in the digital supplement to this Open File Report. The seismic data recorded on the OBS are then converted from their native format (DREA) to the SEGY-standard based on the shot-time tables. The conversion is performed with the Dobs2Sgy.exe software developed and distributed by Prof. Dr. Keith Louden from Dalhousie University. The SEGY data also carry information on the range (or offset) between shot and OBS location. However, the future potential user is advised to verify the values and convert (if necessary) from the unit provided (*km*) to those units used in any subsequent analysis or processing. The final SEGY data after OBS relocation and final shot-time adjustments are provided in the digital supplement to this Open File Report together with the original data. Interested users are asked to contact the first author for conversion- and analyses-codes used in this study.

4.2 Relocation code details

The Haida Gwaii OBS deployment and seismic experiment faced several critical challenges that are not straightforward to overcome. Each ten minutes (600 seconds) the time-server was synced, resulting in small but almost linear segments of deviations from a constant trigger interval. But the largest problem is the significant drift in the shot-time server at two instances. These two instances resulted in large and non-linear (exponential) deviations. As described in section 3, we fist corrected the two large instances of exponential time drift and applied that to the shot-times. Digital data in SEGY format were generated with these corrected shot times for the next step in the analysis: the actual OBS relocation.

4.2.1 Sound Speed Profile

Relocating the OBS using the direct arrivals of the airgun requires a sound speed profile as well as prior knowledge of shot-position, initial guess of the OBS position, as well as times of the actual shots. During the Haida Gwaii seismic experiment, we were unable to collect oceanographic data to either measure sound speed directly, or calculate it from conductivity,

temperature, and depth (CTD) data. A first step to generate a sound-speed profile was to access data from the oceanographic data bank of the Department of Fisheries and Ocean (DFO), which consists of CTD and ARGO data (personal communications Germaine Gatien, February 2013). Although many of these CTD data are in the general location of the experiment, they were acquired in summer times only. During the winter months off Haida Gwaii many storms occur and likely result in a more mixed ocean and rather uniform sound speed. However, we did test the impact on using the detailed summer sound speed profile and a uniform value (1480 m/s). In many instances on several OBS stations, the ray-tracing as part of the relocation code could not converge when the detailed sound speed profile was used, especially for stations on the Queen Charlotte Terrace in much shallower water than e.g. OBS-6 on the abyssal plain in almost 3000 m water depth. However, for OBS-6, both sound speed profiles result in completed inversions. But in an effort to maintain uniformity between all OBS stations, we finally decided to use only the simple sound speed profile. Results on the relocated position for both sound speed profiles are included in section 4.3 for OBS-6.

4.2.2 Parameters of the relocation inversion code

In general, two codes for OBS relocation are available: a code developed and distributed by Prof. Dr. Keith Louden from Dalhousie University and a code developed by Zykov (2006) as part of a PhD thesis. The Dalhousie code was implemented in the relocation analysis for an OBS experiment in the Arctic (Riedel et al., 2014) and is a relatively simple code that solves for the best OBS position given first-arrival picks from the OBS data for which all time-shifts and corrections had to be applied prior to the actual inversion for the OBS relocation. As the Haida Gwaii experiment has multiple challenges with regard to the shot time correction and no direct measurement of the sound speed profile existed, we decided to use the code by Zykov (2006), which allows including additional uncertainties for several parameters in the relocation inversion such as:

(a) Linear drift (R) not corrected prior to inversion ($R = b + k \times T$);
(b) Bias in the sound speed profile (+/- 2 m/s);
(c) Additional offset from an unknown airgun trigger delay (+/- 2 ms);
(d) Shot position (+/- 50 m);

This code therefore offers the necessary flexibility to overcome the specific problems of the Haida Gwaii experiment (mostly the unknown drift-corrections). While originally, the linear drift

correction in the Zykov (2006) code is solved for based on user-defined segments (by manually inserting time intervals for which a piece-wise linear drift is removed), the Haida Gwaii experiment has time-server deviations nominally occurring every 10 minutes (600 seconds). For a total duration of the experiment of ~16 hours, it is impractical to manually define these segments if direct arrivals from the 1930 shots are used. The code was modified and these 10-minute-long linear segments were pre-computed and inserted into the original code. Significant improvements in the inversion results (total residual error) were thus achieved (see sections below). In the cases of OBS-5 and OBS-6 we used 1747 and 1492 arrival times, respectively, as well as the shorter segments of the crossings of the OBS itself for comparison purposes. For all other OBS stations, only the short-distant arrivals (< 6 km distance) were picked and used in the relocation. As the distance to the OBS increases, direct arrivals from the airgun are progressively buried in noise and picking uncertainty becomes significantly larger (especially for OBS-1, which has a sample rate of 5ms to start with).

For details on the mathematical details of the inversion itself, the reader is referred to the PhD thesis by Zykov (2006) and descriptions of two other subsequent OBS experiments by Dash (2007) and Schlesinger (2012).

4.3 Test on parameters using OBS-6

The relocation inversion by Zykov allows including several parameters into the inversion, with some prior knowledge of their uncertainty and a weighting factor defining the ratio between *a priori* information and the regularization applied in the inversion. We have tested the inversion on OBS-6 with various parameters and two sets of first-arrival data, resulting in a total of 16 inversion results. Figure 10 shows the maps of the shot distribution for both scenarios (crossings only, all shots). In order to decide which inversion yielded the “best” result, we tracked the overall misfit, largest misfit, and the resulting X, and Y coordinates, and depths of the OBS (Figure 11, 12). The two first-arrival data sets are the direct arrivals within a short corridor of < 6 km around the OBS itself (direct crossings) and the entire picked arrivals.

Linear drift corrections were applied in two fashions: (a) one singular linear drift, and (b) the above- mentioned 600-second long multi-linear segments. Two sound speed profiles were incorporated (complex profile based on the summer CTD and ARGO data, and a simple profile of one velocity of 1480 m/s). A bias in the sound speed profile was also tested and a gun delay

shift was included. The inversion outcomes are shown in Figure 11 in a map of the different re-located positions, compared to the drop-position. We also show selected results of the individual misfit values versus time after the start of the survey. Some general trends from this test can be seen:

- All inversion results, irrespective of the parameters used, result in an OBS drift of ~200m to the SW (Figure 11);
- Using no linear drift correction always results in a shallower OBS depth than the value obtained from the ship's echo sounder, 2909 m, (Figure 12c);
- Using no linear drift removal, the resulting misfit as a function of time reveals extreme variations, that are apparently correlated, and clearly piece-wise linear;
- Using a simple or complex sound speed profile has a small impact on the resulting horizontal position, but strongly affects the OBS depth and overall pulls the depth closer to the anticipated value of 2909 m (Figure 12);
- Introducing a single linear drift removal reduces the overall misfit significantly, especially for the near-distant arrival times (crossings);
- Introducing the bias in the sound speed profile reduces the misfit, resulting in some change in OBS depth with the horizontal position almost unaffected (< 2 m difference);
- Introducing an offset in gun-delay does not change the resulting relocation position or OBS depth but improves the overall misfit slightly;
- Introducing multi-linear drift removal results in overall best misfit and a more random temporal distribution of the misfits;
- Introducing multi-linear drift removal moves the horizontal position much closer to the drop position and moves the OBS to shallower water depths;

The actual misfit between the picked and predicted direct arrival times reveals further insight into the inversion performance. For OBS-6 we picked a total of 1492 shots on the traces (a total of 1930 shots were fired). A first comparison of the misfit for all shot-data was made (Figure 13) between inversions with and without linear drift removal, simple- and complex sound speed profile as well as the multi-linear drift-removal with sound-speed bias and airgun trigger delay included. The initial inversion without any linear drift removal shows large misfit values that appear to be correlated and vary significantly with sudden large jumps between individual linear-

segments. This behaviour is removed from the data only with the multi-linear drift-removal. The impact of the sound speed profile was tested (see Table 2) and the representative misfit of the travel time data for the two crossings of the OBS is shown in Figure 14. The sound speed profile does not change the overall misfit significantly, and the larger impact is from the linear drift-removal. Finally, the impact of introducing a sound-speed bias and a trigger time delay for the data from the OBS-crossings is compared with the multi-linear drift-removal (Figure 15). It can be seen that the gun offset has no significant impact on the inversion performance.

In an effort to perform the OBS relocation uniformly for all stations under the same assumptions and inversion parameters, we selected the following parameters:

- Simple sound speed profile (1480 m/s);
- Sound speed bias (+/- 2 m/s)
- Gun trigger delay (+/- 2 ms)
- Multi-linear drift correction (600 ms segments)
- As many shots as possible within < 6 km of the OBS station as picking uncertainty is too large for further offsets

It is evident, that the multi-linear drift removal overall results in the smallest misfits. The remaining question is whether to use the solution from the crossings only or from all shots. Data (arrival times) from a near-station environment may best control the depth, and far-distant shots may control the horizontal position best. But far-distant shots overall have a large picking uncertainty. We decided that the final solution for OBS-6 to be carried forward in later analyses is the average between both multi-linear solutions (Table 3).

4.4 OBS-1

This OBS station is located the farthest east in the grid of seismic lines acquired during the survey. OBS-1 is slightly east of the Queen Charlotte transform fault itself. For the OBS relocation we have picked a total of 421 arrivals around the OBS (Figure 16).
The resulting misfit is shown in Figure 17. Results of the three inversion runs performed (no linear drift, single linear drift, multi-linear drift) are reported in Table 3 and coefficients of the multi-linear removal are listed in the Appendix. Using no drift correction or a single linear drift removal does reveal some remaining large misfit values after the relocation, and only the multi-linear drift removal results in a significant reduction in the misfits.

4.5 OBS-2

This OBS station is located about 6km west of OBS-1 on the Queen Charlotte Terrace and is the shallowest of all OBS (~1860 meter water depth). Only one crossing along the central line of the survey is available, and in order to improve the relocation, we picked additional arrivals from the surrounding survey lines to achieve an almost full azimuth circumference (Figure 18). A total of 688 arrival times were used in the inversion. Results are shown in Figure 19.

4.6 OBS-3

This OBS stations is located at the northern end of the central crossing line of the survey (Figure 20). Noise levels on this OBS are very high, especially at far offsets, and arrivals are difficult to detect. We therefore limited the arrivals used in the relocation analysis to the immediate vicinity around the OBS station. A total of 343 arrival times were picked. Using the single linear drift removal only slightly improves upon the total misfit of the inversion, due to the two large deviations in the centre of the arrivals picked (Figure 21). The multi-linear drift removal is capable of addressing these deviations and achieves a reasonably low misfit.

4.7 OBS-4

Station OBS-4 is in the central position of the survey grid where two main lines cross the OBS instrument (Figure 22). A total of 653 arrival times were picked from the traces of the hydrophone record. The picked arrival times are separated from each other by larger gaps when direct arrivals were more difficult to pick. Therefore, the multi-linear drift removal required a large time window and a total of 66 time segments (each 10 minutes long). However, with the multi-linear drift removal the misfit was improved significantly (Figure 23).

4.8 OBS-5

This OBS stations is located at the southern end of the central crossing line (Figure 24). Two separate inversions were tested with a large set of arrival times (Figure 24a) and with a smaller subset of arrivals from the direct crossings (Figure 24b). Again, large misfits are seen when no drift removal is used, but are slightly reduced by using a single linear drift removal. The multi-linear drift removal consisted of 9 segments for the direct crossings, and 24 segments for

the entire set of arrivals. The total misfit between picked and inverted arrival times is much reduced for the multi-linear drift removal (Figure 25).

5 Geophone Orientation Analysis

The orientation of the horizontal geophone components on the seafloor is important for the analysis of S-wave arrivals to determine the S-wave velocity structure. The OBS have four recording channels and the following naming convention is used for the seismic data:

- Channel 1: Hydrophone
- Channel 2: Vertical component (Z-axis)
- Channel 3: horizontal component 1 (North, or Y-axis)
- Channel 4: horizontal components 2 (East, or X-axis)

Typically, a particle motion diagram (also called a hodogram) is created in the x-y plane, which resembles the shape of an ellipse. A representative time window (dependent on wave-shape and frequency content) around the direct arrival of the airgun shots is typically used to define the particle motion in a hodogram. While this particle motion diagram can be used to determine the orientation of the two horizontal axes relative to the shot-azimuth, the extraction of the angle of motion can be difficult when the data are noisy or dominated by amplitudes from non-airgun arrivals, such as earthquakes. The data from the Haida Gwaii experiment were recorded during a still very active time of high seismicity from the aftershock series and thus, the traces have dozens of earthquake arrivals, which sometimes overlap with the airgun data. At a minimum, the data are skewed in amplitude from large-amplitude earthquake arrivals (P- and S-waves), and dominant surface waves, and the horizontal components often have a ringing nature from constant “vibrations” due to the overall high seismicity levels.

It is recognized that this technique is rather crude and heavily dependent on the time- and shot window chosen by the interpreter and has therefore some uncertainty on the calculated orientation angle. More computational intensive approaches can be used, e.g. the approach using an algorithm developed by Rosenberger (2010). This algorithm detects the orientation of maximum motion in the z-direction and projects that motion onto the horizontal (x-y) plane. The angle of this projection to the y-axis is then used in the calculations of the final OBS azimuth

relative to true North. Thus, this algorithm does not rely on the relative motion of the two horizontal components (which is the approach taken with the hodogram). The algorithm scans through the entire data sets (for the given shot range and time intervals provided by the user) and includes arrivals with inclination-angles between 0.3 and 0.99 (where the value '0' is perfectly horizontal motion, and the value '1' meaning perfectly vertical angle of incidence). In order for the (elliptical) particle motion detected to be incorporated in the analysis, the rectilinearity value (parameter $rect_{min}$) has to be at a minimum of 0.6. Data within a time-window of 6 sec (the parameter is referred to as L_T) is used in the calculation, and weighted by an exponential function as described in Rosenberger (2010). The algorithm produces a final histogram distribution of the residual angle between the orientation of the internal OBS axis and the shot azimuth, or in other words, the angle of rotation required to move the internal OBS axes to true North. Results from stations OBS-1, OBS-2, OBS-3, OBS-4, and OBS-6 are shown in Figures 26 – 30. OBS-5 appears to have identical horizontal components, and thus no orientation can be determined. As this algorithm was initially developed for seismological applications, the code assumes that the direct incident P-wave comes from the sub-surface and has an upward motion. However, in the case of a marine OBS instrument, the direct P-wave through the water column creates a down-ward motion onto the geophone and the algorithm then creates an output that is rotated by 180 degrees. Therefore, the resulting histogram distributions can include two solutions (offset by 180 degrees) created by the arrivals through the water column and by the refracted/reflected arrivals from the subsurface. The sign convention in the algorithm is such that negative azimuth values correspond to a counter-clockwise rotation of the OBS to align the N-axis (equivalently channel 3) to true North. All results are listed in Table 4.

6 Single Channel Seismic data and comparison to OBS-data

The active source seismic refraction experiment consisted of two surveys. However, the first survey (Figure 31) was not recorded on the 14 regional OBS stations as battery life did not last long enough to record the airgun shots, and only single-channel seismic data were recorded. A second deployment of six OBS was made, and a second shorter refraction experiment was conducted using the same source and streamer (Figure 3).

A central line was shot in an SW-NE direction across stations OBS-6, OBS-4, OBS-2, and OBS-1 (Figure 32). Around station OBS-1, a short SE-NW oriented segment was acquired (Figure 33). The SW-NE oriented line across station OBS-5 is parallel to the main centre line (Figure 34). A main SE-NW oriented line crosses stations ONS-5, OBS-4, and OBS-3 (Figure 35), followed by a SW-NE oriented line across OBS-3 (Figure 36). The final segment of the survey was a line in NW-SE direction across OBS-6 (Figure 37).

The single channel data is of general sufficient quality to allow for basic interpretations of sediment deformation structures, despite the long shot distance interval of 75m (30 seconds at a speed of 4 knots). The data also are required for a ray-tracing based velocity inversion of the OBS reflection and refraction data as the single-channel data constrain the lateral extent of horizons. A first test in comparing the single-channel seismic data to the wide-angle data on OBS-6 was performed using the SW-NE oriented single channel line and the corresponding eastern and western half of the wide-angle data of the OBS-6 (Figure 38). Within the upper 1 second of travel time, most of the reflections seen on the single-channel data can be matched to arrivals on the OBS data, which are overall of lower frequency content than the streamer data.

7 Initial Refraction Velocity Analysis

After correction of the cumulative time delay, new digital SEGY-formatted data were generated. Using these data, refracted arrivals can be identified the easiest by applying linear move-out, or reducing the seismogram with a constant velocity, as the corresponding refracted arrivals from layers with that velocity appear flattened in the seismogram . We have tested several reducing velocities ranging from 3.5km/s to 6.0 km/s on OBS stations OBS-2, -3, -4, -5 and OBS-6 (Figures 39 – 44).

On station OBS-2, refracted arrivals with velocities of 4.0 and 5.0 km/s are identified on the SW arm of the coverage across the OBS, whereas, the NE portion of the record shows arrivals corresponding to much lower velocities (Figure 39).

OBS-3 is located on the northern end of the central line crossing the Queen Charlotte Terrace. Data from this crossing reveal velocities of 5.0 – 6.0 km/s (Figure 40a), where data from

the transect crossing west towards the abyssal plain show refracted arrivals from within the sedimentary package with velocities of a maximum of 3.5 km/s (Figure 40b).

OBS-4 in the centre of the Queen Charlotte Terrace was crossed twice (in the SW-NE and SE-NW transects) and we show an example from the SE-NW transect with reducing velocities of 4.0 km/s and 5.0 km/s (Figure 41), clearly indicating arrivals at these high velocities underneath the Terrace.

Station OBS-5 was also crossed twice: in a NE-SW transect (Figure 42a, b) and a SE-NW transect (Figure 43a). Arrivals at these velocities occur on each profile, as well as strong refractions at much lower velocity of ~2.5 km/s (Figure 43b).

Three examples of data from station OBS-6 are included (Figure 44) for the station crossing at the beginning of second survey (orientation from SW to NE). Using reducing velocities of (a) 4 km/s, (b) 5 km/s, and (c) 6 km/s it can be seen that refractions from layers with these high velocities have been imaged. Especially the 6.0 km/s arrival is an indicator for crustal material that was reached with the refraction experiment.

8 Long-range refraction data recorded on land stations

Several land stations are within ~50 km of the marine survey lines. The shot tables were used to extract seismic traces from the continuous land recordings in the same manner as the OBS stations to create shot record-type data. The land station data carry seismic information up to 50 Hz, which is lower than what is recorded on the OBS stations (100 Hz and higher). However, this is not detrimental, as the far-range refractions or direct arrivals will have attenuated significantly.

Digital SEGY-data have been created from these land-stations:

- BNB (Barry Inlet)
- HG1B (Mitchell Dam)
- HG3B (Hotspring Cove)
- HG4B (Jedway)
- TSUB (Tasu)
- TKWB (Talunkwan)

- STJA (Cape St. James)

One example of the data on the BNB station from the 2nd survey is shown in Figure 45. Additional processing to enhance the lateral coherency of the arrivals may be possible but require careful amplitude- and frequency-balancing as the data are dominated by noise from the two storm days during the survey as well as low-frequency and high-amplitude earthquake records from the aftershocks.

Acknowledgements

The work conducted as part of the Haida Gwaii Earthquake Response would not have been possible without the support by many individuals. The authors would like to express their special thanks to the Haida Nation for permission to conduct the survey off Gwaii Hanaas and George Wesley who joined the second expedition in January 2013, during which the active source seismic refraction experiment was conducted. Additional thanks goes to the Coast Guard Captains and crew of the two cruises onboard the CCGS John P. Tully, as well as staff from the Canadian Coast Guard Regional Operation Centre in Victoria for their support in scheduling a vessel to conduct the research outside of the usual science patrols. Critical to the success of the work were the two marine mammal observers Rhonda Reidy and Jacklyn Barrs who ensured that the survey was compliant to the DFO seismic operation permit. We also want to thank those members of the GSC who were instrumental in securing the substantial funding required for the offshore component of the earthquake response, including Tom James, Adrienne Jones, Carmel Lowe, and our Director General Daniel Lebel.

9 References

Cassidy, J., James, T., Hyndman, R., Riedel, M., Rogers, G., Schmidt, M., Wang, K., Mulder, T., 2012. The M 7.7 Haida Gwaii Earthquake of October 27, 2012, Simon Fraser University Newsletter December 2012.

Dash, R.K., 2007. Crustal Structure and Marine Gas Hydrate Studies near Vancouver Island using Seismic Tomography, PhD Thesis with the University of Victoria, BC, Canada.

Leonard, L.J. and J.M. Bednarski, 2014. Field survey following the 27 October 2012 Haida Gwaii tsunami. Pure and Applied Geophysics, doi: 10.1007/s00024-014-0792-0.

Riedel, M., Côté, M., Neelands, P. 2014a. Cruise Report PGC2013001PGC, The Mw 7.7 Haida Gwaii Earthquake Ocean Bottom Seismometer Experiment, Instrument recovery and active-source seismic refraction experiment, CCG Vessel John P. Tully, 7-14 January, 2013, Geological Survey of Canada Open File Report 7555.

Riedel, M., Ulmi, M., Conway, K., Standen, G., Rosenberger, A., Hong, J.K., Jin, Y.K. Kim, H.S., Dallimore, S.R., 2014b. Ocean Bottom Seismometer Experiment on the Beaufort shelf and slope region conducted during Expedition ARA04C on the IBRV Araon, Geological Survey of Canada Open File Report 7621.

Rosenberger, A. 2010. Realtime Ground-Motion Analysis: Distinguishing P and S Arrivals in a Noisy Environment, Bull. Seism. Soc. Am., 100, 1252-1262.

Schlesinger, A., 2012. A Study of gas hydrates with ocean-bottom-seismometer data on the East Coast of Canada, PhD Thesis with the University of Victoria, BC, Canada.

Zykov, M., 2006. 3-D travel time tomography of the gas hydrate area offshore Vancouver Island based on OBS data. PhD Thesis with the University of Victoria, BC, Canada.

OBS Station	Drift calibration		Total drift (sec)
	Prior to drop	After drop	
D2-1; Dal-C	Set: Jan 11, 17:28	Calibration: Jan 13, 18:47	0.009580
	Behind by 0.000035 sec	Ahead by 0.000923 sec	
D2-2; NRCan-H	Set: Jan 11, 19:35	Calibration: Jan 13, 17:35	0.004944
	Behind by 0.000007 sec	Ahead by 0.004937 sec	
D2-3; Dal-B	Set: Jan 11, 20:57	Calibration: Jan 13, 15:56	0.003431
	Behind by 0.000030 sec	Ahead by 0.003401 sec	
D2-4; Dal-A	Set: Jan 11, 22:48	Calibration: Jan 13, 17:00	0.000721
	Behind by 0.000011 sec	Ahead by 0.000732 sec	
D2-5; NRCan-E	Set: Jan 12, 00:43	Calibration: Jan 13, 14:27	0.000383
	Behind by 0.00007 sec	Behind by 0.000376 sec	
D2-6; NRCan-D	Set: Jan 12, 02:30	Calibration: Jan 13, 12:50	0.007647
	Behind by 0.000052 sec	Behind by 0.007699 sec	

Table 1. OBS instrument clock drift.

Inversion Number	Parameters	X (m)	Y (m)	Z (m)	dX (m)	dY (m)	dZ (m)	dL (m)	Absolute misfit (ms)	Biggest misfit (ms)
1	sSSP, x, lin, Vc, gun	271836	5809987	2956.8	-171	-151	47.8	228.1	1.6507	5.5916
2	sSSP, x, lin, Vc	271836	5809987	2957	-171	-151	48	228.1	1.6635	5.5597
3	sSSP, x, no lin, Vc, gun	271851	5809984	2899	-156	-154	-10	219.2	5.8395	16.3879
4	sSSP, x, no lin, Vc	271851	5809984	2901	-156	-154	-8	219.2	5.838	16.1976
5	sSSP, x, no lin	271837	5809958	2875	-170	-180	-34	247.6	8.3455	23.4969
6	sSSP, x, lin	271835	5809986	2978.4	-172	-152	69.4	229.5	2.4955	7.7363
7	cSSP, x, lin	271837	5809988	2958.2	-170	-150	49.2	226.7	1.3033	4.7048
8	cSSP, x, no lin	271845	5809974	2899.5	-162	-164	-9.5	230.5	6.9835	19.1687
9	sSSP, all, lin	271819	5810002	2980.3	-188	-136	71.3	232.0	7.3147	24.875
10	sSSP, all, no lin	271850	5810033	2864.9	-157	-105	-44.1	188.9	7.696	33.2259
11	sSSP, all no lin, Vc	271818	5810008	2896.9	-189	-130	-12.1	229.4	7.8302	21.4262
12	sSSP, all, lin, Vc	271816	5810000	2941.8	-191	-138	32.8	235.6	7.2106	22.7995
13	cSSP all, lin	271814	5809999	2938.9	-193	-139	29.9	237.9	7.3346	21.6616
14	cSSP, all no lin	271827	5810016	2894.7	-180	-122	-14.3	217.5	8.0942	24.3535
15	sSSP, all, mlin, Vc, gun	271882	5810034	2898.2	-125	-104	-10.8	162.6	1.4367	17.3001
16	sSSP, x, mlin, Vc, gun	271919	5810055	2864.0	-88	-83	-45	120.9	1.093	6.4587

Table 2. Results of testing the various Zykov (2006) inversion parameters on OBS 6 for simple and complex sound speed profiles, gun delay, bias in sound speed, and with (or without) linear drift removal. The following abbreviations are used in the table: x = crossings only, all = all shots, lin = linear drift removal, no lin = no linear drift removal, mlin = multi-linear drift removal, Vc = sound speed bias, gun = delay in trigger for airgun, sSSP = simple sound speed profile, cSSP = complex sound speed profile.

	X	Y	Z	Absolute misfit (ms)	Largest individual misfit (ms)
OBS-1					
No linear	289638	5827977	1960.6	16.0846	35.8429
Linear	289633	5827980	1932.3	4.1538	18.3055
Multi-linear	*289690*	*5827915*	*1971.8*	*1.8735*	*8.8101*
OBS-2					
No linear	284549	5822896	1862.5	8.0367	19.9884
Linear	284560	5822900	1855.4	5.5064	17.6518
Multi-linear	*284594*	*5822864*	*1847.6*	*0.8877*	*15.5303*
OBS-3					
No linear	277268	5822691	2008.9	4.7812	17.2021
Linear	277269	5822690	2061.7	3.8734	13.2253
Multi-linear	*277389*	*5822748*	*2029.6*	*1.7717*	*10.0065*
OBS-4					
No linear	280875	5819013	2025.5	22.5720	43.1658
Linear	280878	5819008	2063.9	6.6360	22.9679
Multi-linear	*280924*	*5819021*	*2030.5*	*1.6530*	*8.7761*
OBS-5					
No linear, all	284455	5815204	1882.9	9.1435	27.9545
Linear, all	284460	5815212	1879.8	7.3304	21.8454
Multi-linear, all	284497	5815196	1880.0	1.0134	8.7172
No linear, cross.	284454	5815215	1880.0	11.1886	24.0796
Linear, cross.	284478	5815260	1880.0	4.5784	12.7916
Multi-linear, cross.	284545	5815207	1880.0	1.1636	5.4689
Average	*284521*	*5815201.5*	*1880.0*		
OBS-6					
No linear, all	271818	5810008	2896.9	7.8302	21.4262
Linear, all	271816	5810000	2941.8	7.2106	22.7995
Multi-linear, all	271882	5810034	2898.2	1.4367	17.3001
No linear, cross.	271851	5809984	2899	5.8395	16.3879
Linear, cross.	271836	5809987	2956.8	1.6507	5.5916
Multi-linear, cross	271919	5810055	2864.0	1.093	6.4587
Average	*271900.5*	*5810044.5*	*2881.1*		

Table 3. Final results of the OBS relocation analysis performed on all OBS. Included are results for the inversions shown in Figures 14 – 19.

OBS station	Azimuth (°)	Standard deviation around best estimate (°)
OBS-1	+82.7	13.5
OBS-2	-134.0	4.0
OBS-3	-141.0	8.0
OBS-4	-84.0	4.0
OBS-6	+55.0	4.0

Table 4. Results of the horizontal geophone orientation analysis using the Rosenberger (2010) algorithm.

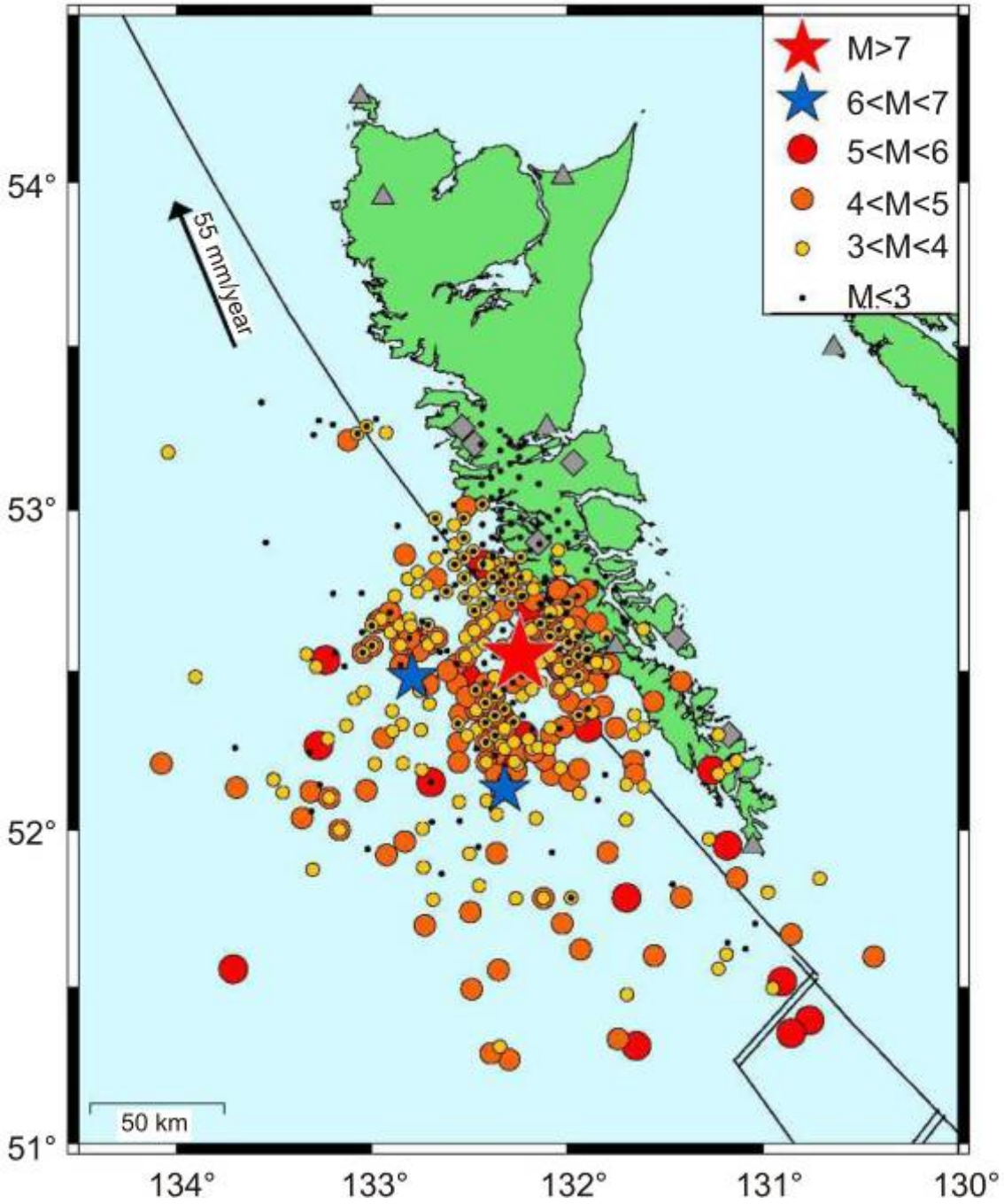

Figure 1. Map showing the preliminary locations of aftershocks with magnitude 3.0 and higher recorded over 30 days after the Mw 7.7 Haida Gwaii earthquake. The epicentre of the main event is shown as a red star and the two largest aftershocks of magnitude Mw 6.0 (or higher) are shown as blue stars (from Cassidy et al., 2012).

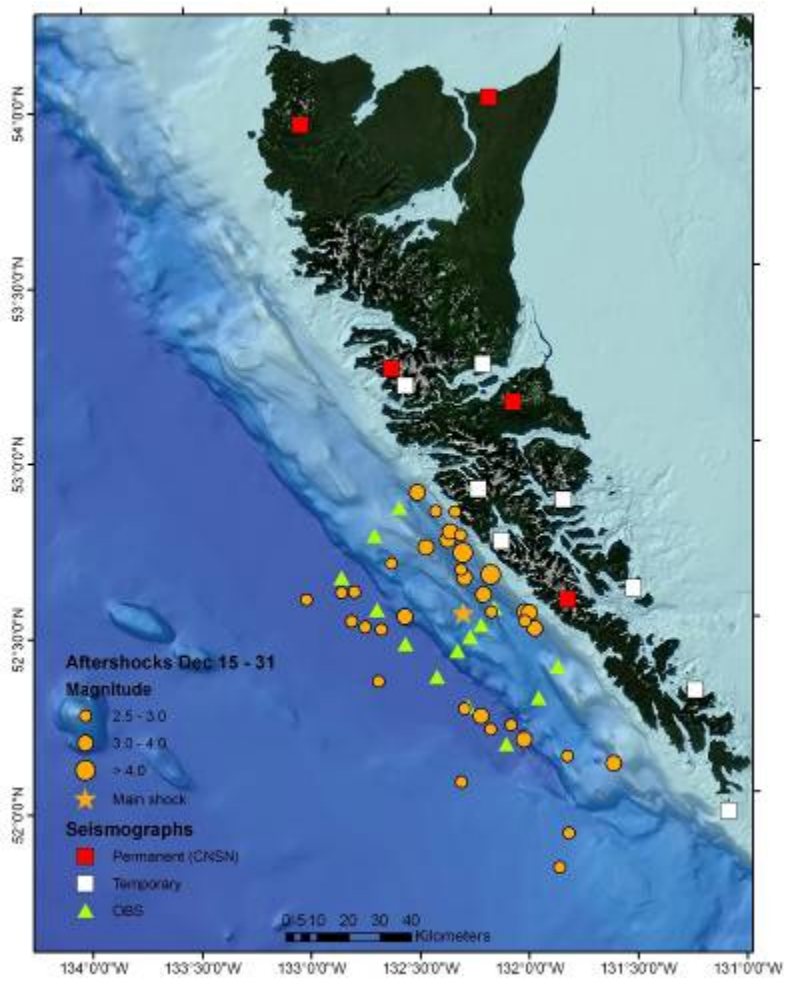

Figure 2. Map showing the OBS stations deployed as regional grid (green triangles) during cruise 2012005PGC and location of land seismometers. Earthquake locations (orange circles) recorded using the land stations only are plotted for the duration of the actual recording period of the 14 regional OBS (for magnitude scale, see legend).

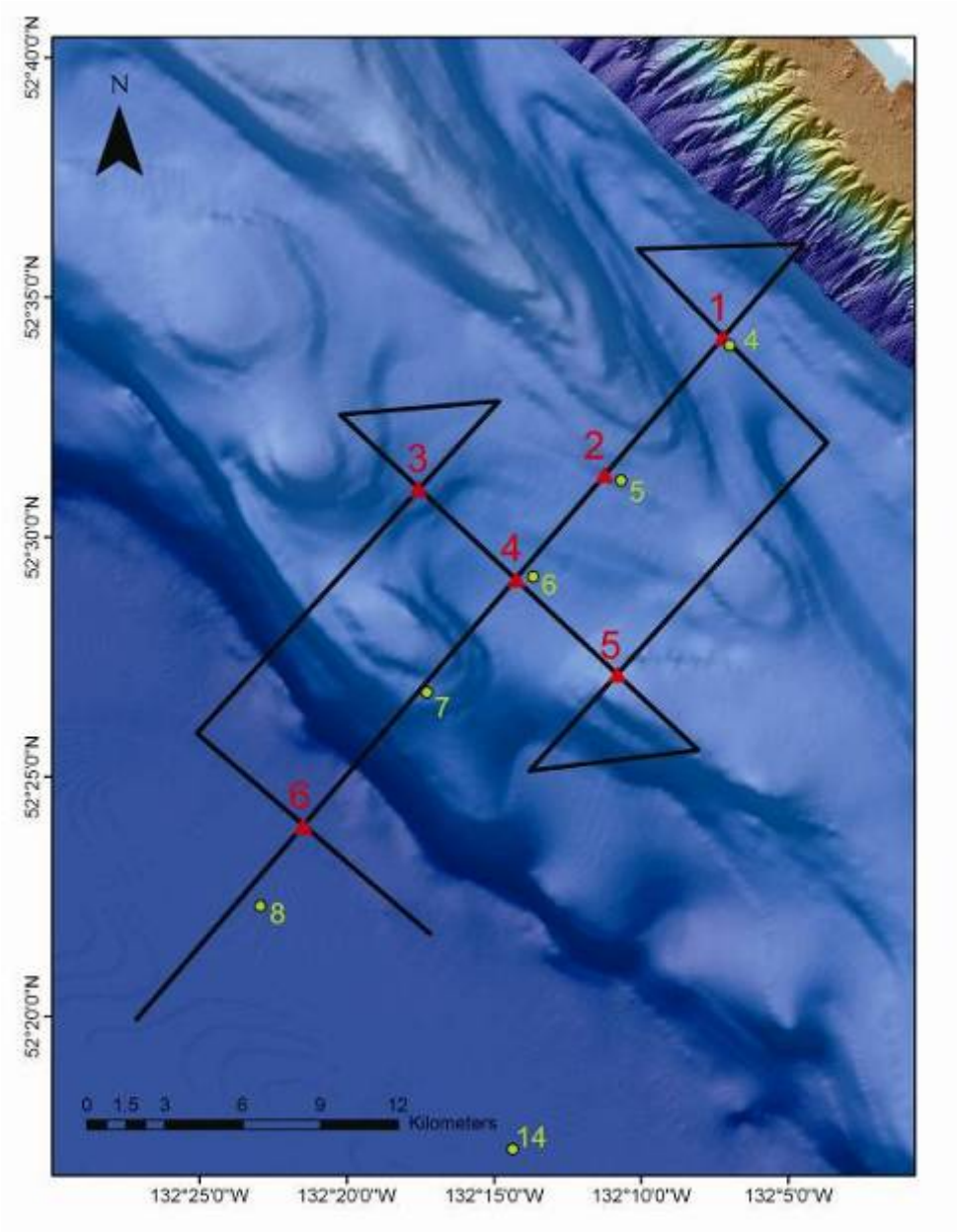

Figure 3. Map of seismic lines acquired during the second active-source seismic refraction survey. The OBS locations from the initial regional grid (green circles) and the 2nd refraction experiment (red triangles) are shown.

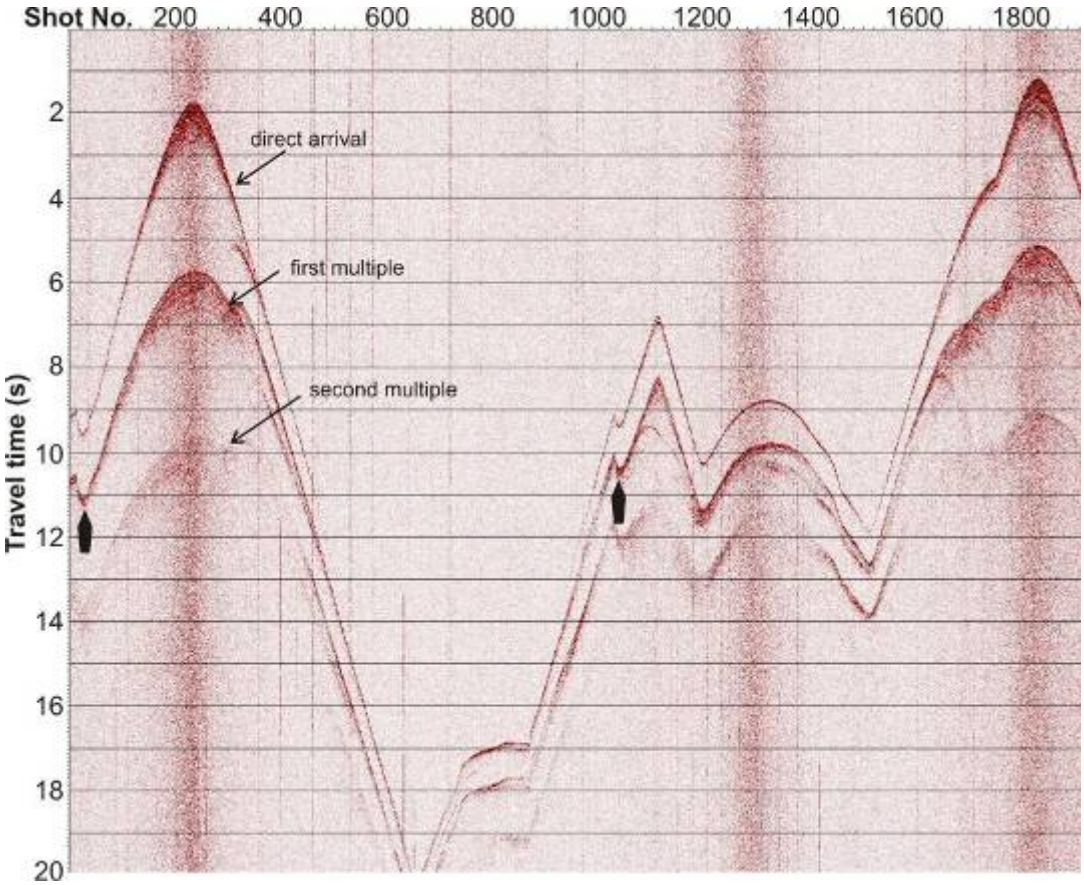

Figure 4. Complete shot-record of OBS-6 showing the direct arrivals (and multiple arrivals) on the hydrophone channel. Note the two incidences of "reversed" arrival times marked by black arrows (compare to Figure 5).

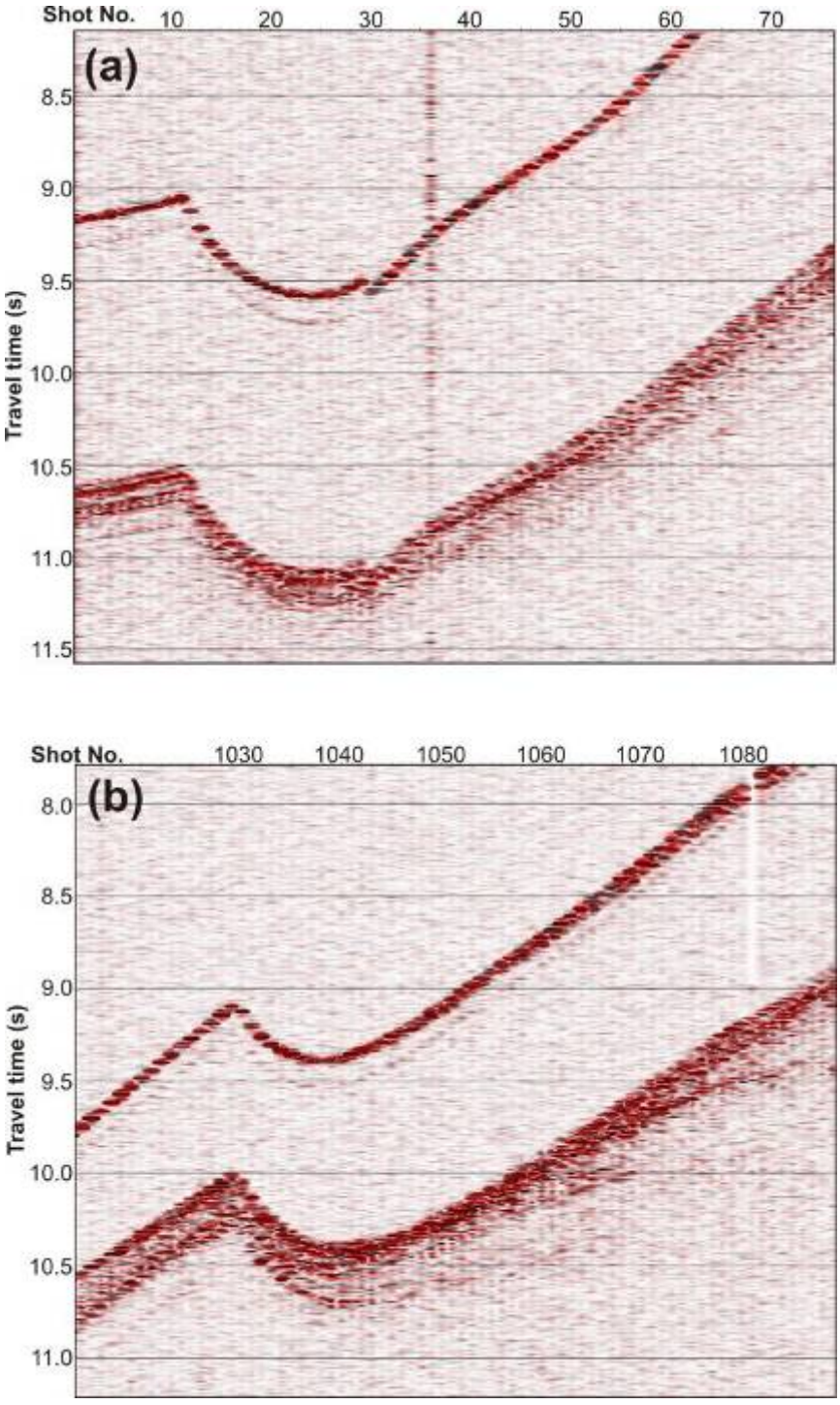

Figure 5. Close-up view on the two incidences of "reversed" direct arrival times on OBS-6: (a) starting at shot number 11 at the start of the survey, and (b) after shot 1029 in the middle of the survey.

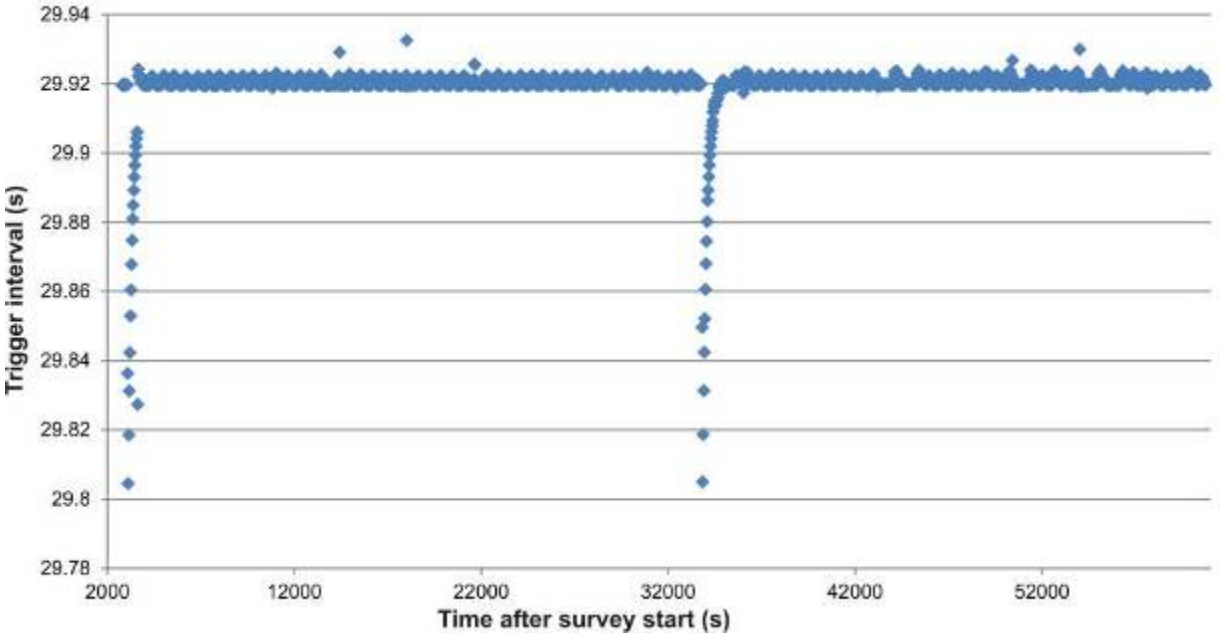

Figure 6. Shot-trigger interval as function of time after beginning of the survey (measured in seconds), showing almost regular intervals around 29.92 s, with two incidences of extreme deviations.

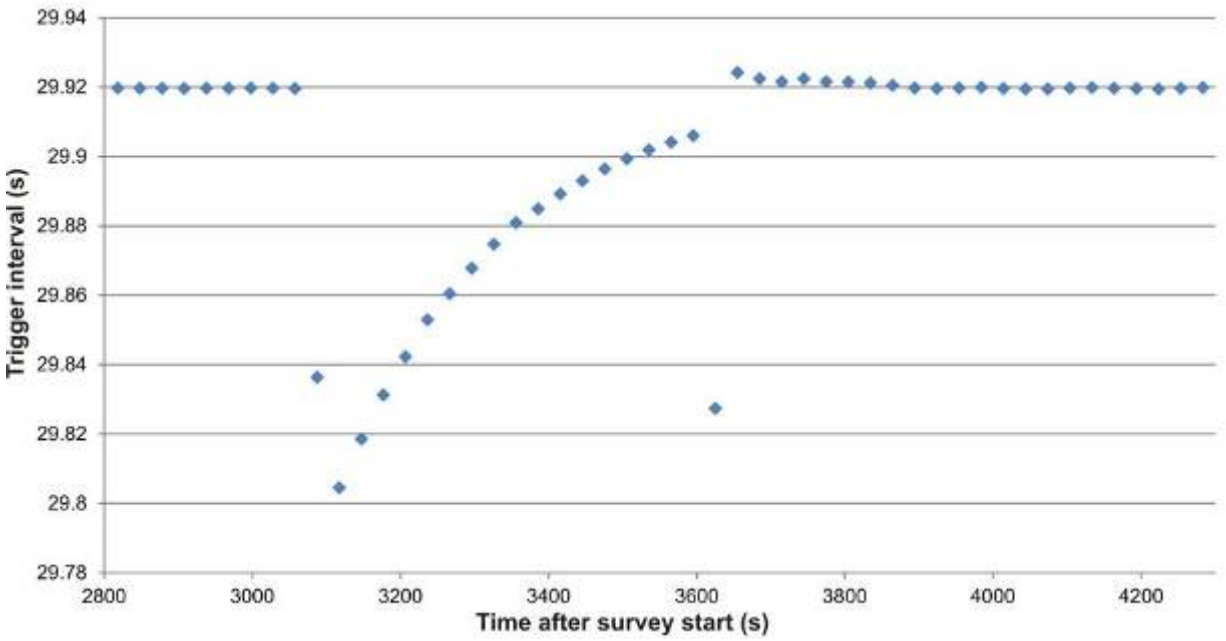

Figure 7a. Close-up view on the shot trigger interval during the first incident of deviation from the regular (intended) interval around 29.92 seconds.

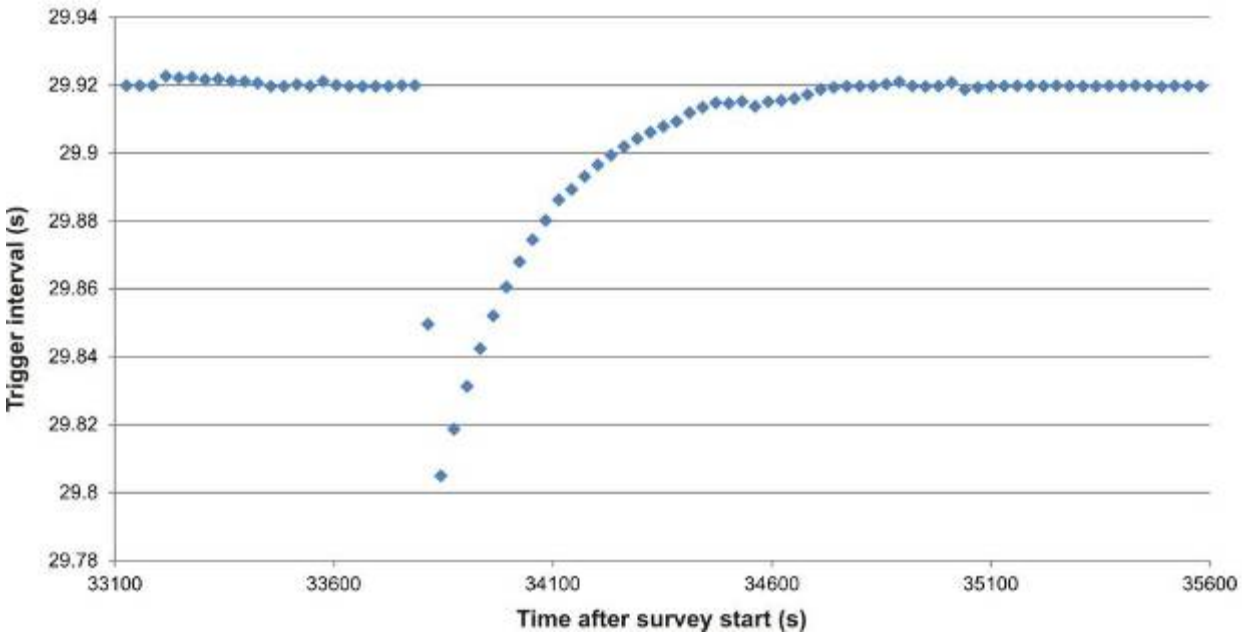

Figure 7b. Close-up view on the shot trigger interval during the first incident of deviation from the regular (intended) interval around 29.92 seconds.

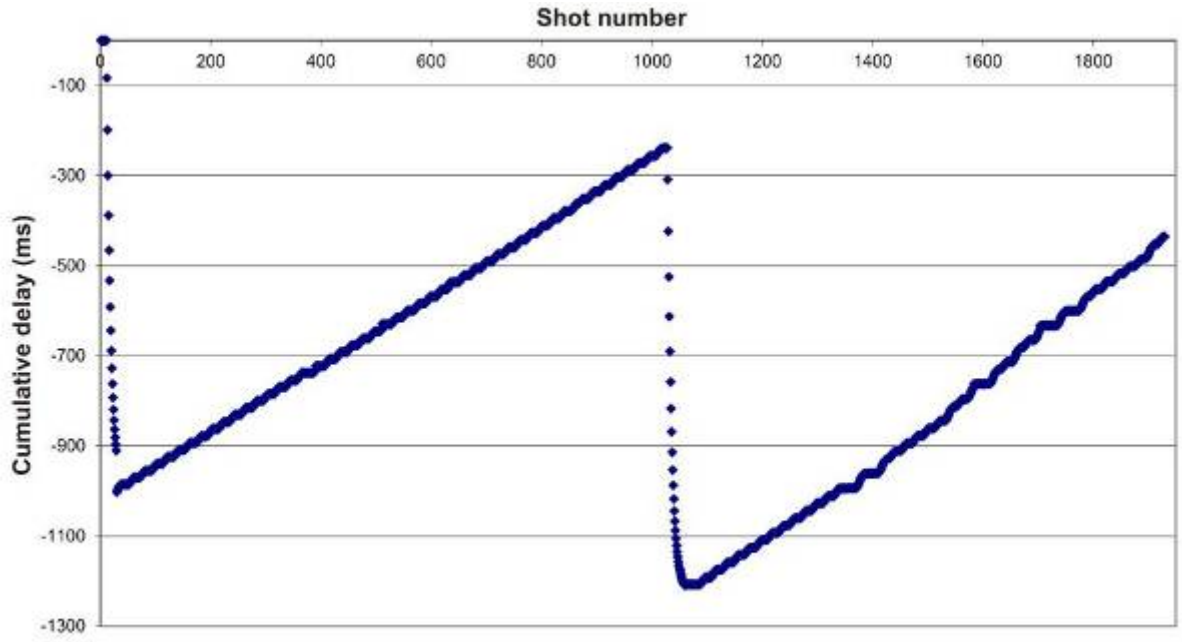

Figure 8. Cumulative delay in the shot-times to be applied to shot times prior to conversion to SEGY standard.

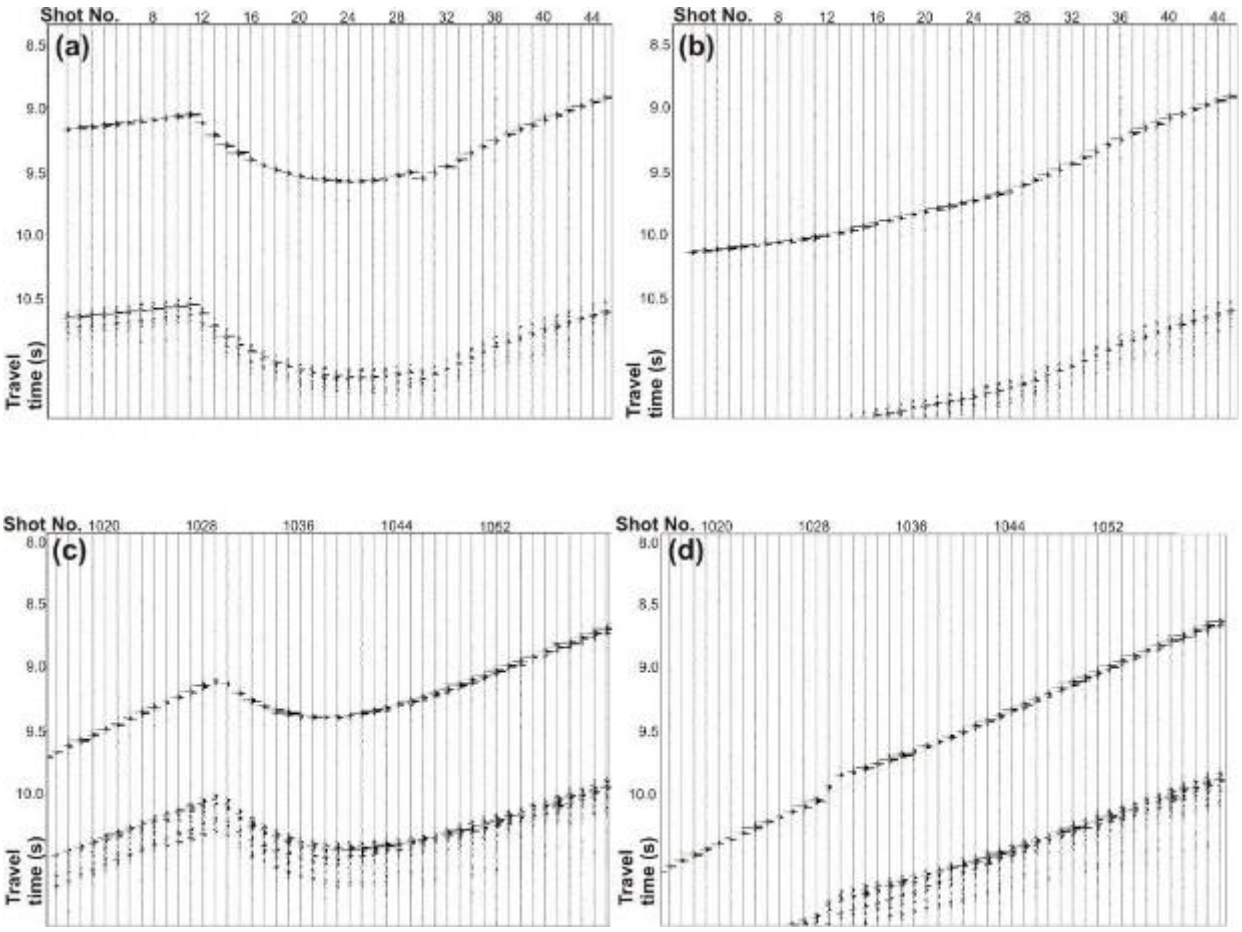

Figure 9. Close up view of shot record of OBS-6 at the incidents of shot arrival time "reversal" (see Figure 5): (a) after shot 11 before applying cumulative delay, (b) after shot 11 after applying cumulative delay, (c) after shot 1029 before applying cumulative delay, and (d) after shot 1029 after applying cumulative delay.

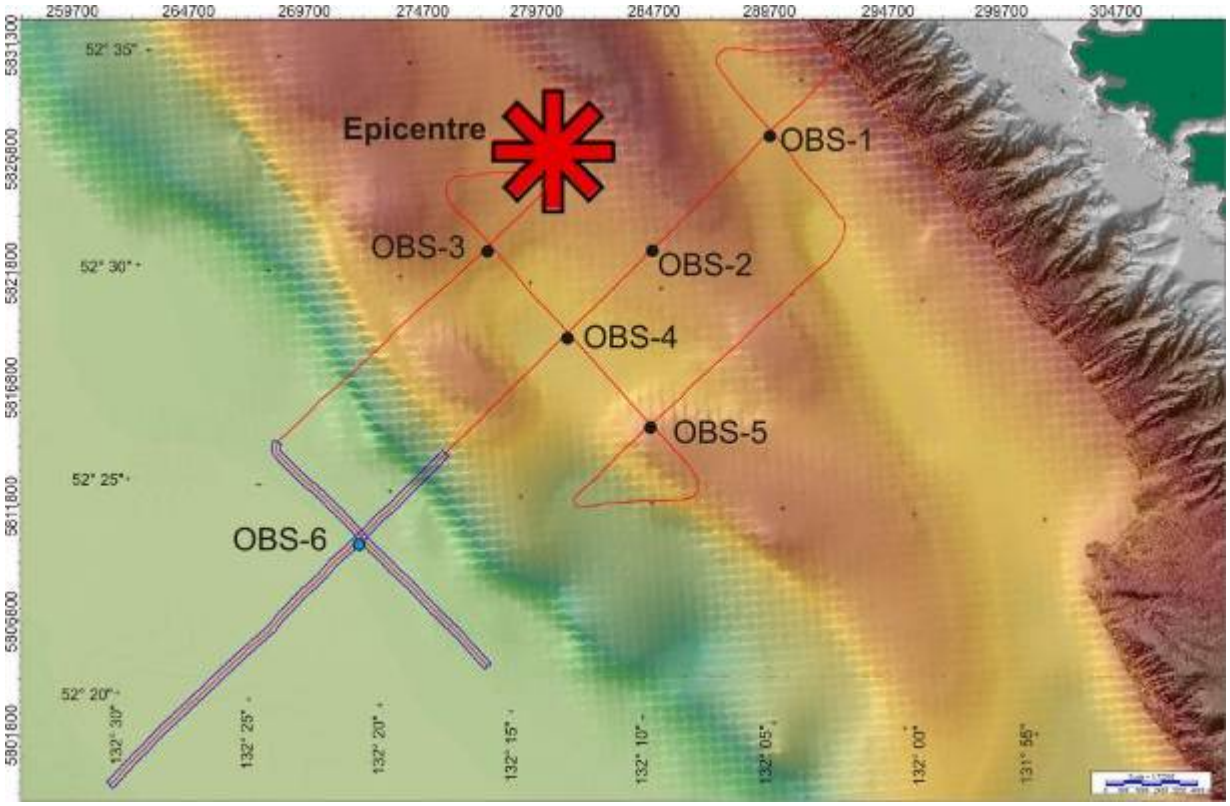

Figure 10a. Map showing distribution of shots around OBS-6 used for relocation analysis in case of the crossings only scenario. Red line is the entire survey, with the region from which direct arrivals were picked highlighted by the double blue lines.

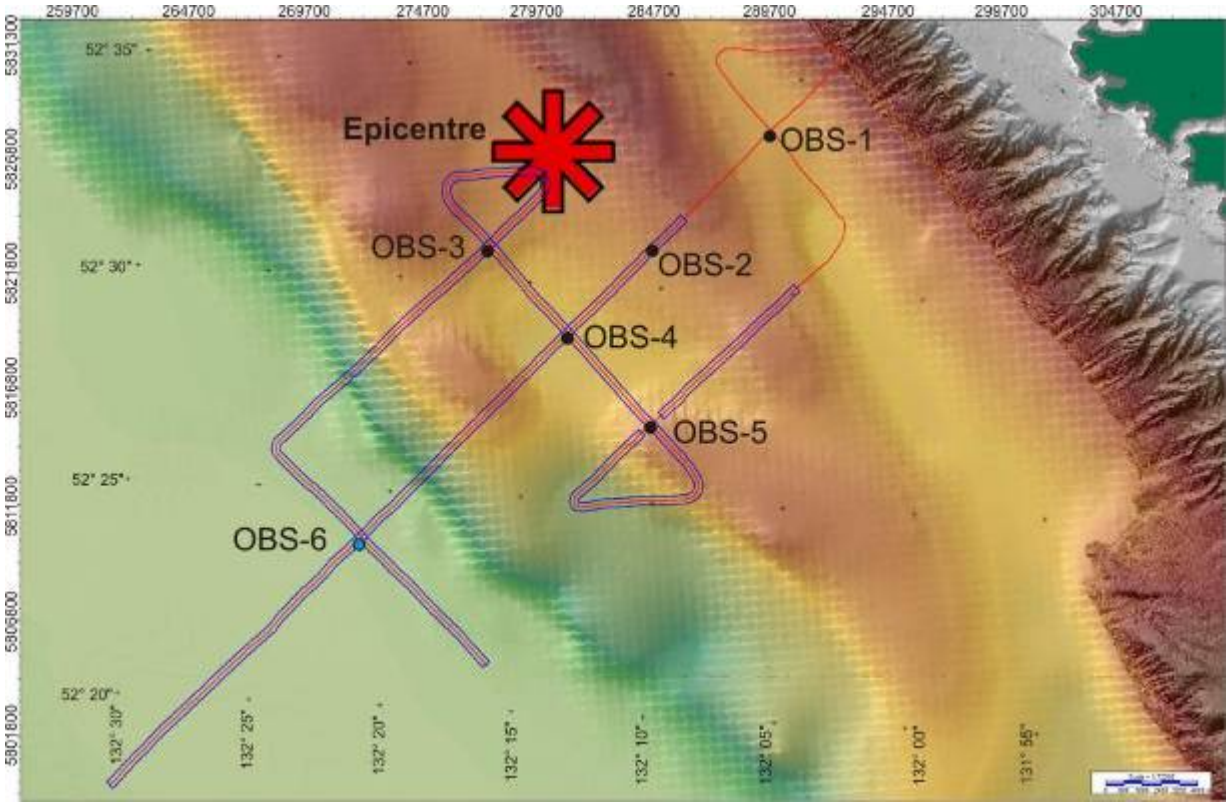

Figure 10b. Map showing distribution of shots around OBS-6 used for relocation analysis in case of the all shots scenario. Red line is the entire survey, with the region from which direct arrivals were picked highlighted by the double blue lines.

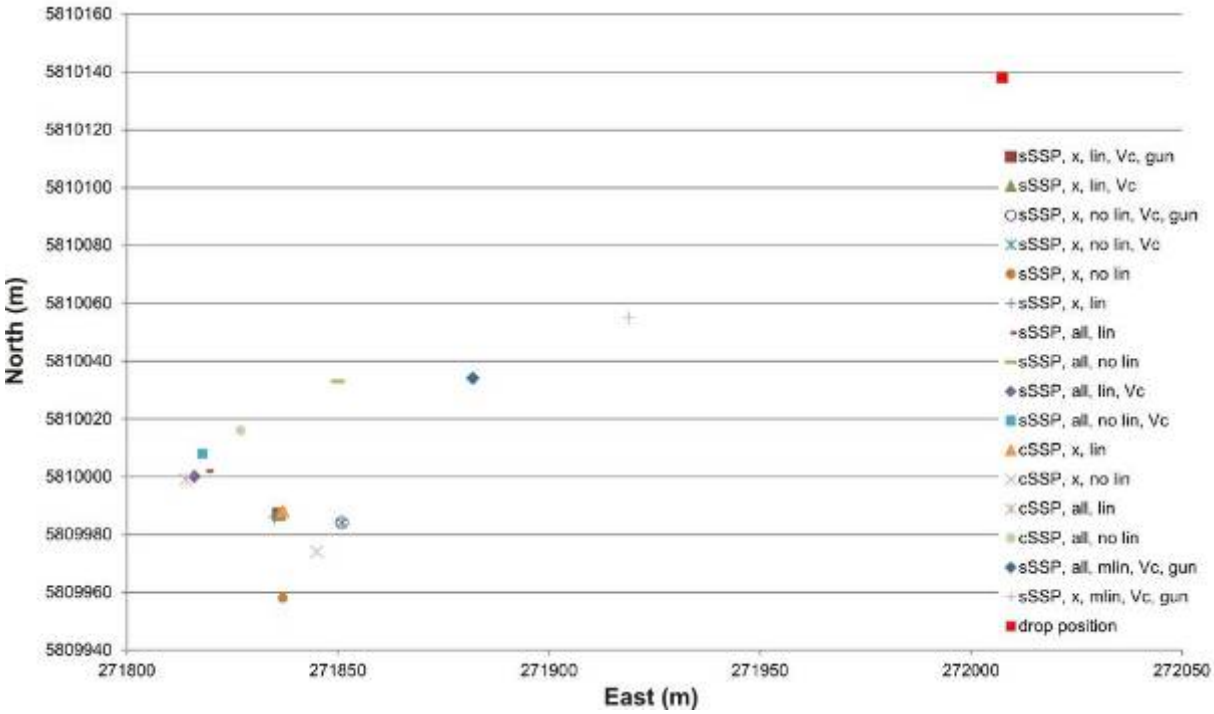

Figure 11. Map showing the location of the OBS-6 drop position (red box) and the re-located positions for all 16 inversion runs tested. Abbreviations used are the same as in Table 2: x = crossings only, all = all shots, lin = linear drift removal, no lin = no linear drift removal, mlin = multi-linear drift removal, Vc = sound speed bias, gun = delay in trigger for airgun, sSSP = simple sound speed profile, cSSP = complex sound speed profile.

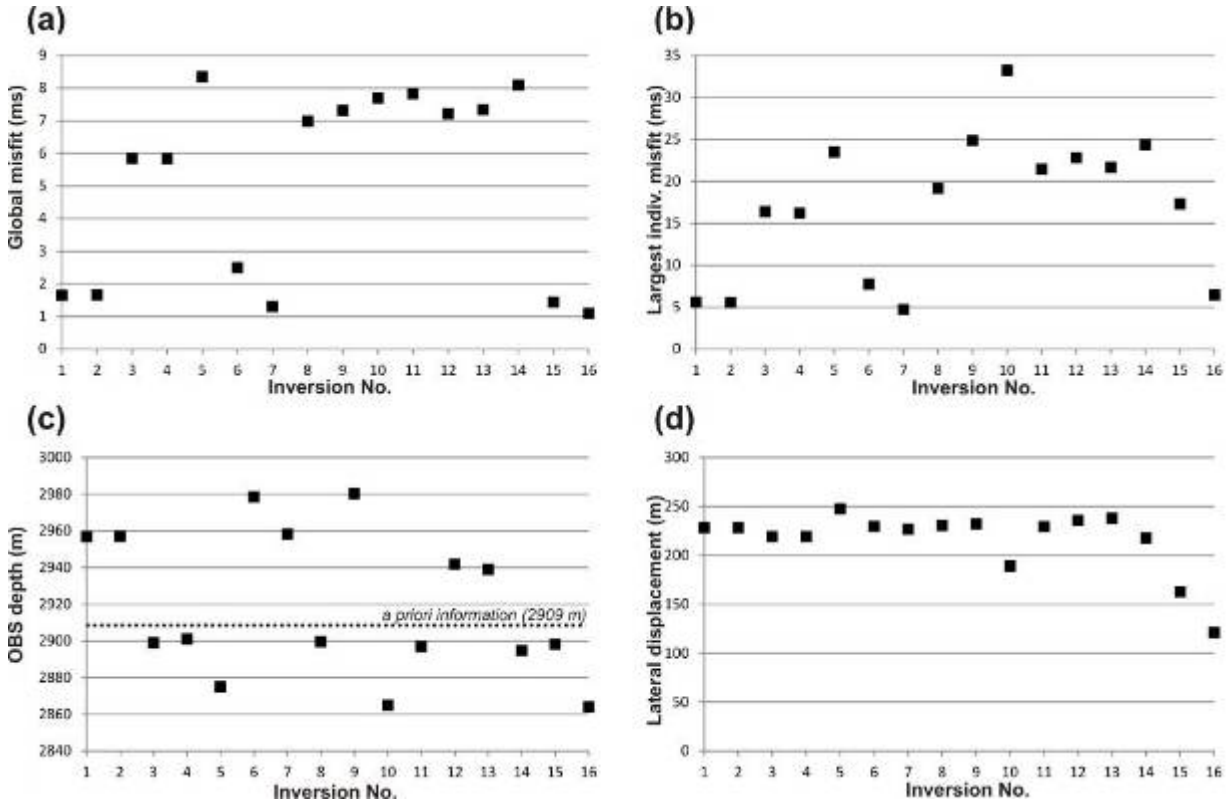

Figure 12. Statistical data for the 16 inversion tests performed for OBS-6. Horizontal axis is inversion number as listed in Table 2. Shown are: (a) global misfit (in ms), (b) largest individual misfit within picked shot period (in ms), (c) re-located depth of OBS station (at drop location, water depth was 2909 m), and (d) lateral shift in meter between drop position and re-located position (in m).

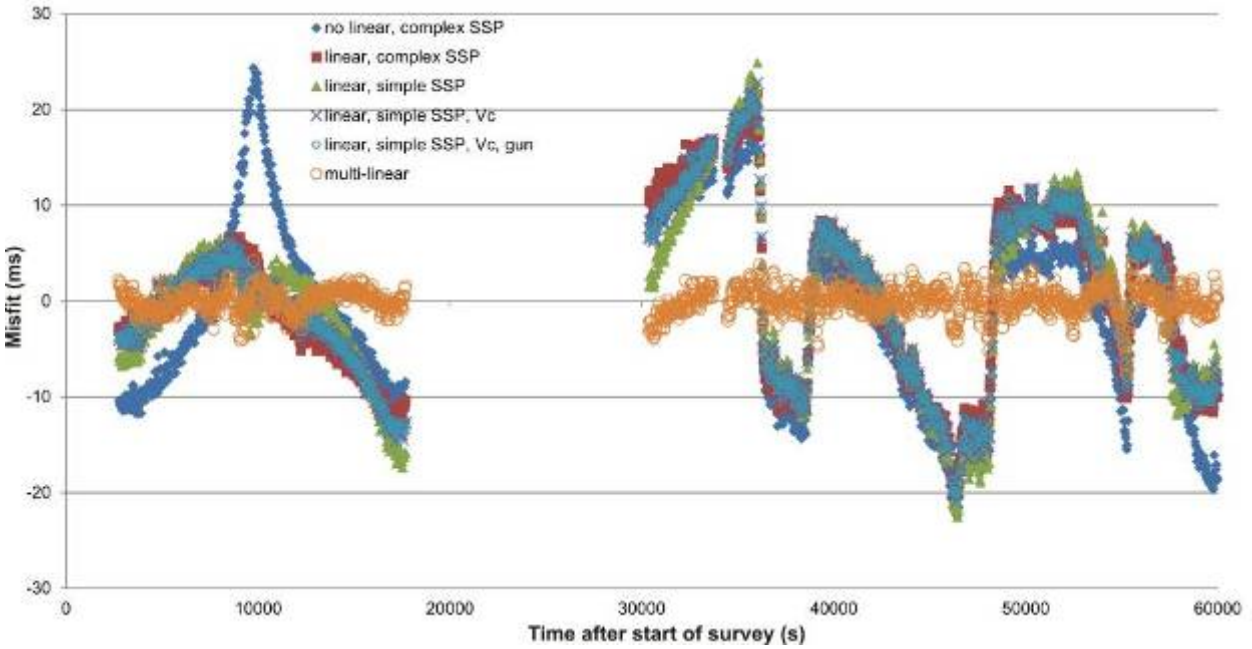

Figure 13. Plot of the misfit (in ms) between picked and predicted direct arrival times of OBS-6 (all shots) for different inversions performed (abbreviations as in Table 2). Note, the large misfits after the non-linear inversion using a complex sound speed profile (blue diamonds) and piece-wise linear segments with sudden vertical jumps. Removing a single linear drift (red squares) improves the overall misfit, but the piece-wise linear segments with sudden vertical jumps still remain in the data. Only a multi-linear drift-removal can correct for these jumps and produce an overall small and random misfit, representing now only the picking uncertainty.

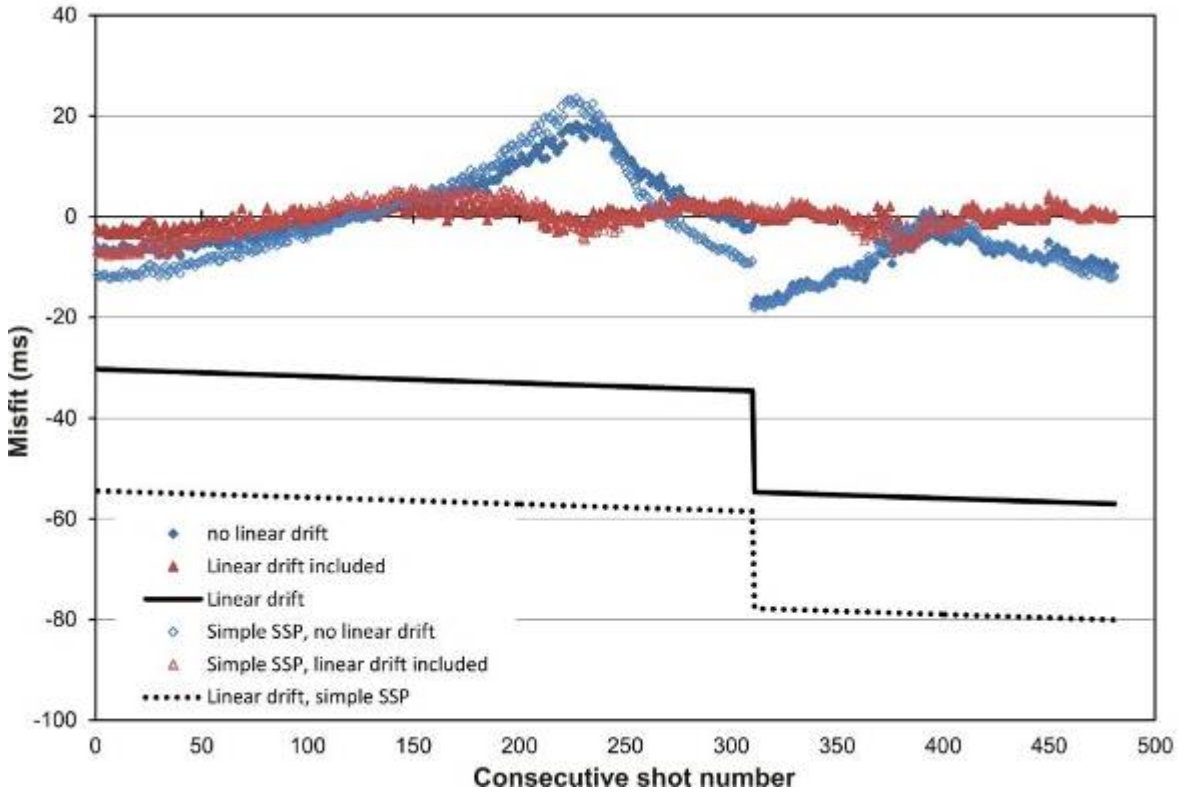

Figure 14. Using only direct crossing above OBS-6, the inversion performance was tested for linear- and no-linear drift removal for the two sound-speed profiles. On average (when summed over all traces), the misfit is insignificantly changed between the complex and simple sound speed profile. The largest impact is from including the linear drift. For comparison purposes, the linear-drift subtracted from the data is shown as black lines. Note, for simplicity, the shot time is not plotted (there is a ~12 hour difference between the two crossings of the OBS-6 station) and a consecutive shot-number is used instead.

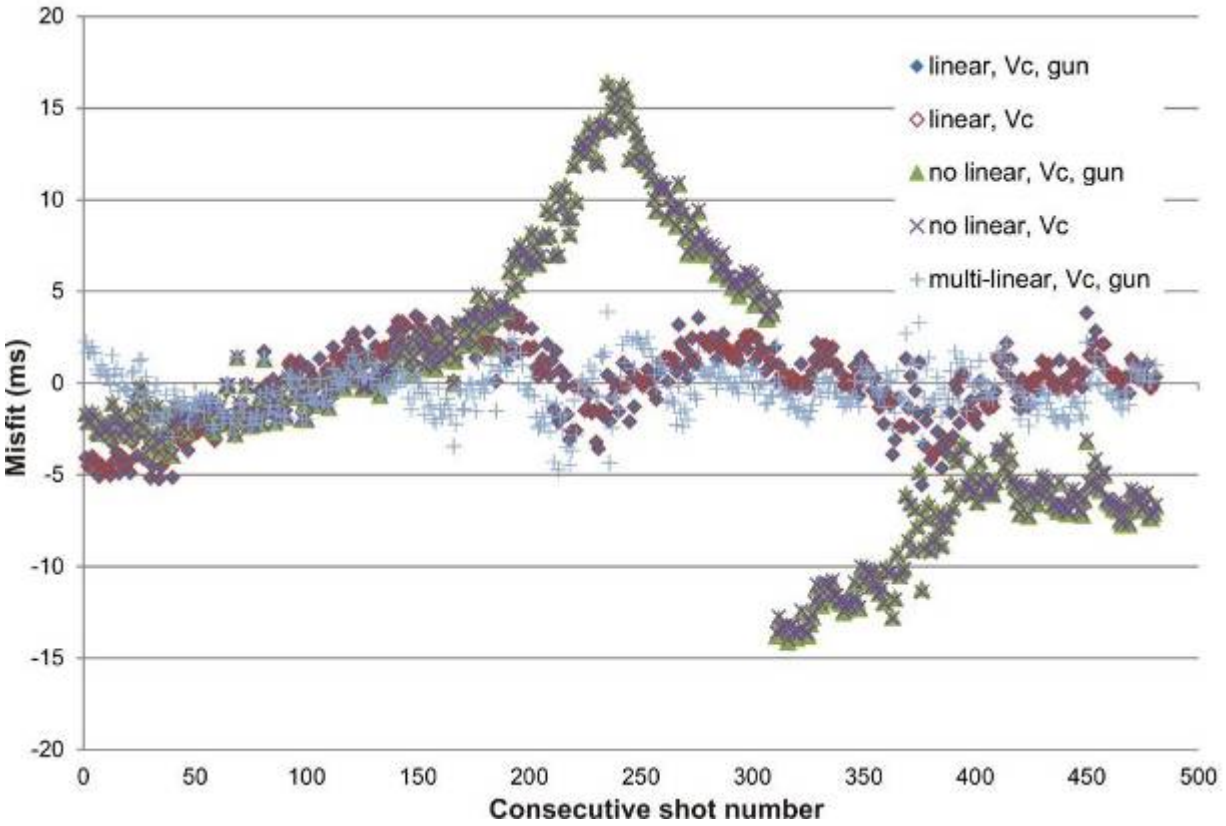

Figure 15. Using only direct crossing above OBS-6, the inversion performance was tested for linear- and no-linear drift removal using the simple sound-speed profile and introducing the sound-speed bias (Vc) as well as airgun trigger time delay offset (gun). On average (when summed over all traces), the misfit is insignificantly changed between solutions with or without the gun-delay included. The largest impact is from including the linear drift-removal and especially the multi-linear drift removal in 600-second intervals (blue crosses). Note, for simplicity, the shot time is not plotted (there is a ~12 hour difference between the two crossings of the OBS-6 station) and a consecutive shot-number is used instead.

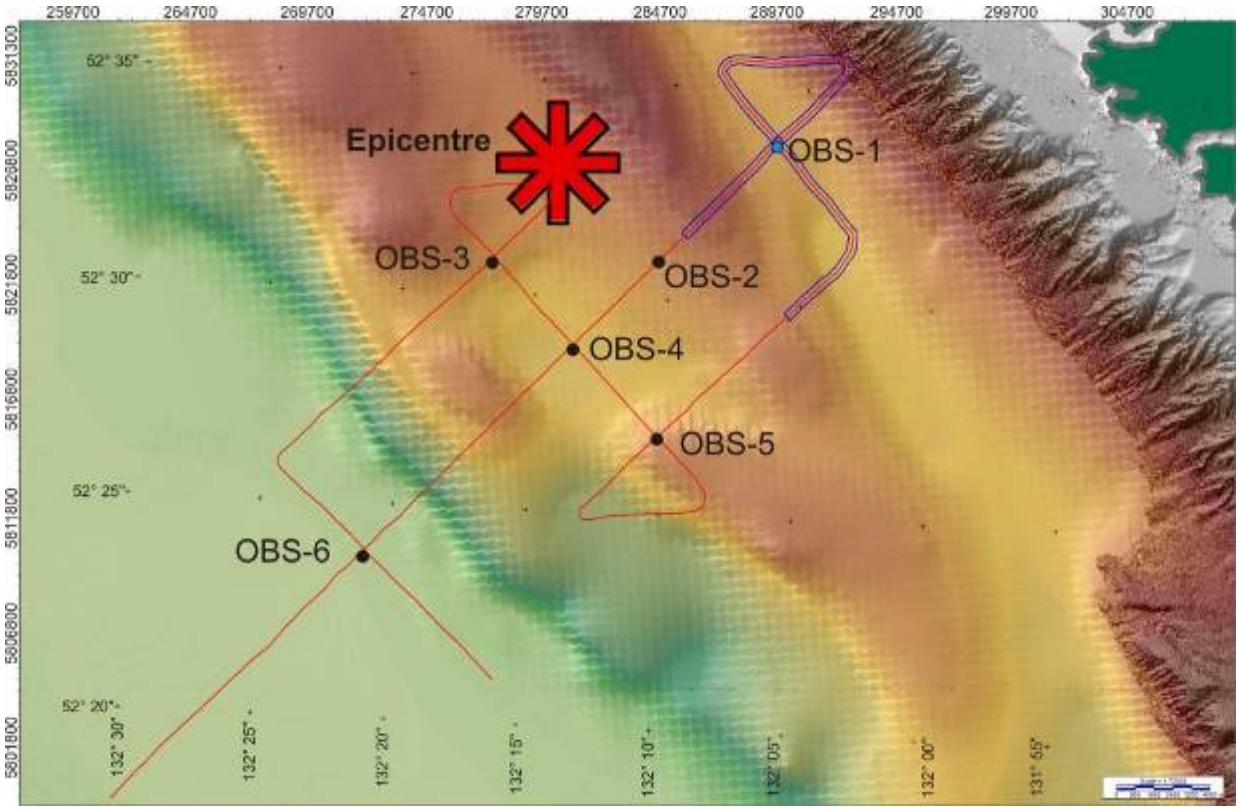

Figure 16. Map showing distribution of shots around OBS-1 used for relocation analysis. Red line is the entire survey, with the region from which direct arrivals were picked highlighted by the double blue lines. The estimated location of the epicentre is shown by the large red star.

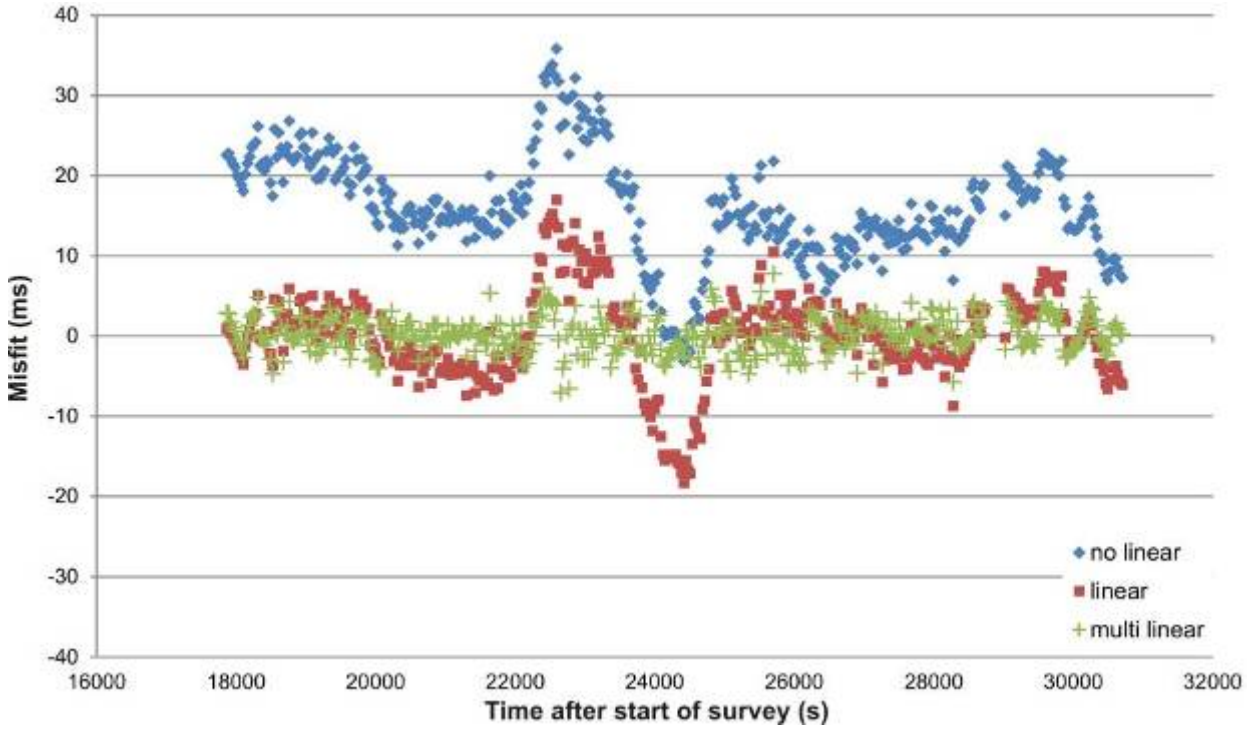

Figure 17. Final result of relocation analysis at station OBS-1. A total of 421 arrival times were picked. The multi-linear drift removal consisted of a total of 18 segments (parameters of the equation coefficients see Appendix).

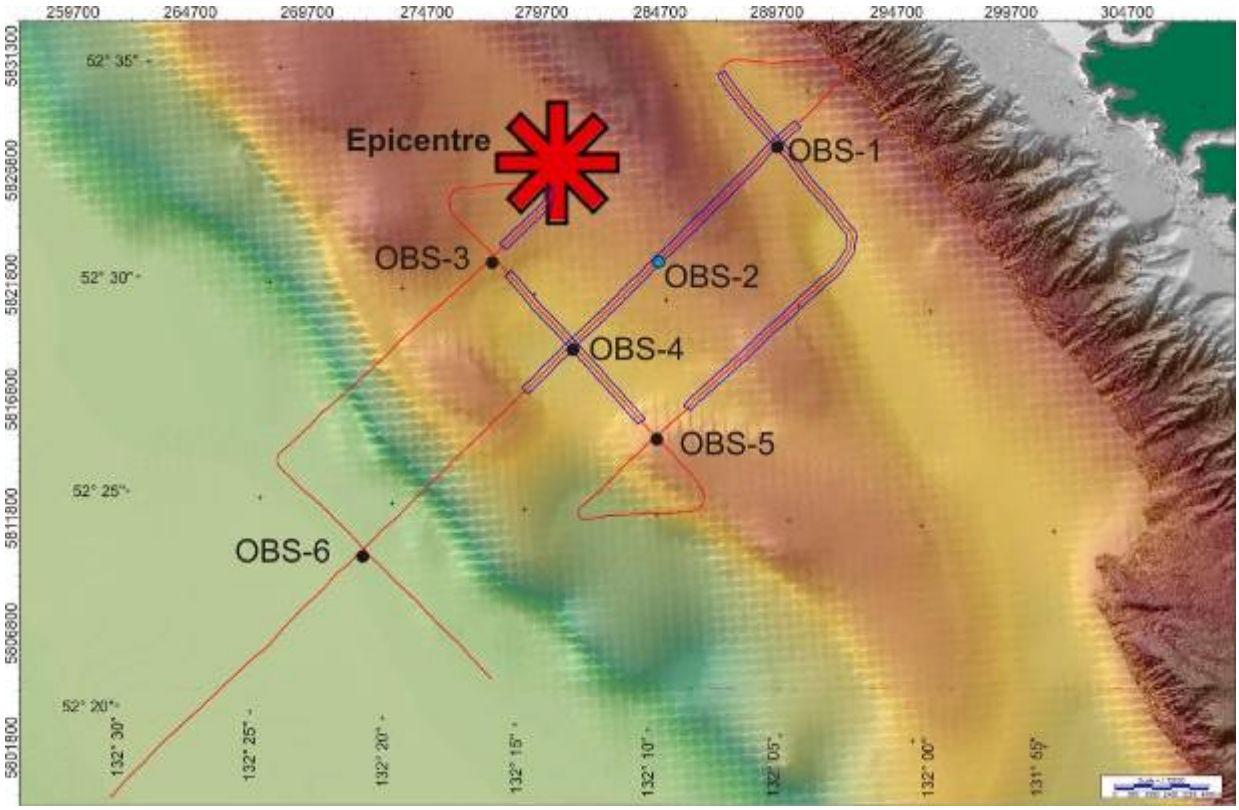

Figure 18. Map showing distribution of shots around OBS-2 used for relocation analysis. Red line is the entire survey, with the region from which direct arrivals were picked highlighted by the double blue lines. The estimated location of the epicentre is shown by the large red star.

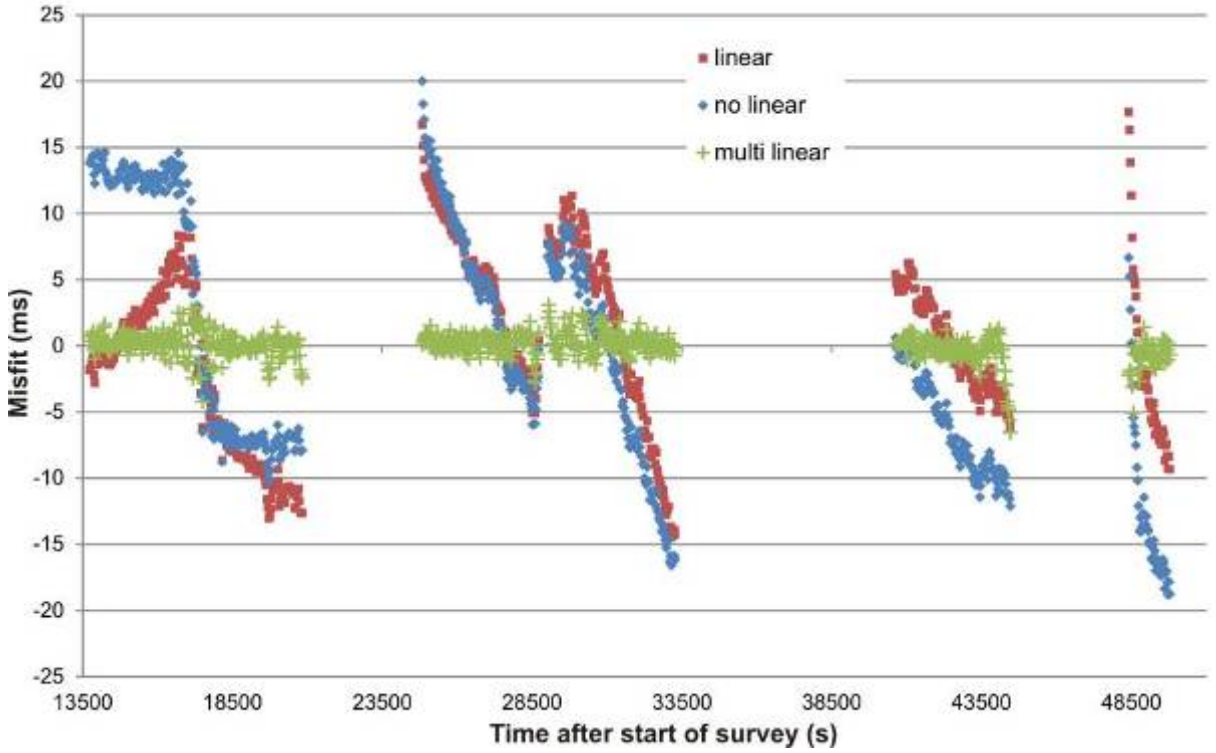

Figure 19. Final result of relocation analysis at station OBS-2. A total of 688 arrival times were picked. The multi-linear drift removal consisted of a total of 60 segments (parameters of the equation coefficients see Appendix).

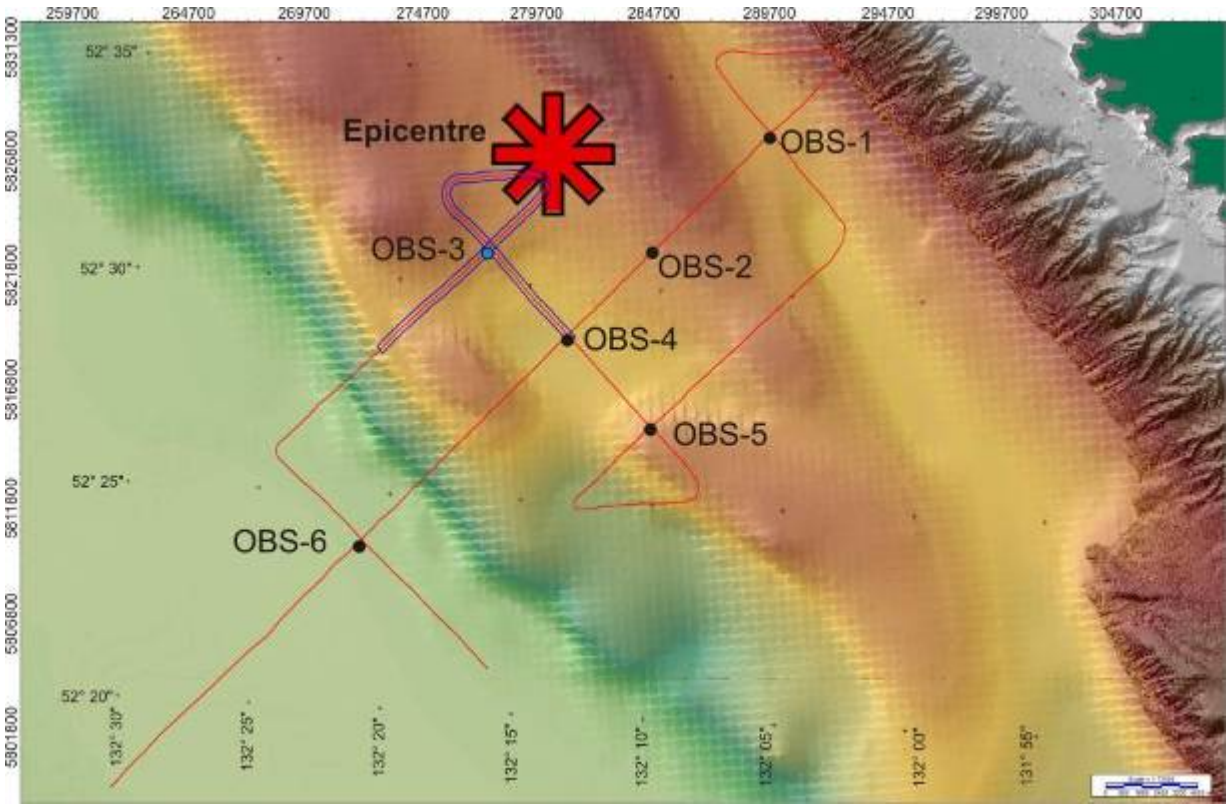

Figure 20. Map showing distribution of shots around OBS-3 used for relocation analysis. Red line is the entire survey, with the region from which direct arrivals were picked highlighted by the double blue lines. The estimated location of the epicentre is shown by the large red star.

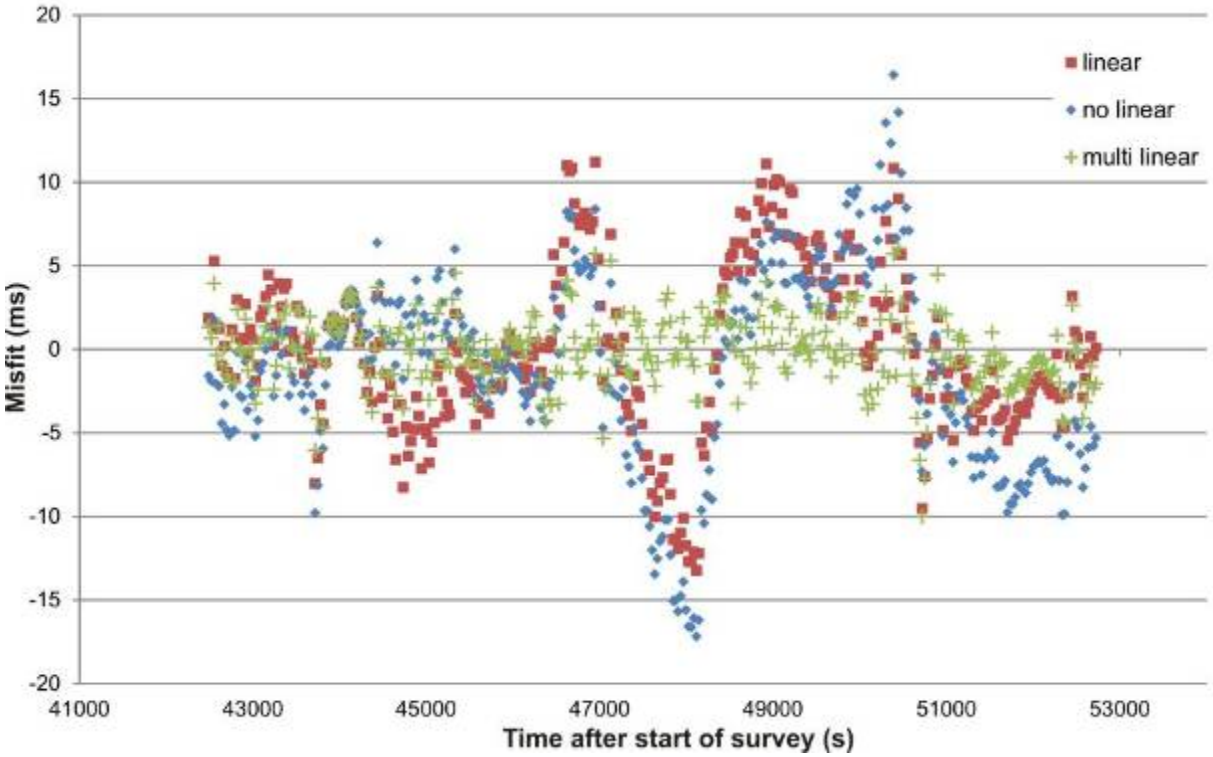

Figure 21. Final result of relocation analysis at station OBS-3. A total of 343 arrival times were picked. The multi-linear drift removal consisted of a total of 20 segments (parameters of the equation coefficients see Appendix).

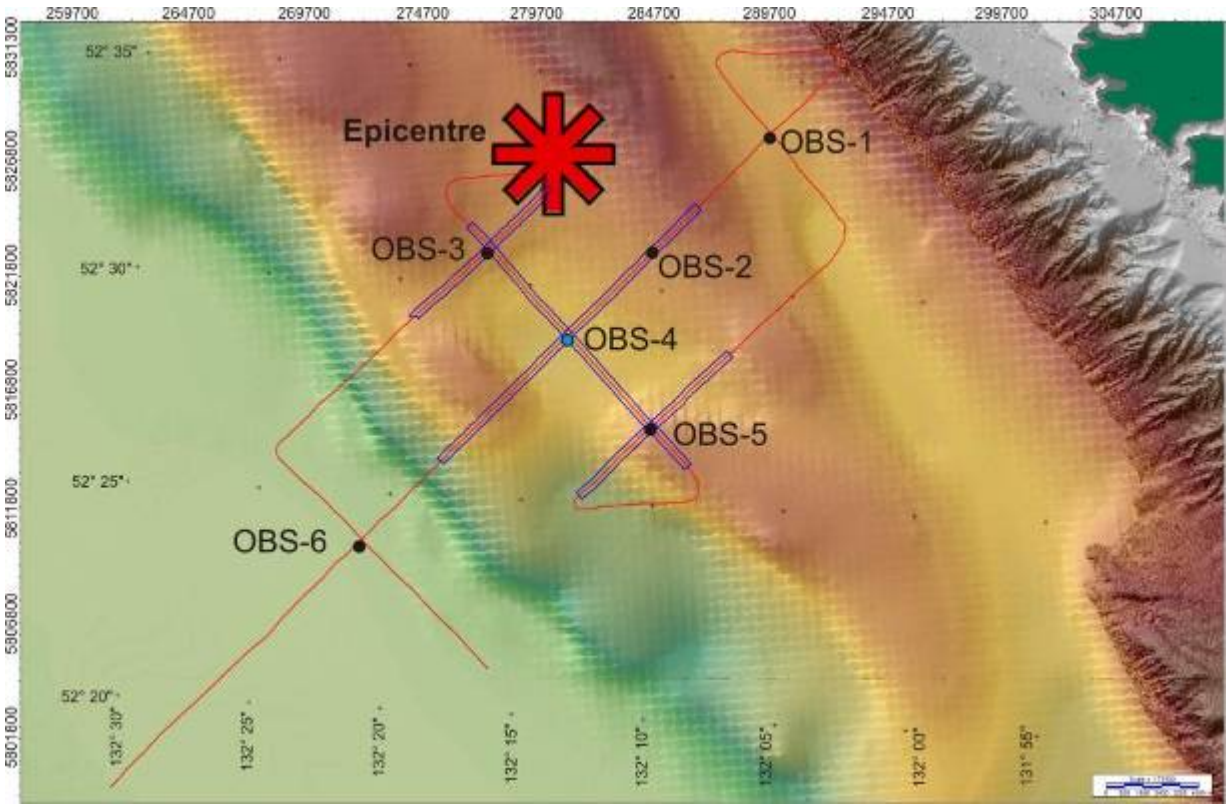

Figure 22. Map showing distribution of shots around OBS-4 used for relocation analysis. Red line is the entire survey, with the region from which direct arrivals were picked highlighted by the double blue lines. The estimated location of the epicentre is shown by the large red star.

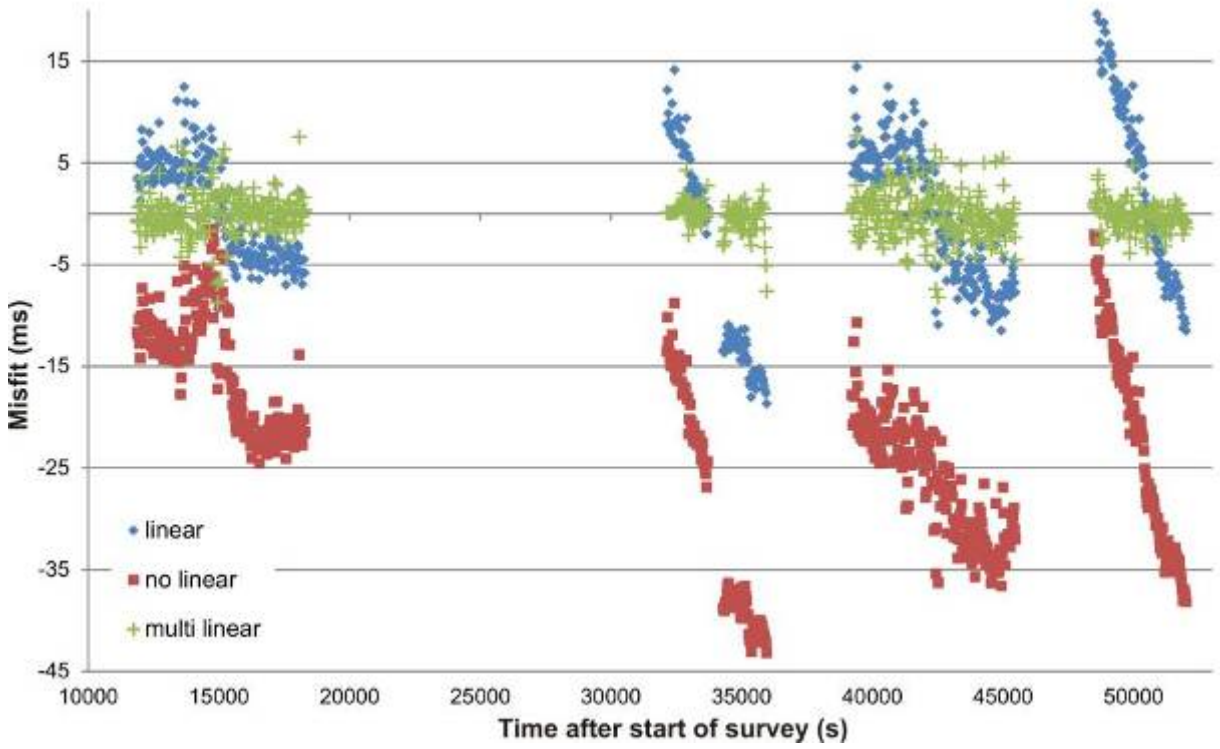

Figure 23. Final result of relocation analysis at station OBS-4. A total of 653 arrival times were picked. The multi-linear drift removal consisted of a total of 66 segments (parameters of the equation coefficients see Appendix).

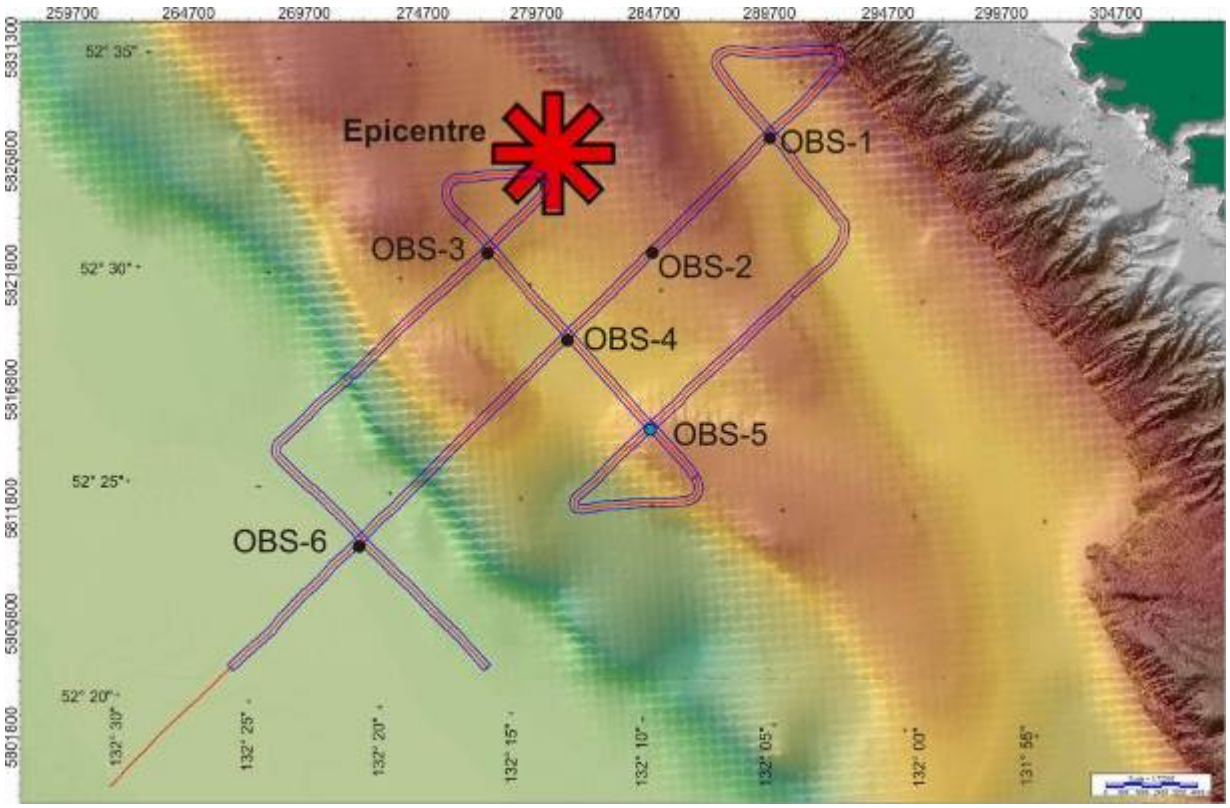

Figure 24a. Map showing distribution of shots around OBS-5 used for relocation analysis for the all shot scenario. Red line is the entire survey, with the region from which direct arrivals were picked highlighted by double blue lines.

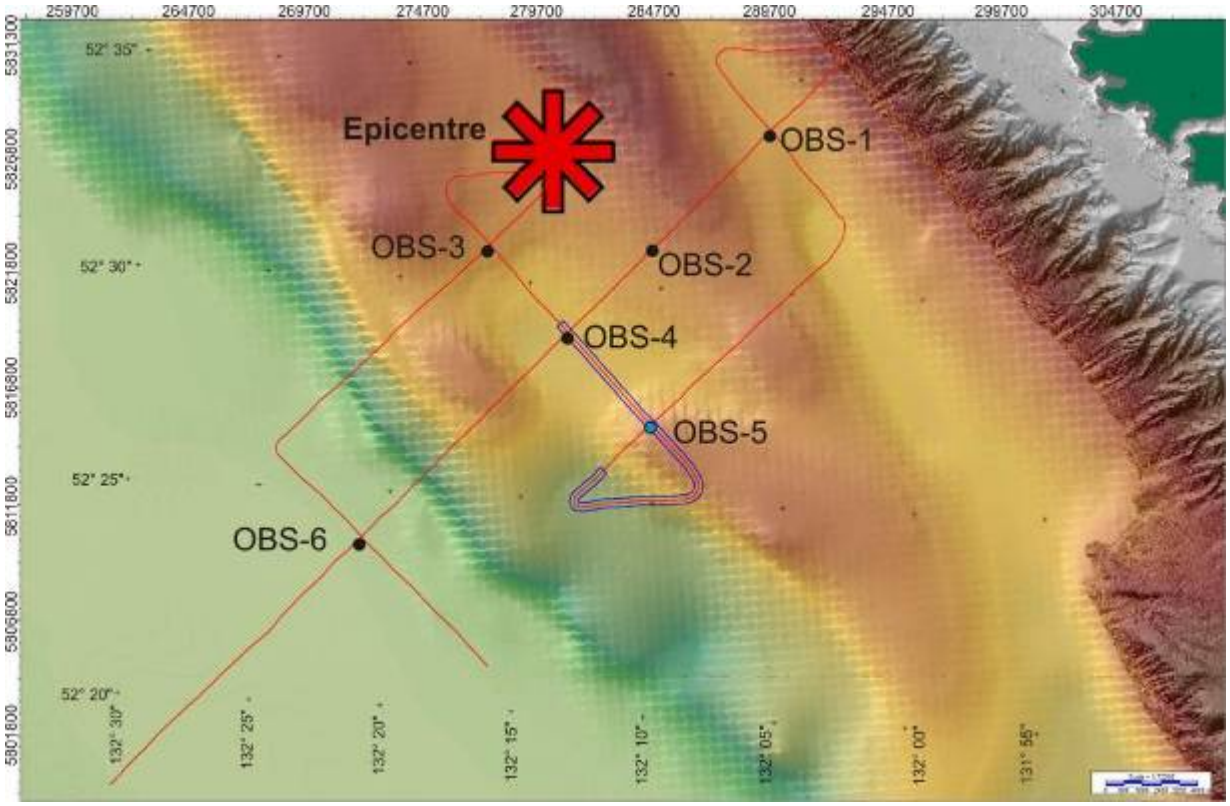

Figure 24b. Map showing distribution of shots around OBS-5 used for relocation analysis for the crossings only scenario. Red line is the entire survey, with the region from which direct arrivals were picked highlighted by the double blue lines.

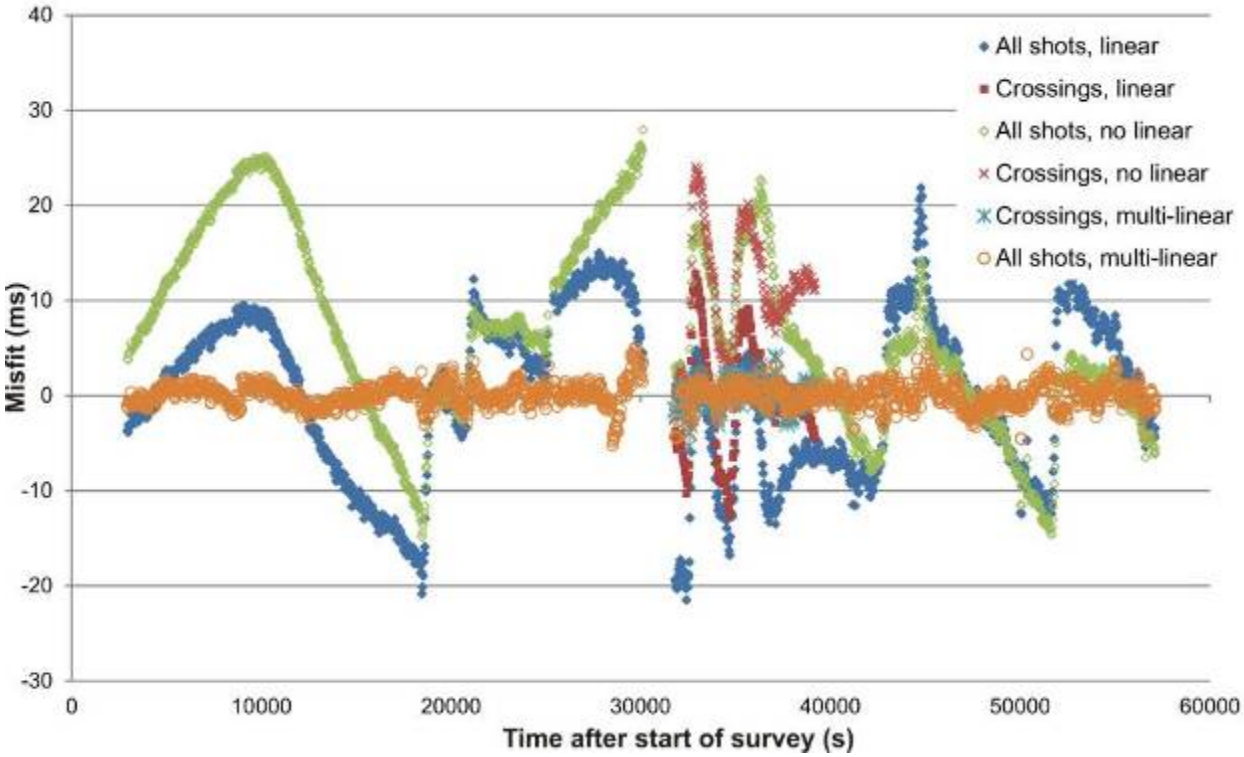

Figure 25. Final result of the relocation analysis at station OBS-5. A total of 247 arrival times were picked for the direct crossings, and 1747 arrival times were picked for the all shot analysis. The multi-linear drift removal on the direct crossings consisted of a total of 9 segments and 24 segments for all shots (parameters of the equation coefficients see Appendix).

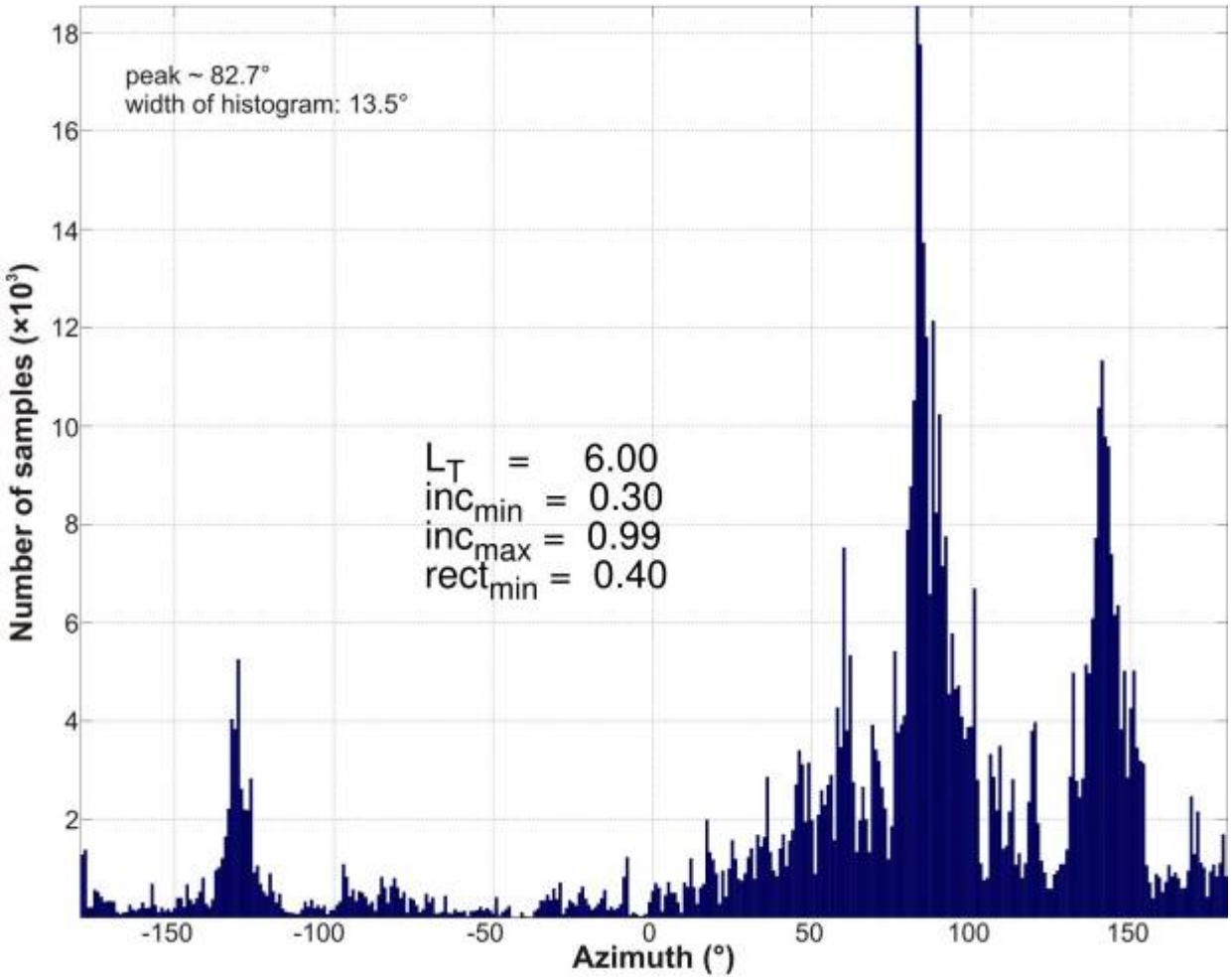

Figure 26. Results of the azimuth analysis of station OBS-1 using the Rosenberger (2010) routine. There are many earthquakes in the seismogram, which result in alternate large peaks, as the OBS station is mostly east of the aftershock area.

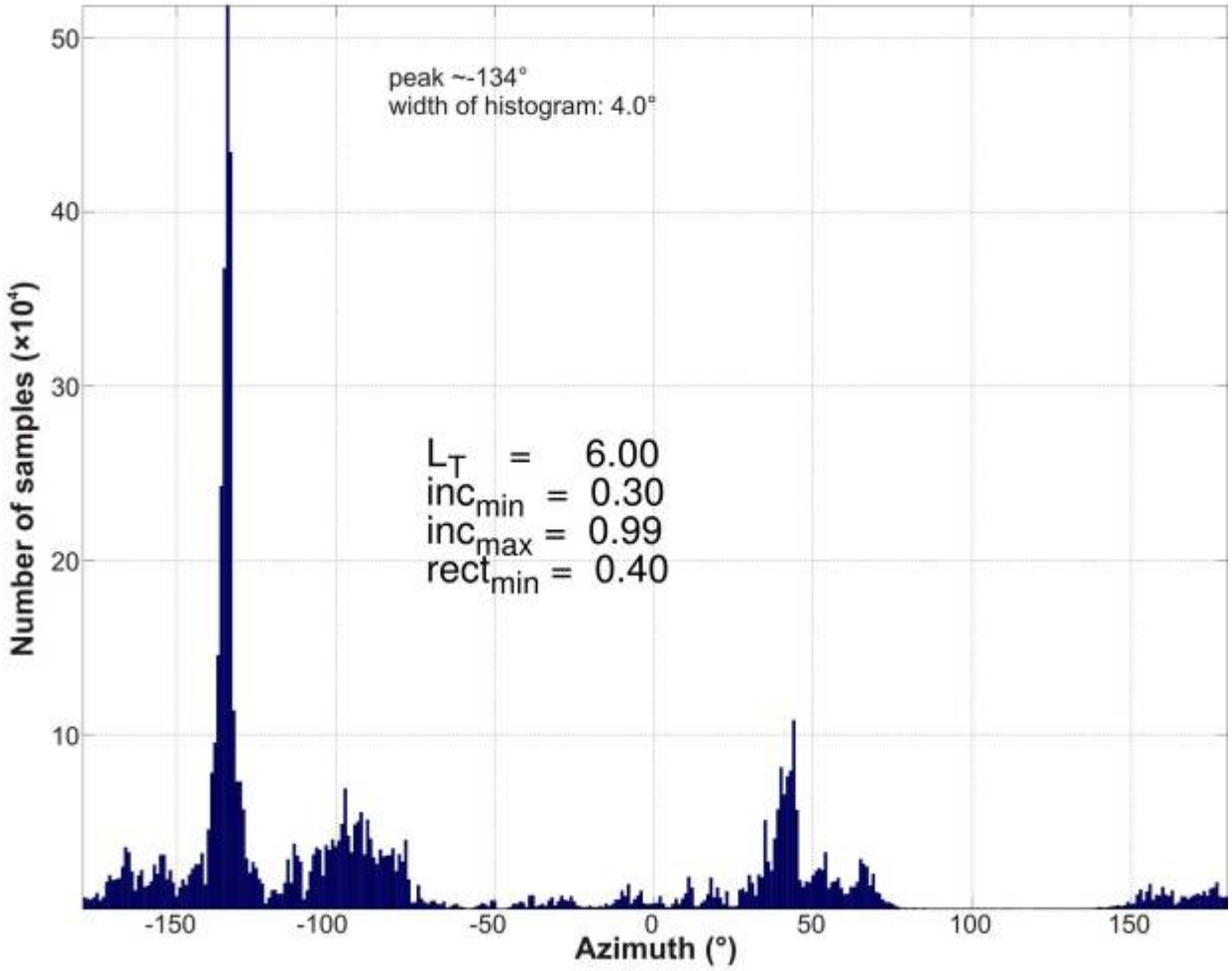

Figure 27. Results of the azimuth analysis of station OBS-2 using the Rosenberger (2010) routine. There are many earthquakes in the seismogram, which result in alternate large peaks, as the OBS station is mostly east of the aftershock area.

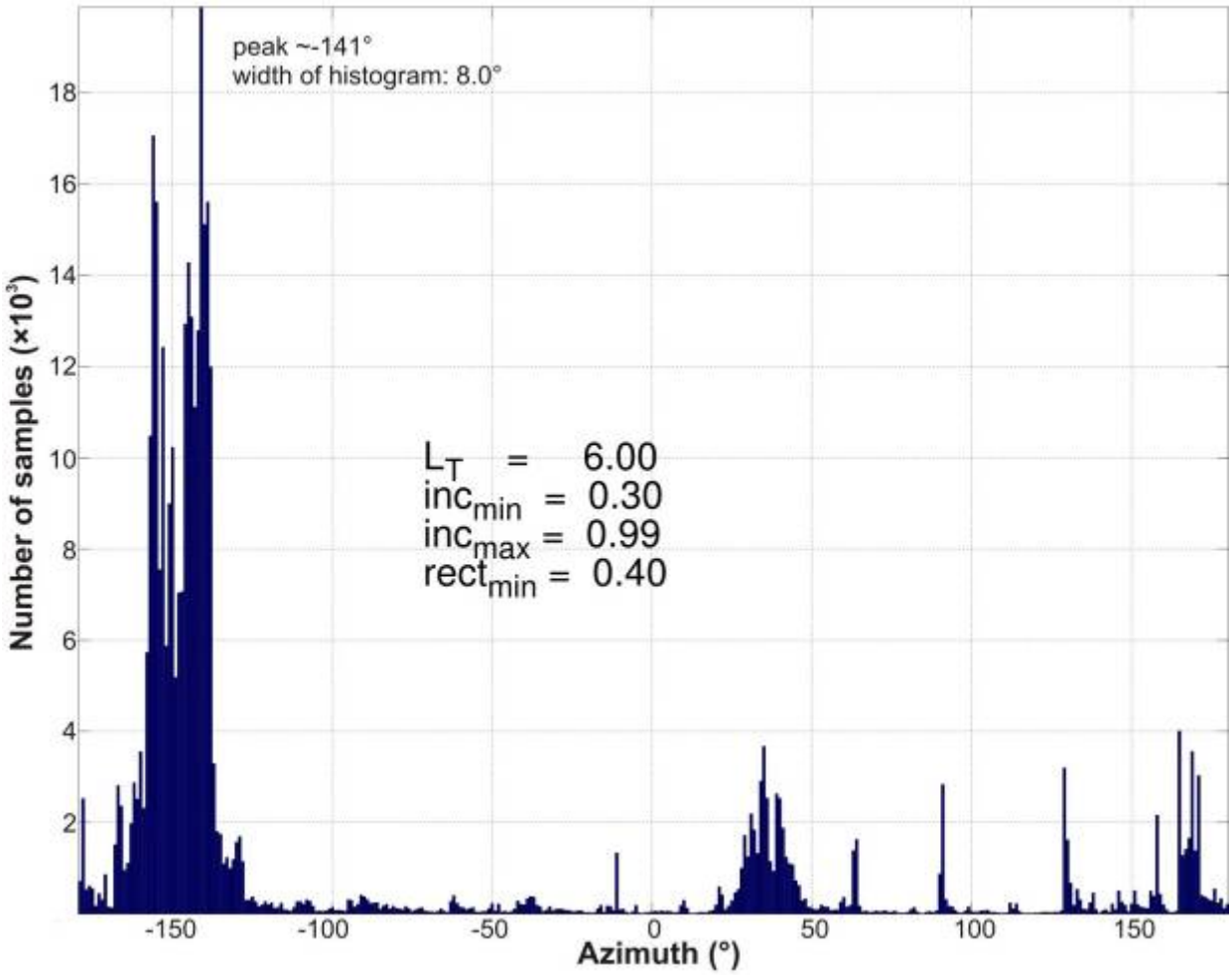

Figure 28. Results of the azimuth analysis of station OBS-3 using the Rosenberger (2010) routine.

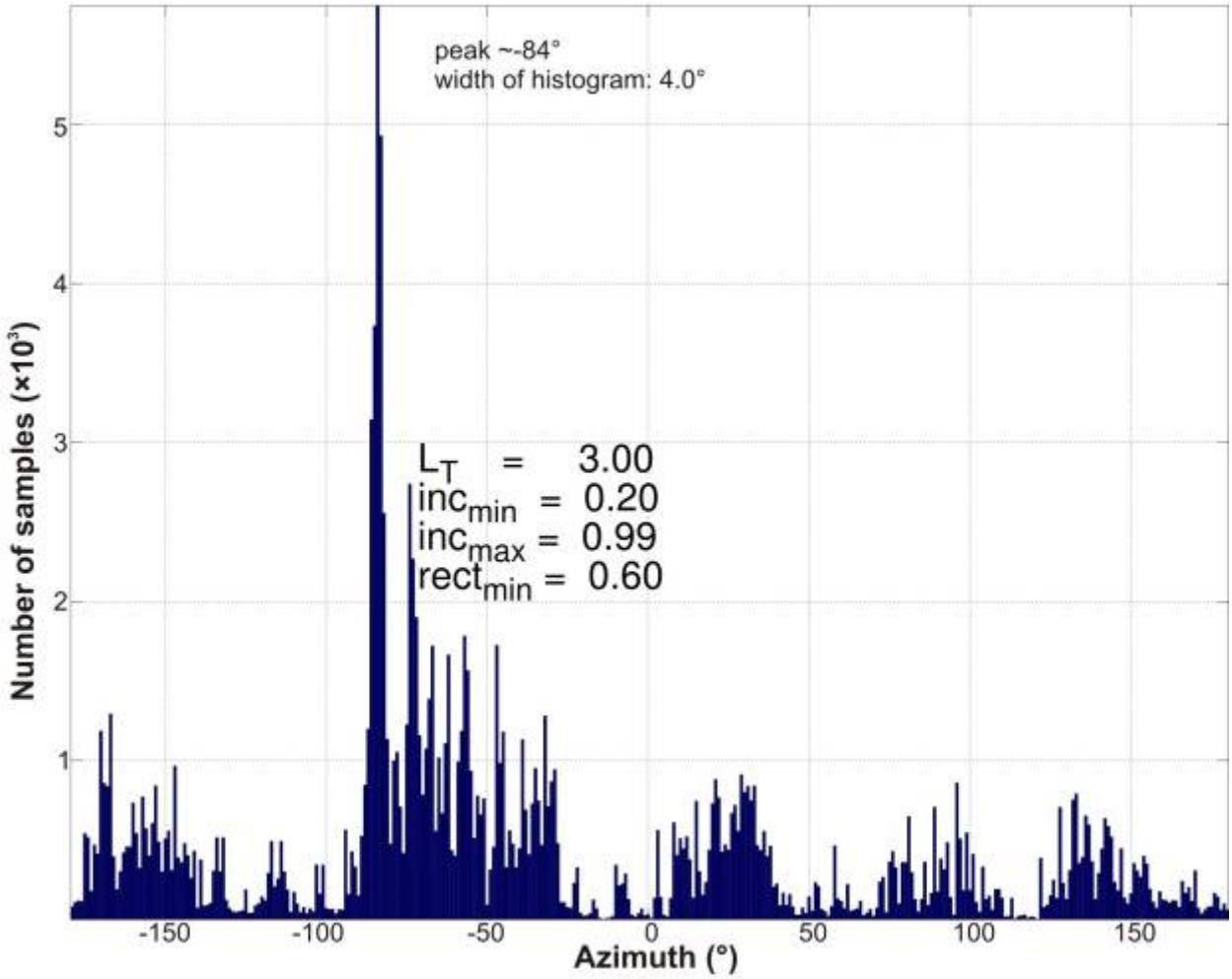

Figure 29. Results of the azimuth analysis of station OBS-4 using the Rosenberger (2010) routine.

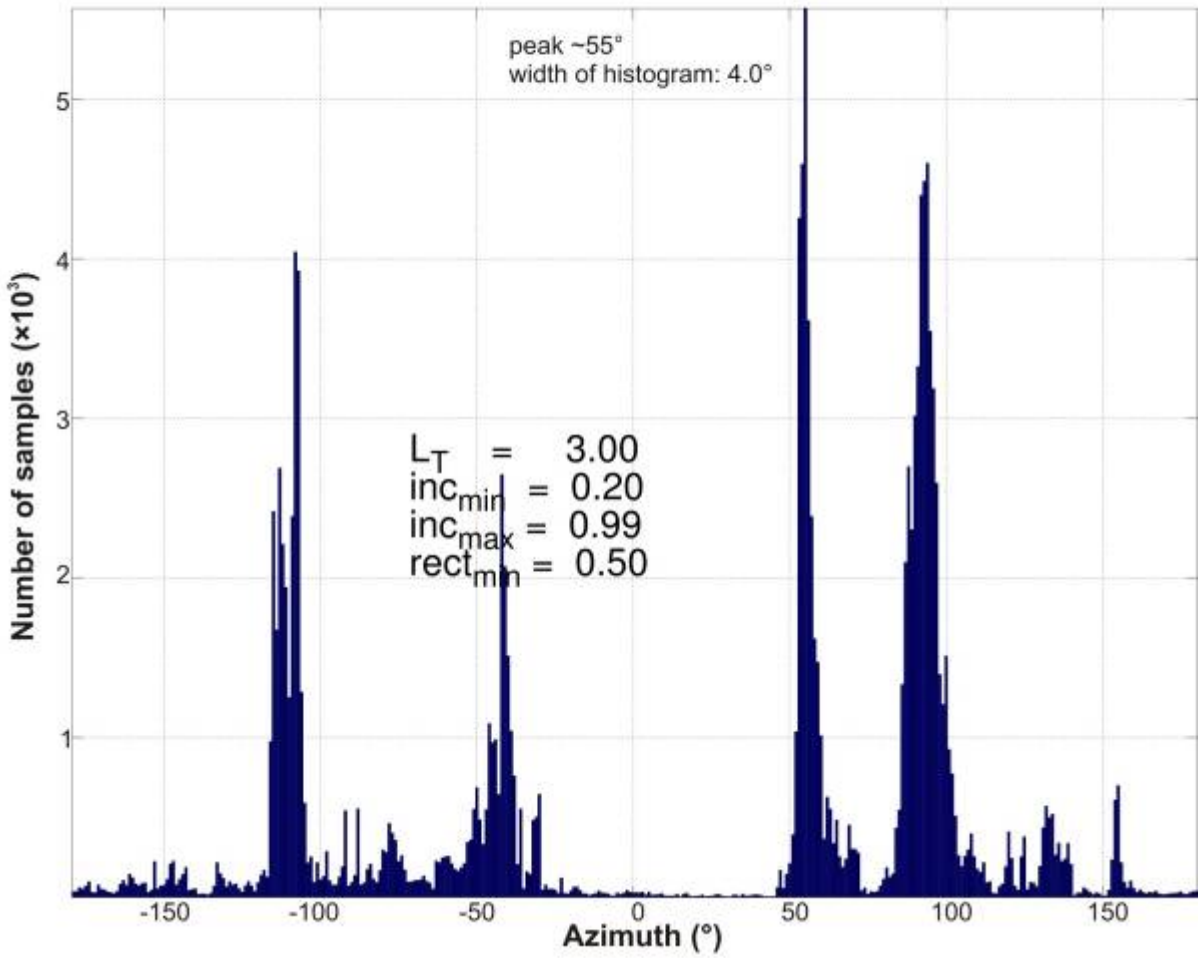

Figure 30. Results of the azimuth analysis of station OBS-6 using the Rosenberger (2010) routine.

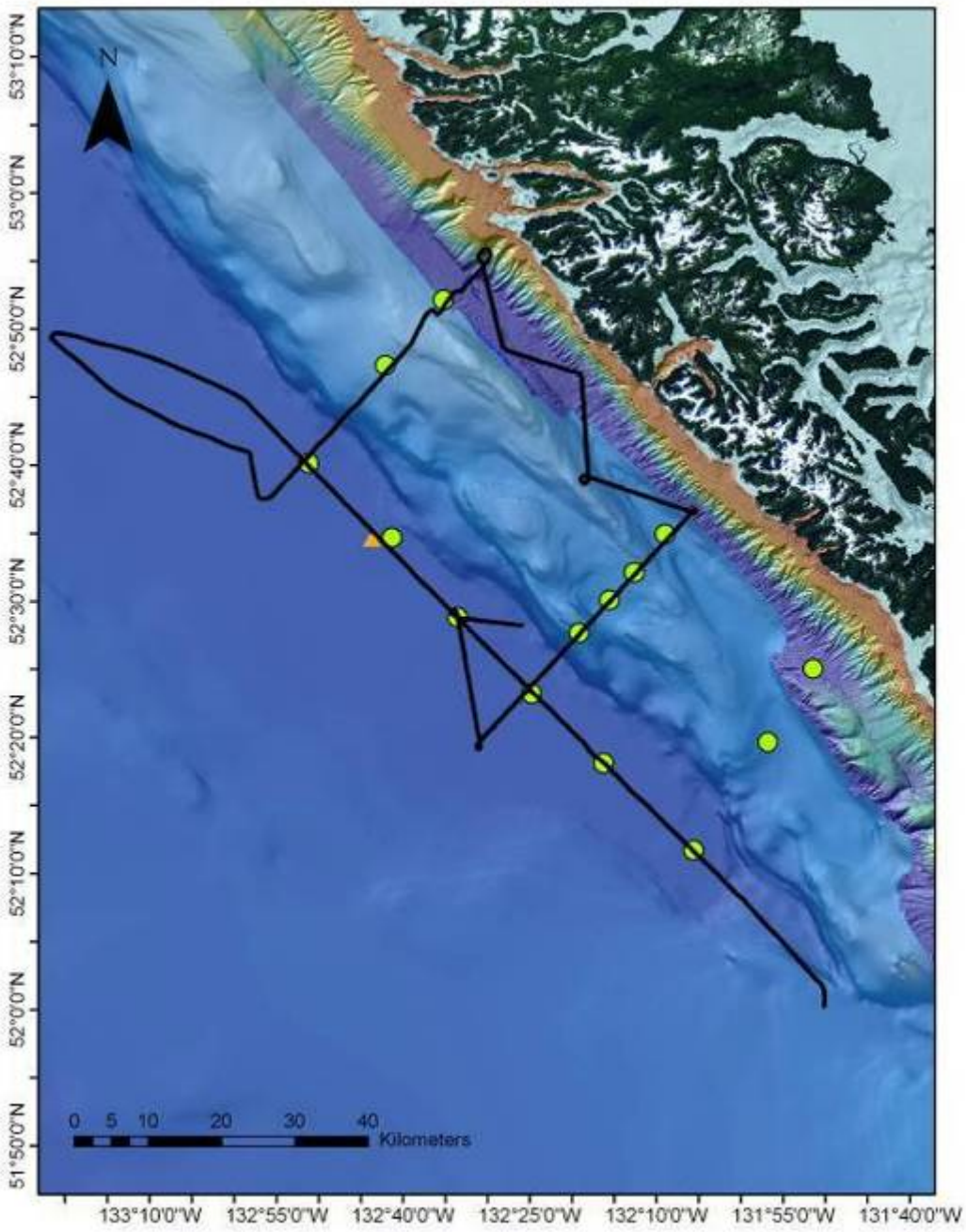

Figure 31. Map of seismic lines acquired during first refraction survey prior to recovery of the regional OBS grid (green circles). The ODAS mooring site (which mandated a slight re-positioning of the nearby OBS) is shown as orange triangle.

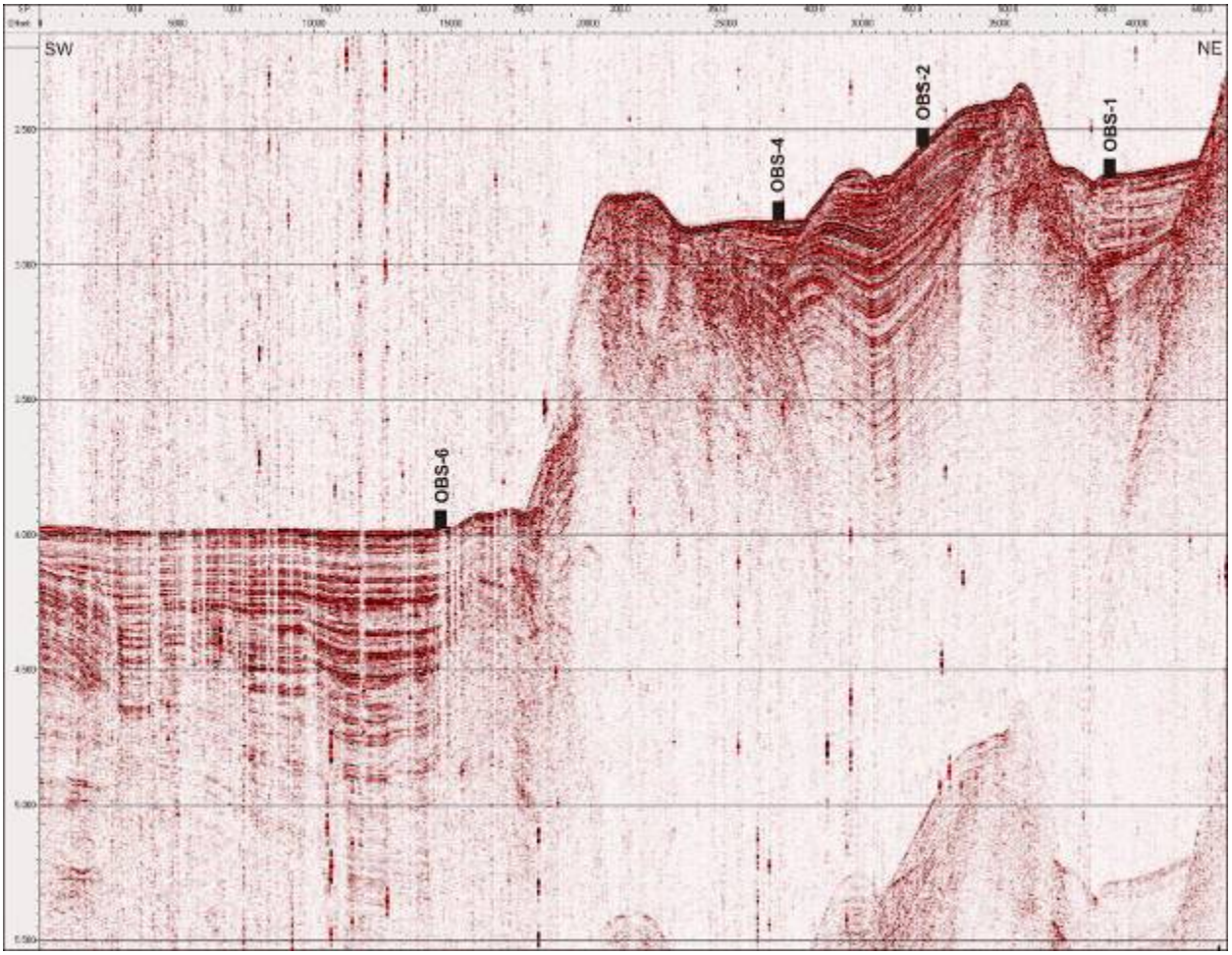

Figure 32. Main central line shot in an SW-NE direction across stations OBS-6, OBS-4, OBS-2, and OBS-1 extending from the abyssal plain across the Queen Charlotte terrace to east of the Queen Charlotte Transform Fault.

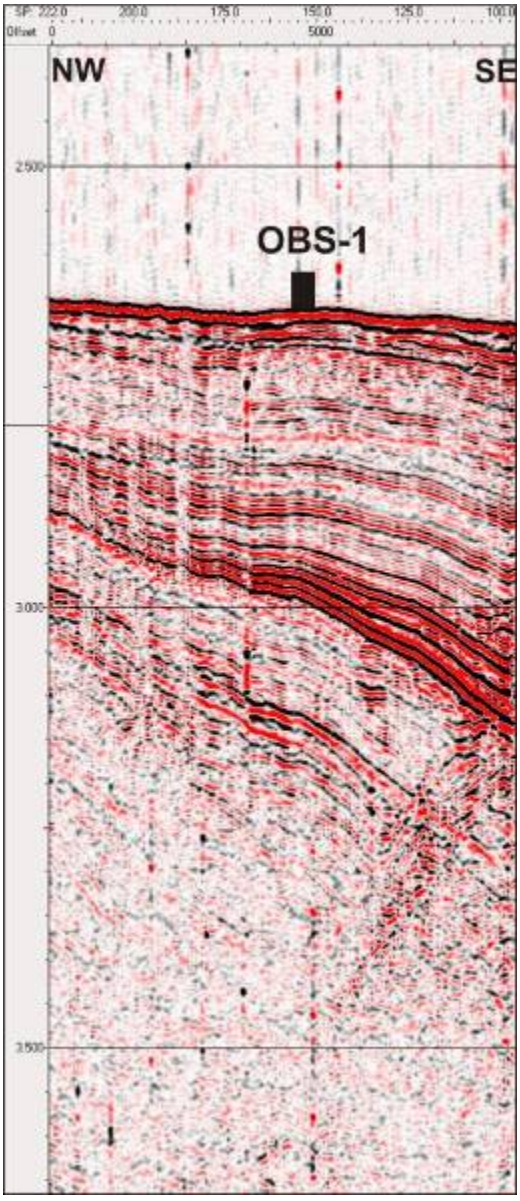

Figure 33. Around station OBS-1 a short SE-NW oriented segment was acquired, almost parallel to the Queen Charlotte Transform Fault.

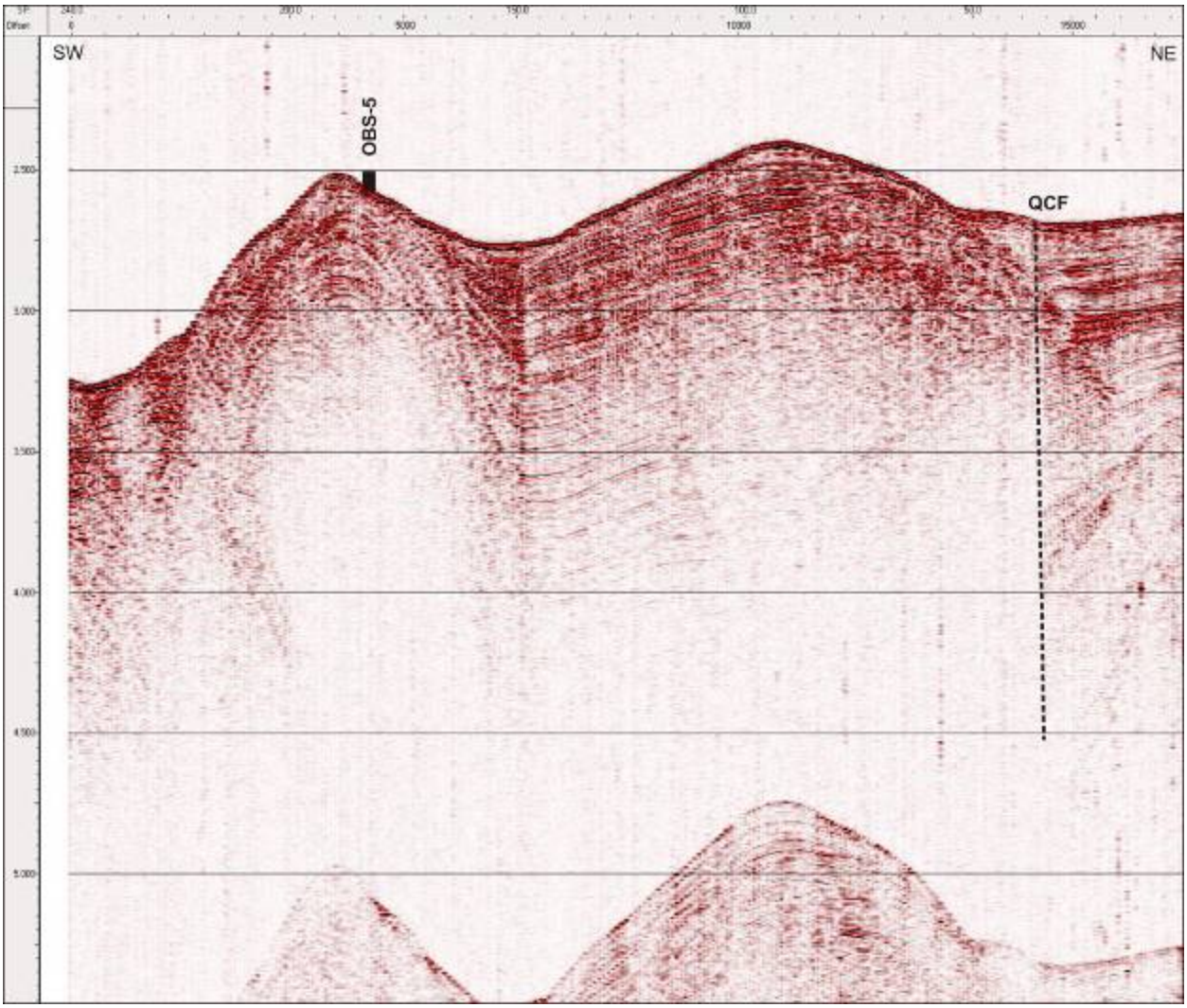

Figure 34. SW-NE oriented line across station OBS-5, parallel to the main centre line. The eastern portion of the line crosses the Queen Charlotte Transform Fault (QCF) and then crosses two ridges of the Queen Charlotte terrace.

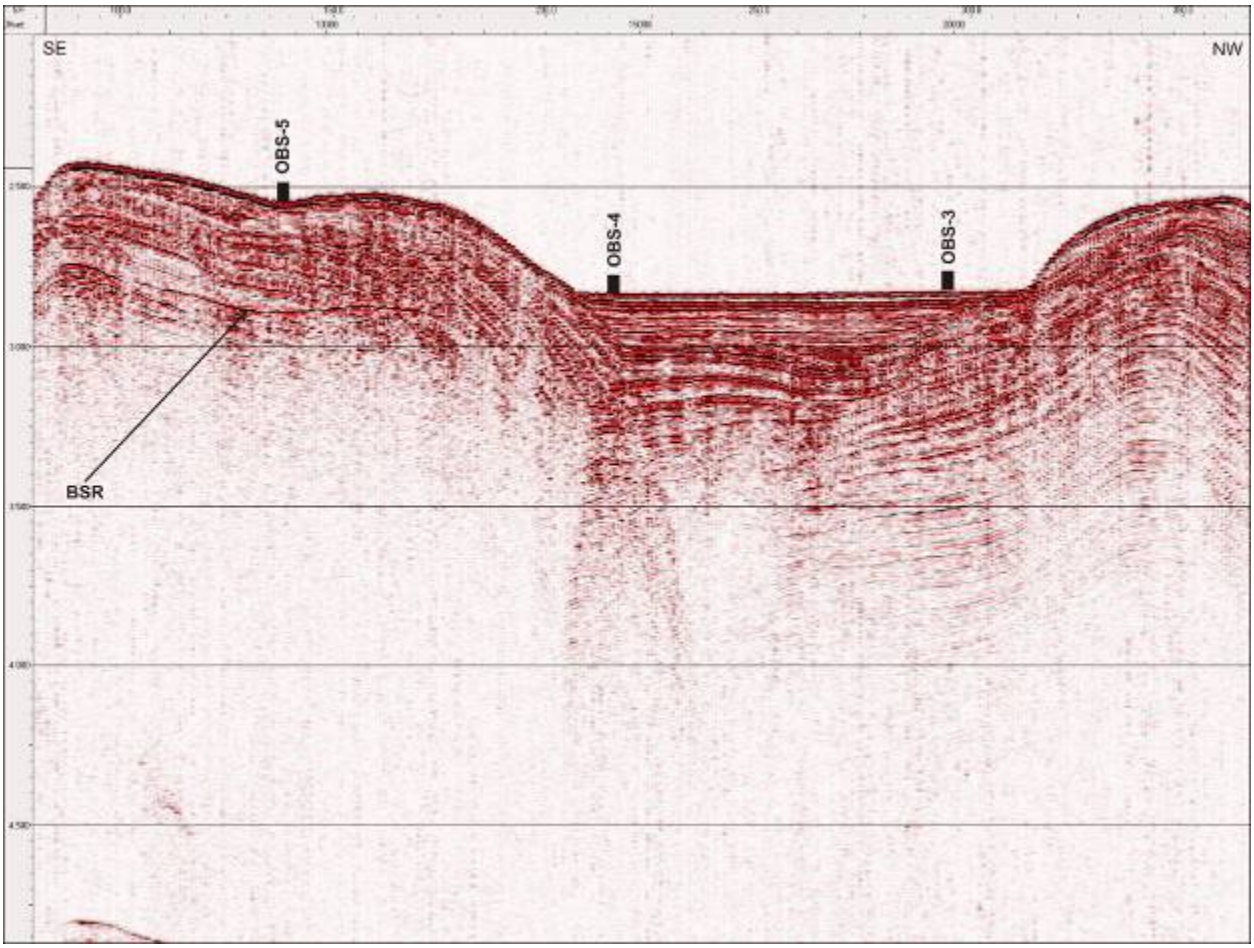

Figure 35. SE-NW oriented line crossing stations OBS-5, OBS-4, and OBS-3. The line crosses a central basin that developed between two elevated ridges of the Queen Charlotte terrace. Note the occurrence of a bottom simulating reflector (BSR) indicating the presence of gas hydrate on the Terrace.

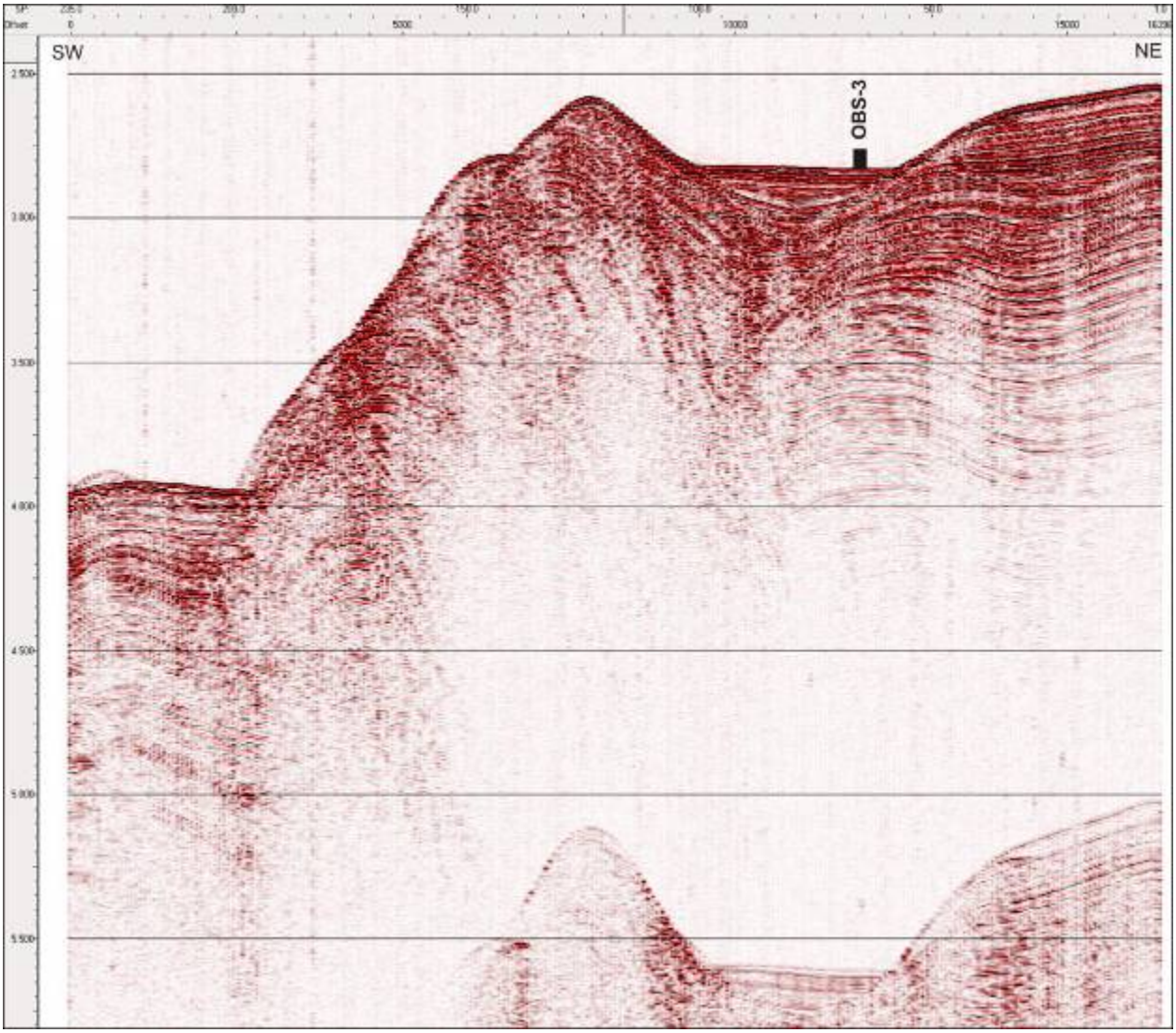

Figure 36. SW-NE oriented line across OBS-3 extending from the Queen Charlotte terrace to the abyssal plain in the west.

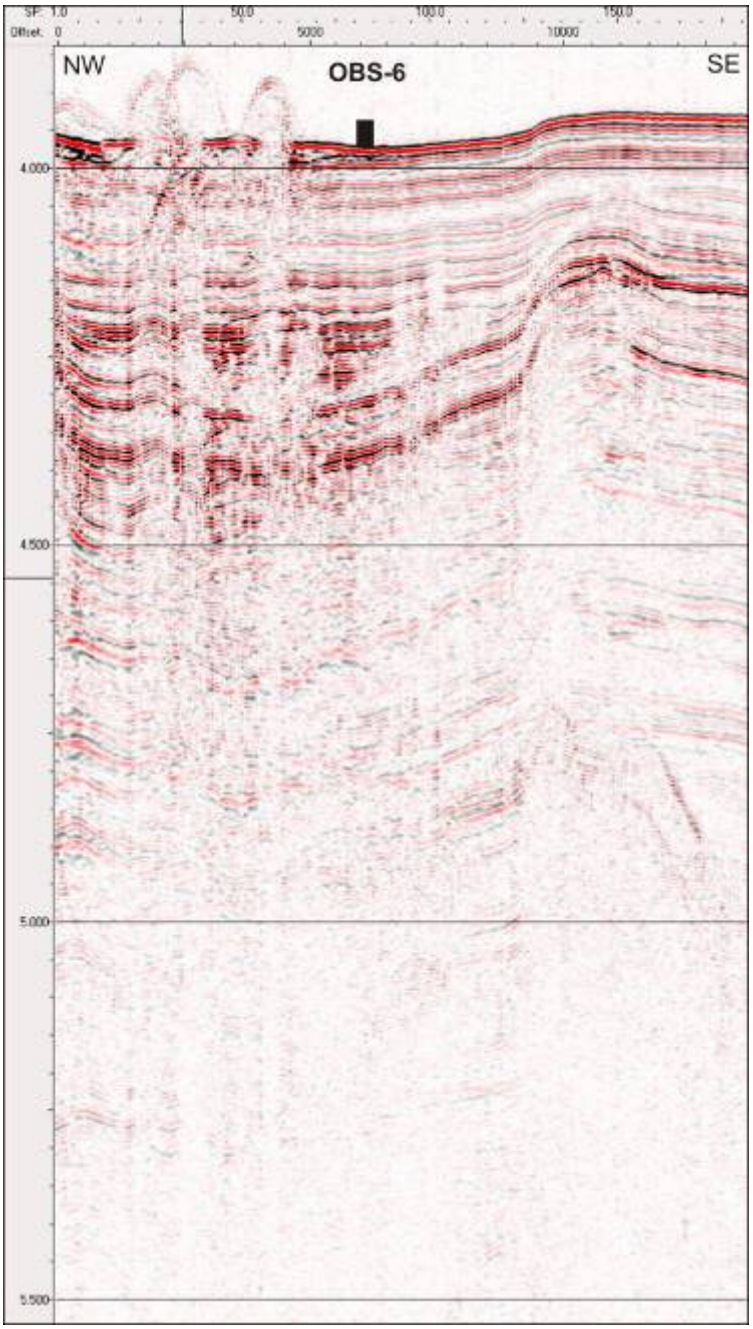

Figure 37. NW-SE oriented line at the end of the survey crossing OBS-6. Note the diffractions in the northern portion of the line from a blocky debris flow.

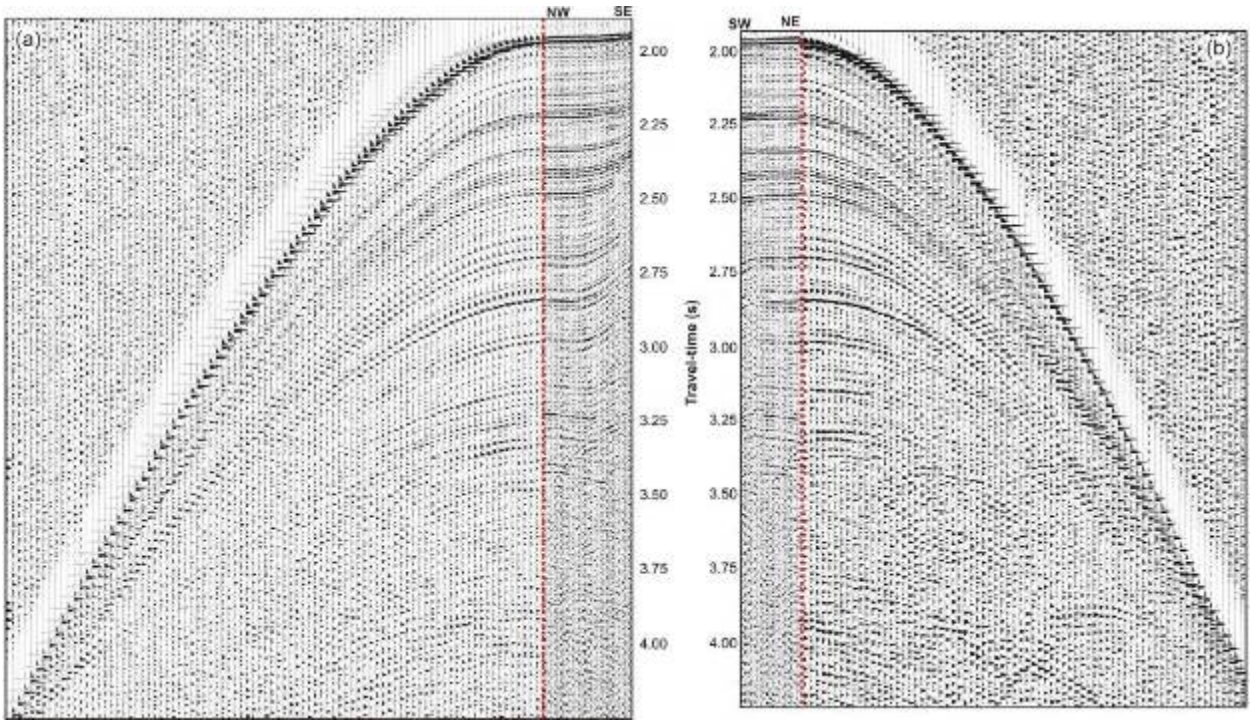

Figure 38. Comparison of the single channel seismic data with the wide-angle OBS data for station OBS-6. The red line indicates the position of the OBS itself. (a) Segment of the NW-SE oriented line (see Figure 32) to the right of the red line with the OBS data to the left of the red line. (b) Segment of the central SW-NE oriented line (see Figure 27) to the left of the red line with the OBS data to the right of the red line. The correlation between the two data sets is excellent for the upper 1.5 seconds, with the deeper data (later arrivals) on the streamer being washed out.

(a)

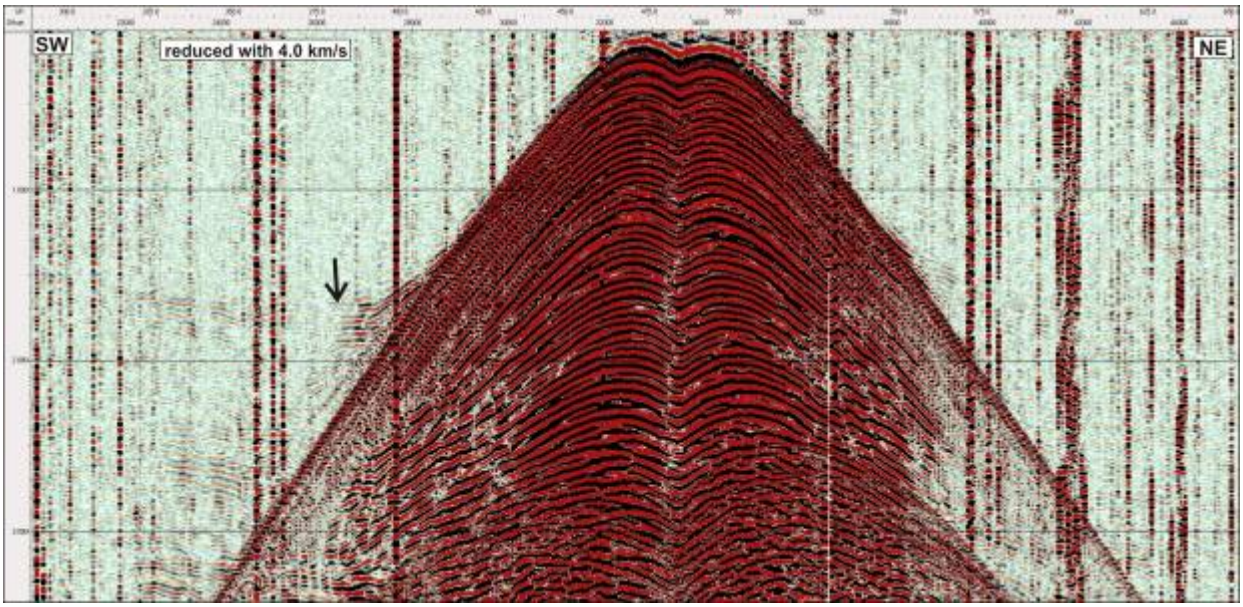

(b)

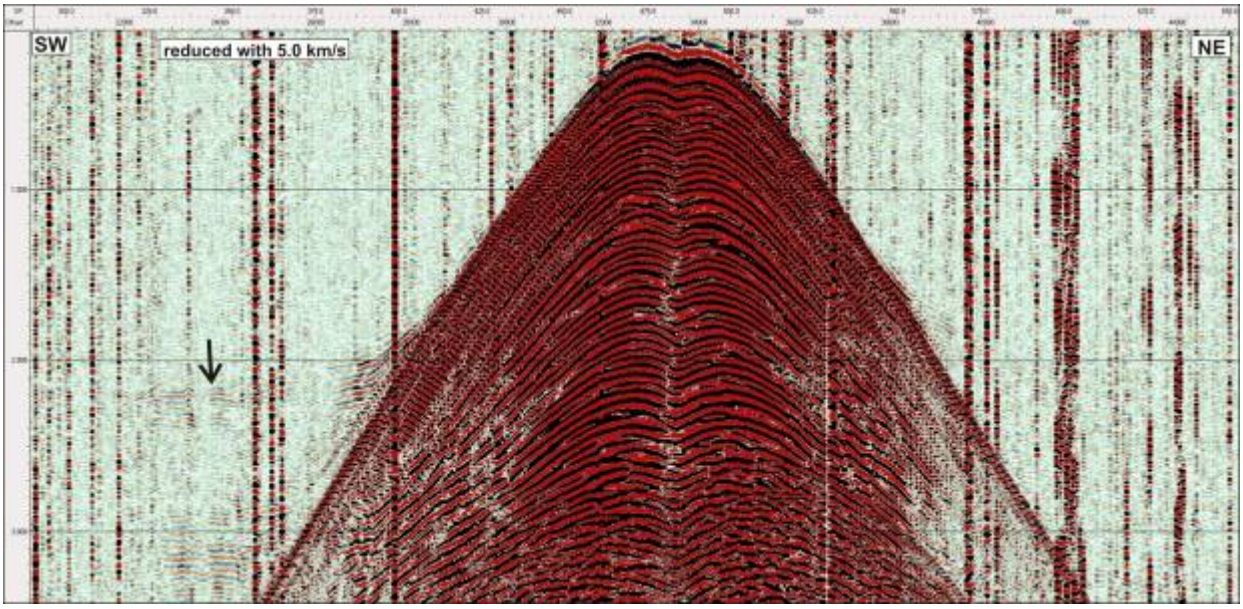

Figure 39. Detection of refracted arrivals on OBS-2 from transect across station of main central line (from SW to NE). Using reducing velocities of (a) 4.0 km/s and (b) 5.0 km/s, refracted arrivals corresponding roughly to this P-wave velocity values appear horizontally flat (refractor-pieces identified by black arrow).

(a)

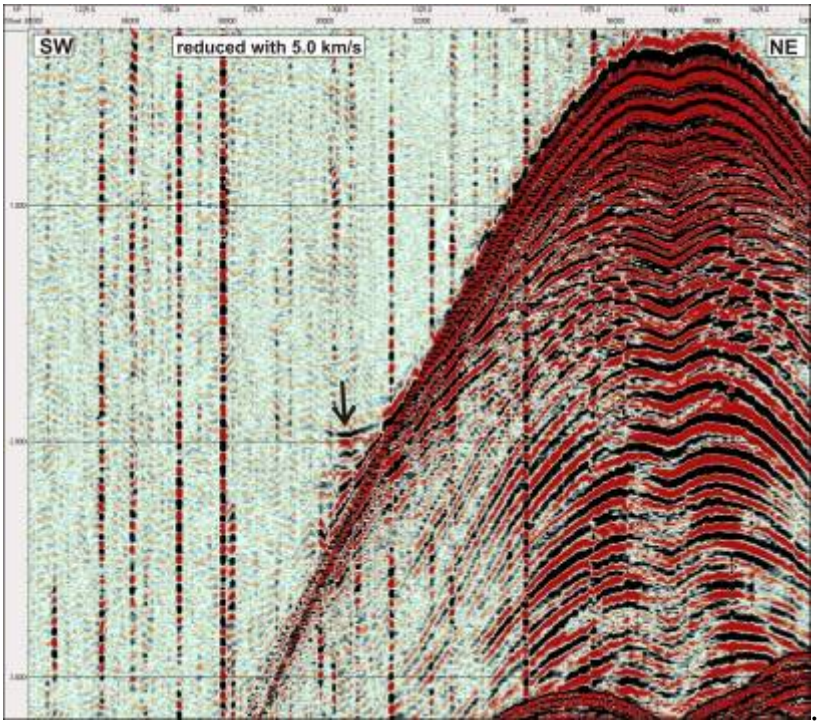

(b)

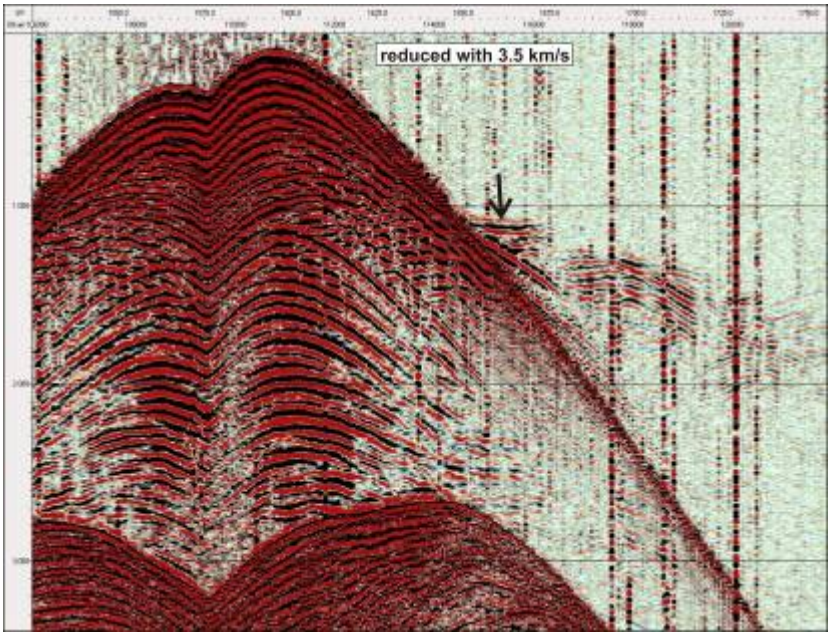

Figure 40. Detection of refracted arrivals on OBS-3 from (a) SE – NW transect using reducing velocity of 5.0 km/s and (b) from the transect across station from NE to SW with reducing velocities of 3.5 km/s. Refracted arrivals corresponding roughly to this P-wave velocity value appear horizontally flat (refractor-pieces identified by black arrow).

(a)

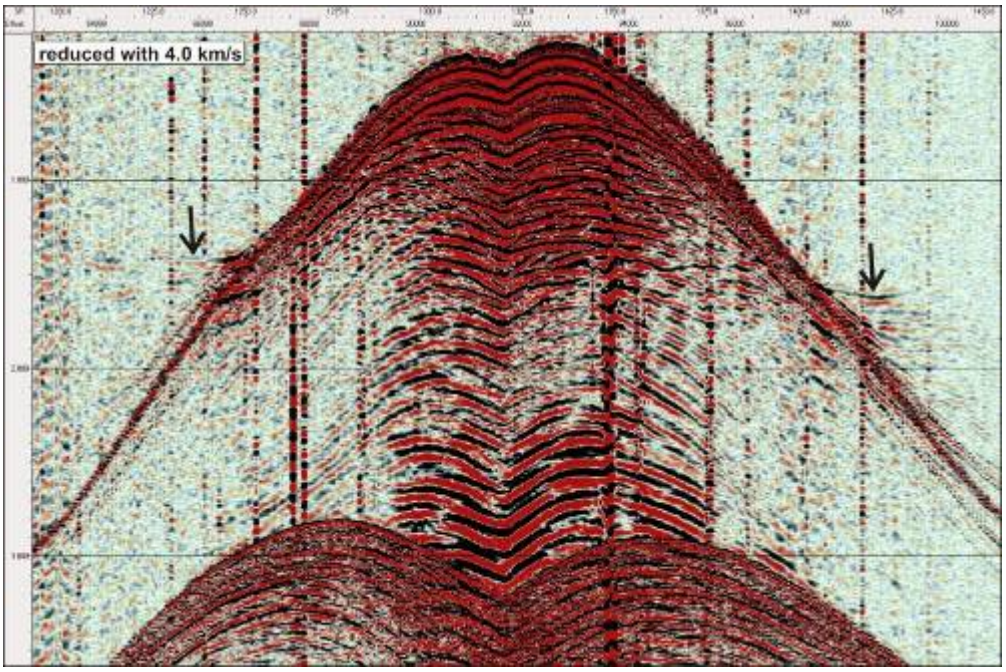

(b)

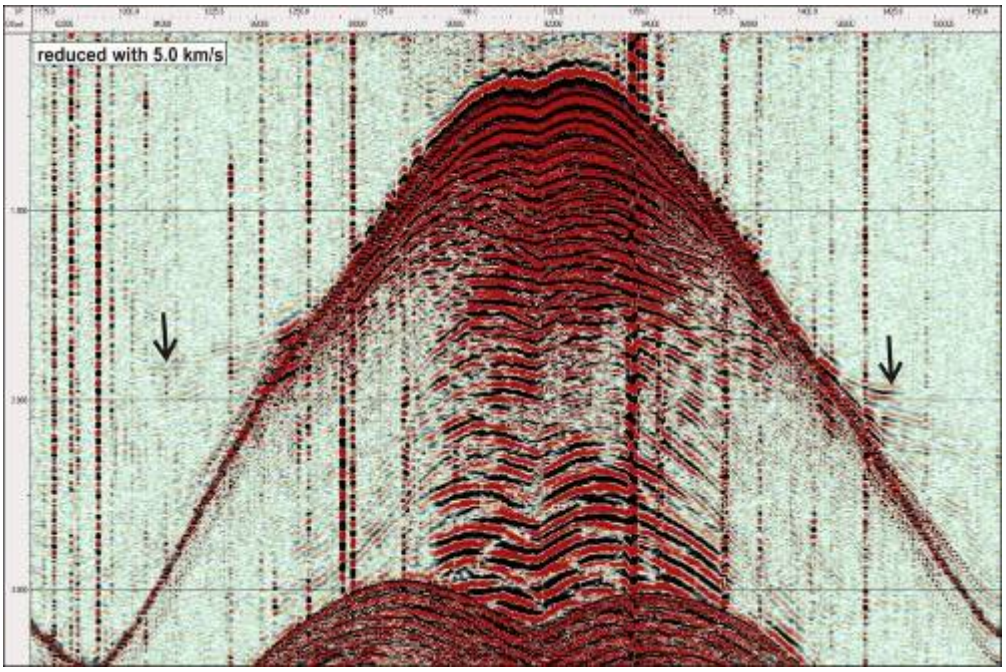

Figure 41. Detection of refracted arrivals on OBS-4 from transect across station at beginning of second survey (from SW to NE). Using reducing velocities of (a) 4 km/s, (b) 5 km/s, and (c) 6 km/s, refracted arrivals corresponding roughly to these P-wave velocity values are horizontally flat (refractor-pieces identified by black arrow).

(a)

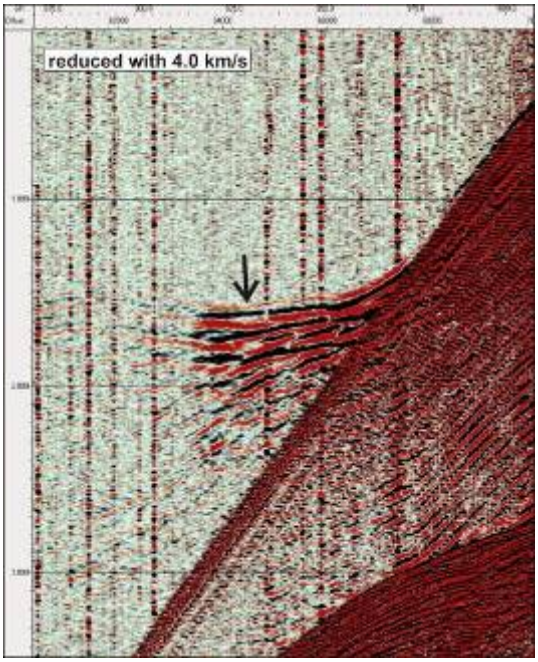

(b)

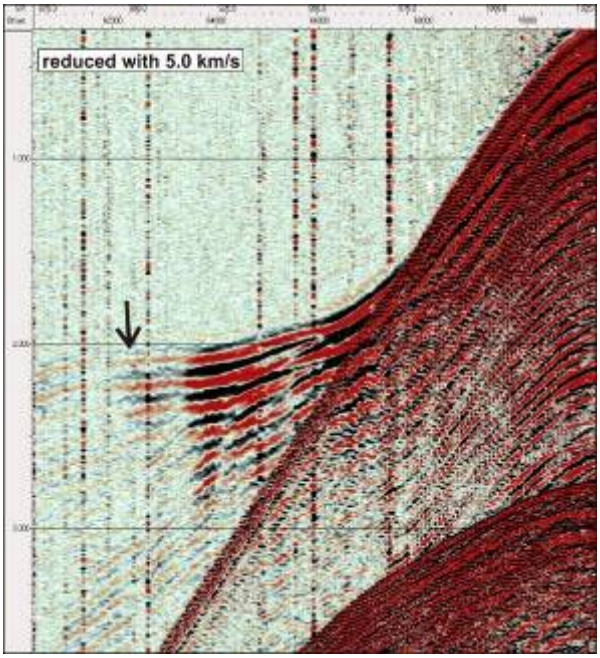

Figure 42. Detection of refracted arrivals on OBS-5 from transect across station (NE to SW) using reducing velocities of (a) 4 km/s and (b) 5 km/s. Refracted arrivals corresponding roughly to these P-wave velocity values appear horizontally flattened (refractor-pieces identified by black arrow).

(a)

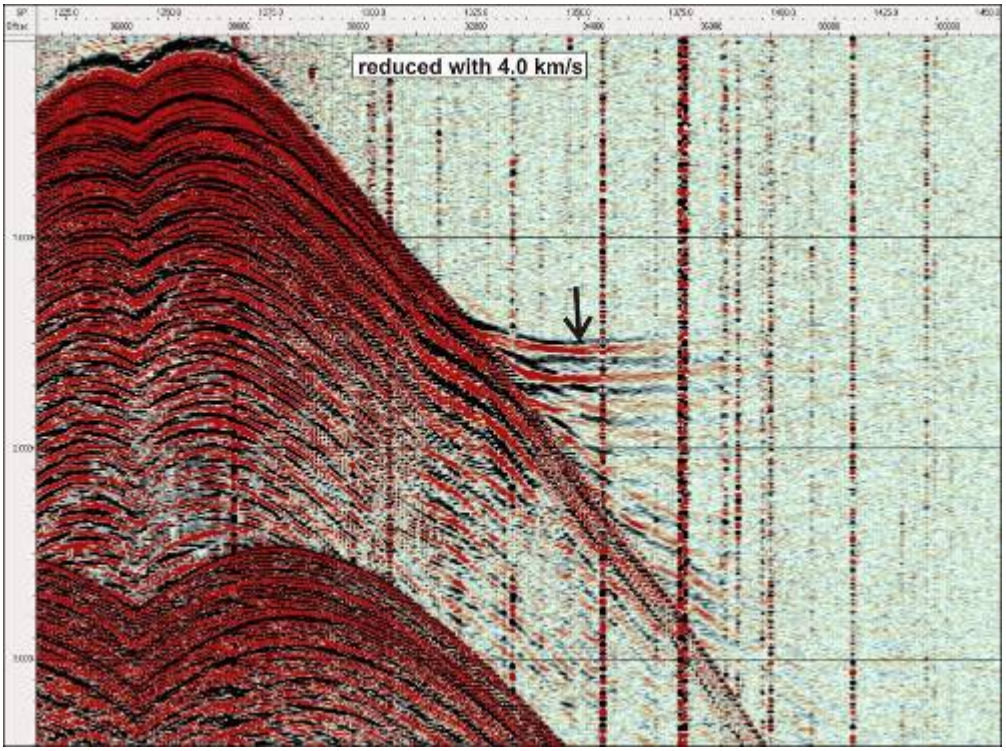

(b)

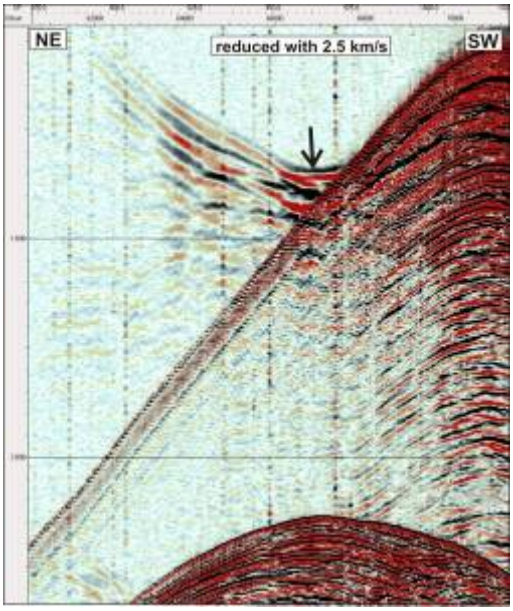

Figure 43. Detection of refracted arrivals on OBS-5 (a) from transect across station (SE to NW) using reducing velocities of 4 km/s and (b) from transect across station from NE to SW using reducing velocities of 2.5 km/s. Refracted arrivals corresponding roughly to these P-wave velocity values appear horizontally flattened (refractor-pieces identified by black arrow).

(a)

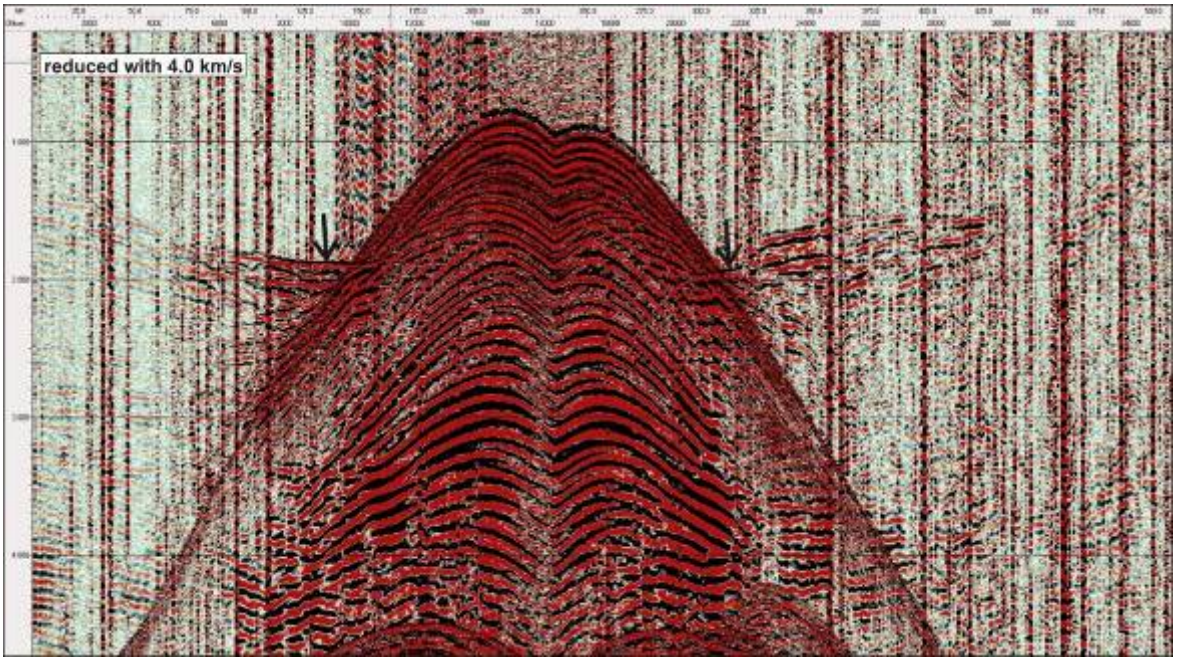

(b)

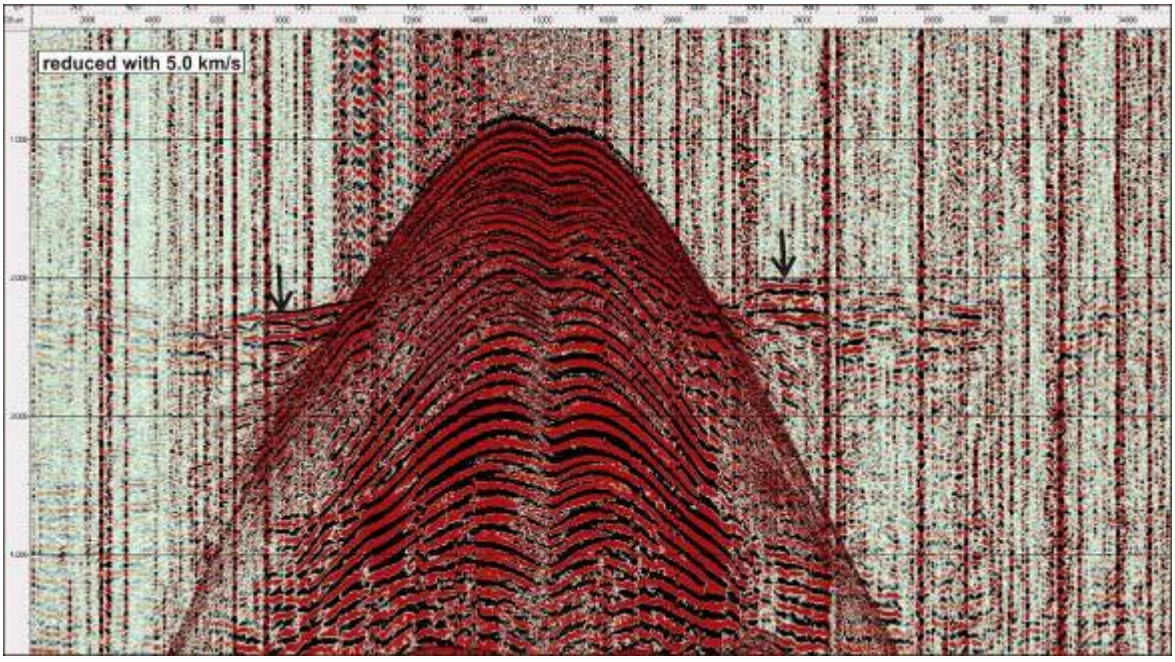

(c)

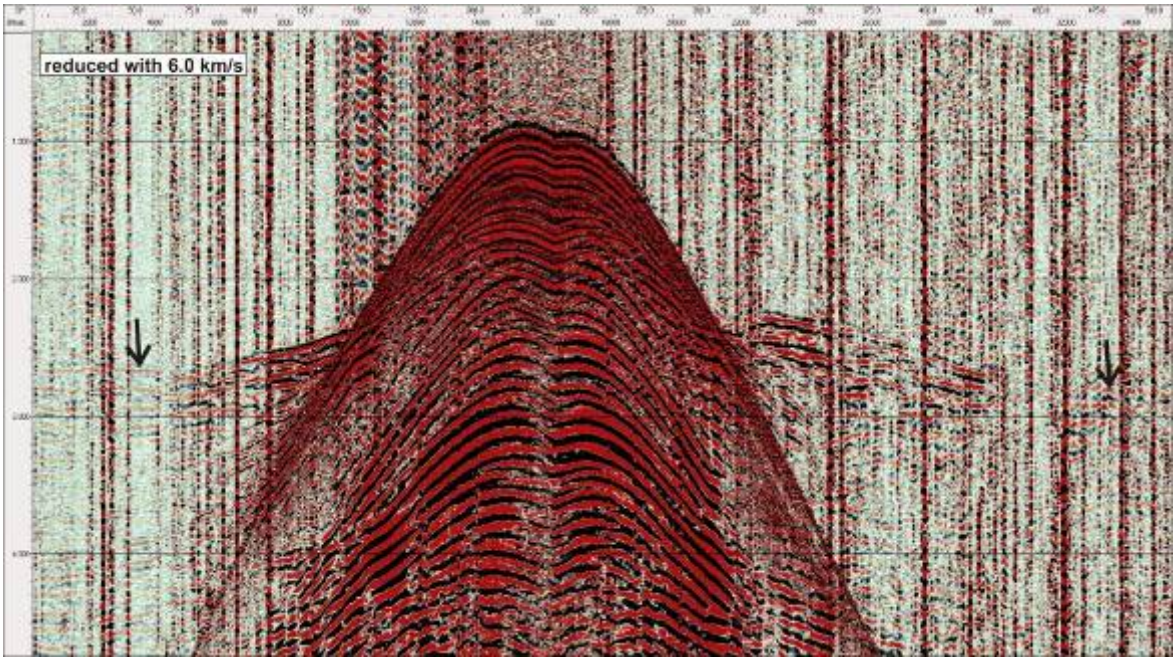

Figure 44. Detection of refracted arrivals on OBS-6 from transect across station at beginning of second survey (from SW to NE) using reducing velocities of (a) 4 km/s, (b) 5 km/s, and (c) 6 km/s. Refracted arrivals corresponding roughly to these P-wave velocity values appear horizontally flattened (refractor-pieces are identified by black arrow).

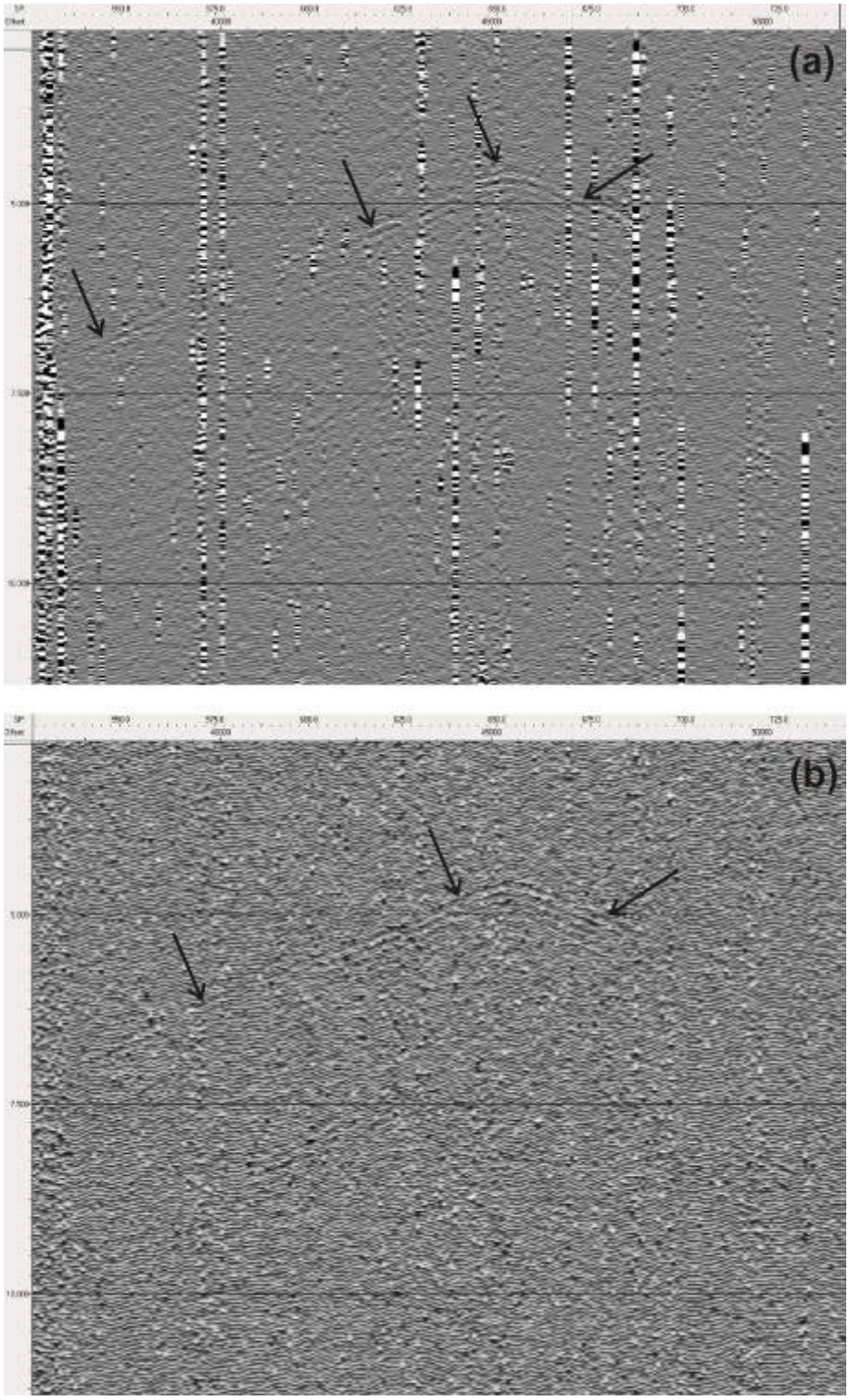

Figure 45. (a) Amplitude and (b) of shot record extracted from land station at Barry inlet (BNB) for second refraction experiment. Arrivals from airgun are highlighted by arrows.

Appendix

(A.1) OBS inversion results

Coefficients of the multi-linear drift removal are given below, together with the start time value (*T'*) (values given in seconds). All intervals are defined as 600 second long segments. The linear drift (*R*) is then calculated within each segment using the equation $R_i = B_i + K_i \times \tau$, where the time τ is used as the difference between actual time (*T*) of the shot and the interval time: $\tau = T - T'$.

A.1.1 OBS-1

Start interval time: 17900 s

B_1	K_1	25.21	-0.12067123
B_2	K_2	29.64	0.00553926
B_3	K_3	30.46	0.00083476
B_4	K_4	25.86	-0.01374931
B_5	K_5	15.75	-0.02325414
B_6	K_6	8.26	-0.00061173
B_7	K_7	5.29	-0.01005653
B_8	K_8	3.57	0.00542965
B_9	K_9	16.02	0.02906139
B_{10}	K_{10}	1.61	-0.04822343
B_{11}	K_{11}	-37.64	-0.08294271
B_{12}	K_{12}	-81.50	-0.05421020
B_{13}	K_{13}	-75.82	0.06586545
B_{14}	K_{14}	-55.65	0.01580915
B_{15}	K_{15}	-33.86	0.05857727
B_{16}	K_{16}	14.46	0.09549422
B_{17}	K_{17}	57.30	0.04372286
B_{18}	K_{18}	77.56	0.01301187

A.1.2 OBS-2

Start interval time: 13800 s

B_1	K_1	13.89	0.00100792
B_2	K_2	14.64	-0.00209138
B_3	K_3	16.42	0.00455961
B_4	K_4	18.37	0.00177088
B_5	K_5	20.52	0.00514574
B_6	K_6	21.18	-0.00593322
B_7	K_7	14.06	-0.02259141
B_8	K_8	1.84	-0.01932833
B_9	K_9	-5.86	-0.00968349
B_{10}	K_{10}	-10.19	-0.00527040
B_{11}	K_{11}	-14.56	-0.00817390
B_{12}	K_{12}	-16.42	-0.00220391
B_{13}	K_{13}	-13.23	0.01933697
B_{14}	K_{14}	-4.72	0.00787216
B_{15}	K_{15}	-1.31	0.00690420
B_{16}	K_{16}	1.02	0.00647796
B_{17}	K_{17}	2.83	0.00582746
B_{18}	K_{18}	4.88	0.00691697
B_{19}	K_{19}	8.25	0.00856095

B_{20}	K_{20}	12.17	0.00259442
B_{21}	K_{21}	11.64	-0.00087101
B_{22}	K_{22}	10.93	-0.00216503
B_{23}	K_{23}	12.37	0.00833640
B_{24}	K_{24}	10.17	-0.01343148
B_{25}	K_{25}	7.66	0.00060419
B_{26}	K_{26}	13.64	0.03543897
B_{27}	K_{27}	33.30	0.01546120
B_{28}	K_{28}	37.66	-0.00583101
B_{29}	K_{29}	33.43	-0.00871356
B_{30}	K_{30}	29.50	-0.01522021
B_{31}	K_{31}	19.05	-0.01766498
B_{32}	K_{32}	9.19	-0.02030642
B_{33}	K_{33}	-4.00	-0.02508526
B_{34}	K_{34}	-5.96	0.01883014
B_{35}	K_{35}	-0.40	0.00208814
B_{36}	K_{36}	-0.10	0.00192780
B_{37}	K_{37}	0.11	0.00218405
B_{38}	K_{38}	0.24	0.00195381
B_{39}	K_{39}	0.35	0.00240396
B_{40}	K_{40}	0.53	0.00239479
B_{41}	K_{41}	0.68	0.00256651
B_{42}	K_{42}	1.13	0.00361545
B_{43}	K_{43}	1.77	0.00326646
B_{44}	K_{44}	2.47	0.00356315
B_{45}	K_{45}	3.69	0.00456788
B_{46}	K_{46}	6.90	0.00935769
B_{47}	K_{47}	4.37	-0.02223256
B_{48}	K_{48}	-6.38	-0.02181393
B_{49}	K_{49}	-19.67	-0.02569314
B_{50}	K_{50}	-32.54	-0.02243549
B_{51}	K_{51}	-42.44	-0.01331833
B_{52}	K_{52}	-46.15	0.01494961
B_{53}	K_{53}	-25.74	0.00130982
B_{54}	K_{54}	-15.64	-0.00300856
B_{55}	K_{55}	-10.73	-0.00786593
B_{56}	K_{56}	-9.91	-0.01316528
B_{57}	K_{57}	-13.29	-0.02033970
B_{58}	K_{58}	-21.37	-0.02685529
B_{59}	K_{59}	-43.36	-0.06387929
B_{60}	K_{60}	-68.18	-0.01135540

A.1.3 OBS-3

Start interval time: 42500

B_1	K_1	-0.00	0.01811893
B_2	K_2	4.56	0.03007583
B_3	K_3	12.39	0.01043332
B_4	K_4	13.26	-0.01375230
B_5	K_5	16.20	0.00538665
B_6	K_6	9.19	-0.02685850
B_7	K_7	-6.97	-0.03241179
B_8	K_8	-24.43	-0.01789353
B_9	K_9	-10.04	0.07686303

B_{10}	K_{10}	15.36	0.01023876
B_{11}	K_{11}	20.57	0.00414118
B_{12}	K_{12}	43.64	0.08403472
B_{13}	K_{13}	64.37	-0.00763948
B_{14}	K_{14}	46.49	-0.04907299
B_{15}	K_{15}	7.59	-0.08604702
B_{16}	K_{16}	-49.36	-0.09633027
B_{17}	K_{17}	-86.11	-0.03859794
B_{18}	K_{18}	-101.82	-0.00891820
B_{19}	K_{19}	-104.10	0.00499772

A.1.4 OBS-4

Start interval time: 11900

B_1	K_1	-17.75	0.00916053
B_2	K_2	-16.95	0.00120601
B_3	K_3	-15.21	0.00358740
B_4	K_4	-6.76	0.01162822
B_5	K_5	2.24	0.02464219
B_6	K_6	14.64	0.02551376
B_7	K_7	18.92	-0.00083925
B_8	K_8	16.75	-0.00428426
B_9	K_9	16.15	-0.00032396
B_{10}	K_{10}	14.74	-0.00537530
B_{11}	K_{11}	11.27	-0.00946774
B_{12}	K_{12}	4.62	0.00216771
B_{13}	K_{13}	2.80	0.00293601
B_{14}	K_{14}	1.81	0.00276996
B_{15}	K_{15}	1.14	0.00278750
B_{16}	K_{16}	0.71	0.00283243
B_{17}	K_{17}	0.39	0.00291519
B_{18}	K_{18}	0.14	0.00308408
B_{19}	K_{19}	0.10	0.00392582
B_{20}	K_{20}	0.14	0.00371054
B_{21}	K_{21}	0.07	0.00391246
B_{22}	K_{22}	0.39	0.00555393
B_{23}	K_{23}	0.62	0.00395225
B_{24}	K_{24}	0.43	0.00427408
B_{25}	K_{25}	0.31	0.00461445
B_{26}	K_{26}	0.22	0.00504686
B_{27}	K_{27}	0.43	0.00658064
B_{28}	K_{28}	0.99	0.00720869
B_{29}	K_{29}	1.62	0.00760342
B_{30}	K_{30}	2.43	0.00840884
B_{31}	K_{31}	3.47	0.00867159
B_{32}	K_{32}	4.71	0.00896353
B_{33}	K_{33}	6.92	0.01143839
B_{34}	K_{34}	10.82	0.01322442
B_{35}	K_{35}	17.78	0.01832377
B_{36}	K_{36}	18.68	-0.02084550
B_{37}	K_{37}	1.70	-0.04155855
B_{38}	K_{38}	-21.66	-0.03072338

B_{39}	K_{39}	-33.63	-0.01737106
B_{40}	K_{40}	-47.46	-0.02013965
B_{41}	K_{41}	-31.28	0.09422327
B_{42}	K_{42}	-1.89	0.00499102
B_{43}	K_{43}	-0.67	0.00262654
B_{44}	K_{44}	2.38	0.01308236
B_{45}	K_{45}	5.79	0.00412245
B_{46}	K_{46}	8.42	0.00869880
B_{47}	K_47	8.89	-0.00727703
B_{48}	K_{48}	8.97	0.01343254
B_{49}	K_{49}	11.07	-0.01073785
B_{50}	K_{50}	10.23	0.01172414
B_{51}	K_{51}	6.01	-0.02098858
B_{52}	K_{52}	-7.29	-0.01825163
B_{53}	K_{53}	-24.03	-0.03099197
B_{54}	K_{54}	-34.76	-0.00654454
B_{55}	K_{55}	-42.94	-0.01894459
B_{56}	K_{56}	-46.69	0.00362315
B_{57}	K_{57}	-23.83	0.07790896
B_{58}	K_{58}	0.56	0.01179540
B_{59}	K_{59}	4.64	0.01224465
B_{60}	K_{60}	8.45	0.01031363
B_{61}	K_{61}	13.47	0.01316774
B_{62}	K_{62}	14.34	-0.01449998
B_{63}	K_{63}	0.72	-0.03166558
B_{64}	K_{64}	-16.12	-0.02912780
B_{65}	K_{65}	-36.13	-0.04448869
B_{66}	K_{66}	-62.07	-0.02034692

A.1.5.1 OBS-5 crossings only

Start interval time: 32000

B_1	K_1	-52.46	-0.01485736
B_2	K_2	-36.59	0.17339800
B_3	K_3	-0.62	0.00787214
B_4	K_4	33.21	0.08314800
B_5	K_5	51.87	-0.01768086
B_6	K_6	44.60	-0.03495044
B_7	K_7	23.91	-0.06190964
B_8	K_8	-7.26	-0.05313393
B_9	K_9	-33.73	-0.00676878

A.1.5.2 OBS-5 all shots

Start interval time: 3000

B_1	K_1	29.81	0.00181100
B_2	K_2	12.34	-0.00391616
B_3	K_3	6.36	0.09555552
B_4	K_4	25.87	-0.00980396
B_5	K_5	25.88	0.05565184
B_6	K_6	38.24	-0.00086323
B_7	K_7	43.69	0.03760203
B_8	K_8	56.50	0.00159370
B_9	K_9	14.96	-0.02598925
B_{10}	K_{10}	-14.44	0.18066595
B_{11}	K_{11}	8.69	-0.00887868
B_{12}	K_{12}	20.62	0.06914542
B_{13}	K_{13}	36.64	-0.01379163
B_{14}	K_{14}	31.16	-0.02765243
B_{15}	K_{15}	15.76	-0.04517657
B_{16}	K_{16}	-6.11	-0.03534008
B_{17}	K_{17}	-29.30	-0.00347286
B_{18}	K_{18}	-23.80	0.06368920
B_{19}	K_{19}	3.85	0.00640102
B_{20}	K_{20}	20.47	0.11546829
B_{21}	K_{21}	17.85	-0.10129089
B_{22}	K_{22}	-29.99	-0.00853438
B_{23}	K_{23}	-28.49	0.14245108
B_{24}	K_{24}	-10.81	-0.00387014

A.1.6.1 OBS-6 crossings only

Start interval time: 3000

B_1	K_1	-116.58	0.00989376
B_2	K_2	-78.59	0.02011352
B_3	K_3	-28.15	0.05034418
B_4	K_4	29.37	0.02995001
B_5	K_5	40.36	-0.00344631
B_6	K_6	21.76	-0.00534167
B_7	K_7	-21.99	-0.00158025
B_8	K_8	-32.78	0.02213178
B_9	K_9	-7.58	-0.00122809
B_{10}	K_{10}	-32.01	-0.01698764

A.1.6.2 OBS-6 all shots

Start interval time: 3000

B_1	K_1	-54.38	0.00189814
B_2	K_2	-52.12	0.00083796
B_3	K_3	-48.57	0.00760651
B_4	K_4	-43.93	0.00727575
B_5	K_5	-39.29	0.00789952
B_6	K_6	-33.93	0.01163896
B_7	K_7	-28.18	0.01030070
B_8	K_8	-21.94	0.00805104
B_9	K_9	-14.75	0.01585495
B_{10}	K_{10}	-4.47	0.02143568
B_{11}	K_{11}	7.56	0.02190143
B_{12}	K_{12}	22.03	0.02259751
B_{13}	K_{13}	30.12	0.00340905
B_{14}	K_{14}	29.64	-0.00431420
B_{15}	K_{15}	25.21	-0.00924783
B_{16}	K_{16}	19.31	-0.01047964
B_{17}	K_{17}	15.31	-0.00574051
B_{18}	K_{18}	11.10	-0.00753610
B_{19}	K_{19}	6.72	-0.00867252
B_{20}	K_{20}	2.15	-0.00847217
B_{21}	K_{21}	-2.87	-0.00768749
B_{22}	K_{22}	-8.13	-0.00934012
B_{23}	K_{23}	-14.55	-0.01101679
B_{24}	K_{24}	-20.47	-0.00969445
B_{25}	K_{25}	-21.98	0.00994146
B_{26}	K_{26}	-11.72	0.00179142
B_{27}	K_{27}	-6.96	0.00163965
B_{28}	K_{28}	-4.09	0.00145159
B_{29}	K_{29}	-2.43	0.00114824
B_{30}	K_{30}	-1.47	0.00123974
B_{31}	K_{31}	-0.83	0.00142835
B_{32}	K_{32}	-0.45	0.00124230
B_{33}	K_{33}	-0.24	0.00135231
B_{34}	K_{34}	-0.17	0.00118622
B_{35}	K_{35}	-0.17	0.00142402
B_{36}	K_{36}	-0.21	0.00148830
B_{37}	K_{37}	-0.23	0.00195460
B_{38}	K_{38}	-0.22	0.00219223
B_{39}	K_{39}	-0.08	0.00306167
B_{40}	K_{40}	0.24	0.00351728
B_{41}	K_{41}	0.51	0.00345341
B_{42}	K_{42}	0.78	0.00407027
B_{43}	K_{43}	1.60	0.00586986
B_{44}	K_{44}	2.43	0.00427849
B_{45}	K_{45}	3.59	0.00684717
B_{46}	K_{46}	6.09	0.00824443
B_{47}	K_{47}	10.35	0.01096195
B_{48}	K_{48}	16.77	0.00879343
B_{49}	K_{49}	20.77	0.00579540
B_{50}	K_{50}	25.13	0.00729811
B_{51}	K_{51}	28.81	-0.01718587
B_{53}	K_{53}	26.27	0.02010079

B_{54}	K_{54}	37.04	0.01059114
B_{55}	K_{55}	42.18	0.01578071
B_{56}	K56	28.72	-0.08548127
B_{57}	K_{57}	-12.48	-0.01543554
B_{58}	K_{58}	-19.54	-0.00359991
B_{59}	K_{59}	-23.37	-0.01218525
B_{60}	K_{60}	-22.87	0.03118168
B_{61}	K_{61}	3.35	0.03287351
B_{62}	K_{62}	10.70	-0.00212125
B_{63}	K_{63}	10.06	-0.00020392
B_{64}	K_{64}	8.30	-0.00281903
B_{65}	K_{65}	5.94	-0.00141633
B_{66}	K_{66}	3.34	-0.00785975
B_{67}	K_{67}	-2.32	-0.00734860
B_{68}	K_{68}	-8.24	-0.01680300
B_{69}	K_{69}	-15.76	-0.00380148
B_{70}	K_{70}	-20.96	-0.01644212
B_{71}	K_{71}	-28.10	-0.00743601
B_{72}	K_{72}	-34.14	-0.01611755
B_{73}	K_{73}	-45.26	-0.01418928
B_{74}	K_{74}	-39.27	0.01320548
B_{75}	K_{75}	-37.91	-0.01038958
B_{76}	K_{76}	-27.42	0.06068923
B_{77}	K_{77}	5.73	0.01693272
B_{78}	K_{78}	9.41	0.00019420
B_{79}	K_{79}	11.77	0.00428186
B_{80}	K_{80}	13.98	-0.00606019
B_{81}	K_{81}	12.86	0.00269779
B_{82}	K_{82}	15.59	-0.00093199
B_{83}	K_{83}	15.89	-0.00000143
B_{84}	K_{84}	12.83	-0.01667530
B_{85}	K_{85}	5.30	-0.01365799
B_{86}	K_{86}	-2.28	-0.01625832
B_{87}	K_{87}	-14.42	-0.03361993
B_{88}	K_{88}	-21.70	0.02458934
B_{89}	K_{89}	-5.96	0.01213476
B_{90}	K_{90}	1.62	0.00819419
B_{91}	K_{91}	5.60	0.00231852
B_{92}	K_{92}	2.93	-0.01776148
B_{93}	K_{93}	-8.43	-0.02449729
B_{94}	K_{94}	-21.77	-0.02404597
B_{95}	K_{95}	-32.83	-0.01569051
B_{96}	K_{96}	-42.20	-0.01312515